Dissertation

Toughening and modeling of photopolymers used in 3D printing by experimental and computational methods

carried out for the purpose of obtaining the degree of Doctor technicae (Dr. techn.), submitted at TU Wien, Faculty of Mechanical and Industrial Engineering, by

Alexander Hochwallner

Mat.Nr.: 1226741

under the supervision of

Univ.Prof. Dipl.-Ing. Dr.mont. Jürgen Stampfl

Institute of Materials Science and Technology, E308

Vienna, 01-2023

Reviewed by

....

Peter Krajnc   Robert Liska

Faculty of Chemistry and Chemical Technology   Institute of Applied Synthetic Chemistry

University of Maribor   TU Wien

Smetanova Ulica 17   Getreidemarkt 9/163

2000 Maribor, Slovenia   1060 Vienna, Austria

I confirm, that going to press of this thesis needs the confirmation of the examination committee.

Affidavit

I declare in lieu of oath, that I wrote this thesis and performed the associated research myself, using only literature cited in this volume. If text passages from sources are used literally, they are marked as such.

I confirm that this work is original and has not been submitted elsewhere for any examination, nor is it currently under consideration for a thesis elsewhere.

I acknowledge that the submitted work will be checked electronically-technically using suitable and state-of-the-art means (plagiarism detection software). On the one hand, this ensures that the submitted work was prepared according to the high-quality standards within the applicable rules to ensure good scientific practice "Code of Conduct" at the TU Wien. On the other hand, a comparison with other student theses avoids violations of my personal copyright.

_____   _____
       City and Date   *Signature*

I. Acknowledgements

"If you wish to make an apple pie from scratch, you must first invent the universe." – Carl Sagan

II. Table of contents

III. Abstract

Photopolymers are a class of materials that show polymerization reactions upon exposure to light. This unique property is the basis for stereolithography, one of the most precise methods in 3D printing. Unfortunately, the material properties of common photopolymers do not meet the requirements for demanding applications. Especially fracture toughness is low due to rigid, highly crosslinked polymer networks. Recent developments in molecular chemistry, and the invention of hot lithography guide a way to leave the brittleness behind and make high performance 3D printed parts.

This work aims at unraveling the structure property relations in state-of-the-art photopolymer compositions and understanding toughness by investigating different toughening approaches. The focus lies on toughening by deliberately introducing heterogeneities into otherwise homogeneous photopolymers. One of the most used technical plastics, ABS, is a prime example for the success of heterogenous polymers.

Multi-phase photopolymers were produced in different ways using core-shell rubber particles, polymerization induced phase separation, and a custom hybrid additive manufacturing technique. All approaches showed substantial increase of elongation at break while only slightly compromising stiffness. The hybrid printing method is of high technological importance as it enables selective toughening of additively manufactured parts which minimizes the need for toughening agents.

To further investigate the matrix material and facilitate simulation-based material developments in the field of photopolymers, a computational reactive molecular dynamics representation of meth/-acrylate based resins was investigated. The computational method was used to study reaction kinetics and mechanical properties by means of tensile properties and dynamic mechanical response. The model was compared to experimental values showing excellent agreement. This indicates the usability and value of molecular modeling for aiding the development of cutting-edge photopolymer materials.

IV. Kurzfassung

Materialien, die durch die Bestrahlung mit Licht Polymerisationsreaktionen zeigen und dabei aushärten, nennt man Photopolymere. Dieses Verhalten ist die Grundlage der Stereolithographie, eines der präzisesten 3D-Druckverfahren. Allerding ist diese Klasse an Materialien, durch die chemisch vernetzte Molekülstruktur, meist spröde. Dadurch werden die potentiellen Anwendungsfelder dieser Technologie deutlich eingeschränkt. Durch neue Entwicklungen im Bereich der Polymerchemie und Prozesstechnik ergeben sich Möglichkeiten, Polymere zu verdrucken, die höhere Bruchzähigkeiten aufweisen.

Die vorliegende Arbeit behandelt die Beziehung zwischen der Struktur und den thermomechanischen Eigenschaften von modernen Photopolymeren. Es wird untersucht, welche Mechanismen hauptverantwortlich für eine hohe Bruchdehnung sind, und es werden verschiedene Strategien verfolgt, die Bruchdehnung zu maximieren und gleichzeitig die Steifigkeit hoch zu halten. Des Weiteren wird eine Methode präsentiert, Photopolymere mittels Molekulardynamiksimulationen zu beschreiben, wodurch die Vorhersage von Materialeigenschaften und Reaktionskinetik möglich werden soll.

Die Ansätze zur Steigerung der Bruchdehnung zielen darauf ab, in ein ansonst homogenes Photopolymer, Heterogenitäten einzubauen. Diese mehrphasigen Werkstoffe wurden mittels Core-shell Nanopartikel, Phasenseparation während der Polymerisation, und einem hybriden 3D-Druckverfahren hergestellt. Mit allen Verfahren konnte eine signifikante Steigerung der Bruchdehnung erreicht werden, bei nur geringer Abnahme der Festigkeit. Von besonderer Relevanz ist dabei das hybride Druckverfahren, da es selektive Modifikation von Bauteilen zulässt. Es konnte außerdem gezeigt werden, dass das Potenzial zur Steigerung der Bruchdehnung stark von dem Matrixmaterial abhängig ist. Mittels Molekulardynamiksimulationen verschiedener Systeme konnten präzise Übereinstimmungen mit experimentellen Ergebnissen aus Zugversuch und dynamisch mechanischer Analyse gefunden werden. Dies kann als wichtiger Meilenstein in Richtung simulationsbasierter Photopolymerentwicklung angesehen werden.

1 Introduction

For any given technological application, the choice of material has tremendous influence on the design of a product, as only the materials properties give a design its functionality. However, often the properties are a limiting factor. Be it electrical conductivity in electrical applications, or the strength in structural applications. The availability of suitable materials is a critical aspect that defines the design space for engineers. To expand this space, the discovery and development of new materials with better properties and manufacturing techniques is essential and a key enabler for technological advances. From the perspective of a materials scientist, this motivates to intensively trying to understand what defines a material's properties and use this knowledge to develop advanced materials.

It is well known today that the properties of a material arise from a combination of effects that happen at different length scales. While the chemical constitution builds the foundation, the microstructure also plays an important role for the properties. Eventually, the shape of a part must not be excluded from consideration. Examples for the importance of the microstructure can be found everywhere in nature. Wood, one of the oldest structural materials used by humankind, is highly hierarchically structured which has influence on the macroscopic properties. Furthermore, a lot of different woods exist with widely varying mechanical properties, though the molecular constituents are very similar. In order to fully understand such a complex material, it is necessary to study each aspect not only separately but also how they influence each other. Hierarchically structured materials are not only found in nature, also technical materials like plastics can show microstructures which will be discussed later.

Besides the properties, the respective manufacturing method is of high technological and industrial relevance. Today, the benchmark for polymer processing is injection molding which can produce large quantities of parts at low production cost. The necessary mold, however, is rather expensive and make lower quantities not feasible. This gap is being tried to fill using alternative manufacturing methods like 3D printing. The versatility of this technology makes it an interesting alternative to conventional methods. It is now possible to manufacture parts without the need of conventional tools, directly from a digital model. New designs, not producible before, are becoming possible, giving engineers increased freedom in the design process. This idea of virtually unlimited freedom of design has sparked a hype that the industry has yet to live up to. Though the remarkably high age of the additive manufacturing idea, a

broad industrial adoption is still not realized. The reasons for this are manifold and highly application dependent. A general shortcoming is the lack of available high-performance materials which are necessary for demanding applications. 3D printing methods usually require the raw material to be in a narrowly defined processing window to be processable by the respective 3D printing machine. This limits the freedom in material development and explains the difficulties in coming up with high performance materials for a broad adoption of 3D printing methods.

Especially challenging in terms of materials development is stereolithography. With its light-based approach however, this method gives superior spatial resolution and is therefore a popular choice among 3D printing technologies. Stereolithography involves covalent crosslinking of a resin, which tends to yield brittle final materials. While there exist resins with increased toughness, a good balance between stiffness and toughness is hard to achieve.

This work starts where synthetic chemistry ends and tries to explore methods to toughen photopolymer materials. It starts with investigating the influence of different compounds on the final mechanical properties. Then, a number of different toughening approaches are explored. The focus lies on deliberately producing an inhomogeneous microstructure to increase energy dissipation during deformation and giving a fracture mechanical advantage over the homogenous material. In this regard, ABS can be seen as a role model. This block copolymer is known to form a matrix-inclusion microstructure that yields high stiffness without the brittle behavior of the styrene homopolymer. Because of its superior properties it is very attractive to manufacture ABS parts in a 3D printing process. But machines that are capable of processing ABS are inferior when it comes to spatial resolution. Whereas light based stereolithography machines, which deliver the best resolution, are limited to the intrinsically brittle materials that commonly are homogenous. For the purpose of investigating heterogeneous photopolymers, microstructures were added using well known methods like nano particles and phase separation, but also novel methods involving a hybrid 3D printing process that combines stereolithography with inkjet printing are presented. The major advantage of using this second 3D printing method is the ability to selectively deposit a second material. In contrast to particles and phase separation, the second phase can now be added in a regular fashion.

The final part of this thesis then deals with simulation methods in an effort to model different aspects of photopolymers that are potentially relevant for accelerated material development in the future. While molecular dynamics simulations are heavily used in biophysics and related fields, it is not widely adopted in polymer development. A simulated polymerization algorithm

is used to go from the molecular representation to a polymer network. From this network different mechanical properties are evaluated and compared to real world measurements.

This text is divided into five chapters. The first being the introductory chapter that briefly introduces the fundamental topics relevant also in the later chapters. The following chapter briefly describes the methods and materials used. After this the main findings of this work are summarized in two chapters. One being the more experimental section of the toughening approaches, the other one presents the findings from the simulation activities. The final chapter summarizes and tries to put everything into perspective.

1.1   3D Printing

3D Printing, or the more descriptive term additive manufacturing, refers to processes in which a part is created by adding material in a layer-wise fashion. This layer-by-layer formation of a part is what discriminates additive manufacturing from traditional manufacturing methods like drilling or casting. This fundamental difference enables the production of parts with complex geometric shapes that were not achievable with the established manufacturing methods. A possible field of application is therefore the manufacturing of light weight components which often are designed in a complex cellular fashion [1]. Besides the enhanced freedom of design, the great potential for automating the production process makes 3D printing attractive for manufacturers. With a faster time between an idea and the prototype, development cycles can be streamlined. Even minor changes in the design can be implemented rather easily.

Since the patent filed by Charles Hall in 1984 [2], in which stereolithography was first described, many different variations of 3D printing have been developed. The range of materials that can be processed with additive manufacturing methods was extended to metals [3] and ceramics [4]. Even printing of concrete was made possible [5]. This enables the automation of the main task in building houses, namely erecting walls, which can help create affordable housing. The field of bioprinting and tissue engineering are fields of lots of ongoing research and plentiful exciting possible applications [6].

Looking at the manifold achievements of additive manufacturing one is tempted to ask what 3D printing cannot do. But the challenges are often process inherent. One major limitation is that a certain material is tightly bound to a distinct method. Changing the material almost certainly makes changes in the process necessary, or an entirely new process has to be developed. For that reason, material development in 3D happens within tight boundaries. The

material has to have the properties dictated by the processability parameters. Only then one can think about the material properties required by a certain application.

A lot of applications demand high performance materials. But many 3D printing materials cannot meet the high requirements. Especially when comparing them to established materials which are manufactured conventionally they cannot compete [7], [8].

1.1.1 3D printing methods

Additive manufacturing processes can be categorized by the way the individual layers are formed. According to the ASTM, the groups of methods are called binder jetting, direct energy deposition, materials extrusion, material jetting, powder bed fusion, sheet lamination and vat polymerization [9]. Only materials which are suitable for the respective layer forming technique can be processed. It follows that the process and the material form a system, and the two components cannot be considered independently. A method based on extrusion, of course, requires a material which is possible to be extruded. A powder-based method can only work with powdered materials which bring its own characteristic challenges in preparing and handling of the underlying material. To find an additive manufacturing method for a certain application one has to consider mainly the material properties and precision of the method that can handle the target material. The optimal solution must be determined for every specific case individually. Other aspects that need to be considered are the speed of the building process and the cost of the device and the material.

To give an idea of the diversity of available methods for only one class of materials, namely polymers, an overview of some available methods for polymer additive manufacturing is given in Figure 1. The depicted methods [10] use different principles of layer formation. In method a (fused deposition modeling) and d (selective laser sintering), the layer is formed from a solidifying thermoplastic that was molten, or sintered respectively, by a source of thermal energy. Methods b (laser-stereolithography) and c (digital light processing) use a liquid resin which can be cured by photochemical activation. It solidifies where it was exposed to light. The light source can either be a laser or a light emitting diode. Method e (inkjet 3D printing) also works with a photochemically curable material, with the difference that here the resin is selectively deposited before curing instead of selectively cured. For process f (sheet lamination)

the layer is provided already in the form of a foil. It is then shaped using some sort of cutting device, a laser in this case, and then the layers are bonded.

It is important to note, that each individual process has its specific advantages and disadvantages that need to be considered carefully when planning to adopt a specific process. For this work, only resin-based methods are relevant which will be discussed in the next section.
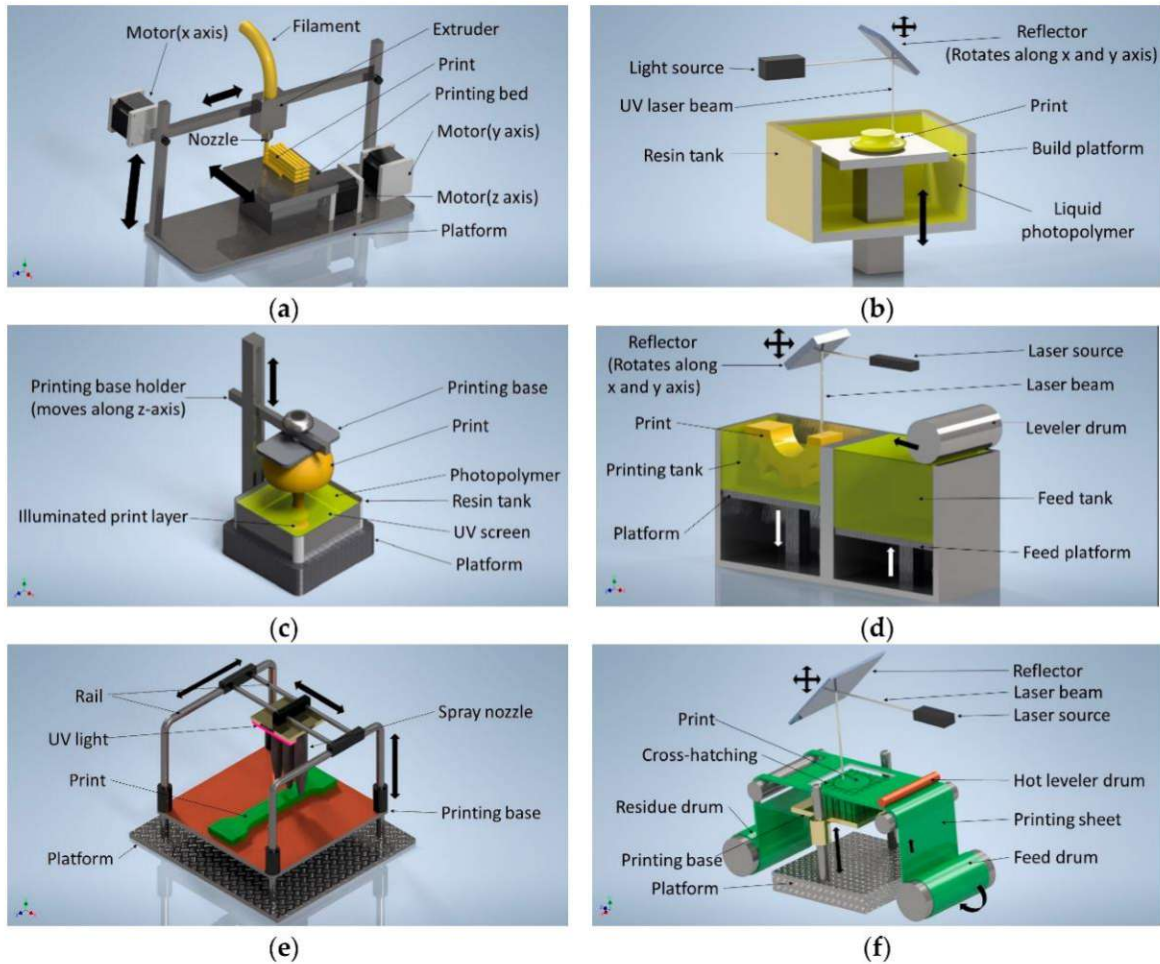
Figure 1: a) The layers are formed by solidification of an extruded thermoplastic material. b) A laser is used to cure a photopolymer. c) A photopolymer is cured using a DLP light engine. d) Powder particles are merged using the energy provided by a laser. e) An inkjet printhead is used to selectively deposit a photopolymer. The layer is cured with a light source immediately after deposition. f) The layers are cut out of a foil using a laser and merged with thermal energy. Figure taken from [10].

1.1.2 Lithography-based additive manufacturing

When high resolution and good surface quality are desired, stereolithography is the method of choice in many cases [11]. This process uses a light-curable, also called photoreactive resin or photopolymer, together with a corresponding light source. As light sources, laser-scanner systems are used or alternatively so-called digital light processing devices (DLP). The main advantage of DLP over the laser-scanner method is that an entire layer can be exposed at once, while a laser spot is confined in space, making scanning necessary. This gives an advantage of DLP over laser-scanners regarding building speed which is especially true for parts with large cross-sections. In terms of surface quality, laser-scanning systems are preferable because continuous laser paths can be realized that render contours smoothly. In contrast, DLP cross sections are composed of individual pixels. This can lead to poor surface quality especially in areas with high curvature. An effect that is well known from any digital displaying device. Another major difference between a laser-based system and a DLP system is the power density that arrives at the resin. A laser focuses all the emitted power in the spot. A DLP system covers a much larger area which means that the power densities are generally lower at a DLP pixel compared to a laser spot. This means the resin used has to work with the respective power density for successful printing.

Not all photopolymers are equally suited for both, DLP and laser exposure. Photopolymers cover a wide range of material properties and also the polymerization kinetics are different from resin to resin. This was investigated in [12] where a resin was diluted by a monofunctional methacrylate and evaluated regarding the printability in a laser system and a DLP system. To see the influence of the mono-functional diluent, exposure tests were conducted at different laser speeds. For this purpose, a defined amount of resin was put into the exposure area and cured with different laser speeds. Three different outcomes were observed. Either all of the resin was solid after exposure, no solidification, or a disc was cured and part of the resin remained liquid on top of that disc. The results of the exposure tests are given in Table 1 with the three outcomes color coded in green, red and white respectively. It shows a clear trend towards longer exposure times of materials with higher amounts of monofunctional reactive diluent. It can be concluded that a high content of monofunctional reactive diluent slows down the polymerization speed and longer exposure times are needed. That requires slow scanning speed to get fully cured layers which makes laser-scanner systems unpractical for resins that show slow polymerization reactions. Subsequent printing tests conducted in [12] then showed that with high content of monofunctional reactive diluent, small features could be resolved with

DLP that could not be resolved using a laser scanner. This can be explained by the high power densities in the laser spot together with a slow scanning speed which leads to significant over-polymerization.

Table 1: Exposure tests with different amounts of a monofunctional reactive diluent (HSMA [13]). The values are the measured height of the cured disk in mm. Green background means the disk was entirely cured. Red background means no solid material was obtained. Table taken from [12].

		HSMA content [wt%]								
		0	10	20	30	40	50	60	70	80
Laser speed [mm/s]	100	1,04	1,01	0,96	0,94	0,87	0,60	0,81	0,80	1,14
	250	0,90	0,95	1,00	0,93	0,73	0,87	0,89	0,67	0,55
	500	0,92	0,99	0,77	1,06	0,90	0,41	0,75	0,75	X
	1000	1,08	1,30	0,75	0,87	0,68	X	X	X	X
	1500	1,23	1,01	0,77	0,76	X	X	X	X	X

Crucial for a successful printing process is the strength of the material after exposure, also called the green part strength. The periodic coating and exposure cycles stress the part already at building time. Only if the material does not fail under this load, the printing process can be finished successfully. This is critical, especially for very delicate structures.

Besides the reactivity, also the viscosity of a resin must be within the processing window that is required by the stereolithography machine of choice. To expand the range of materials which can be processed with resin based additive manufacturing, the so called hot lithography process was developed [14]. It uses a special heating method to lower the viscosity of highly viscous resins and enables their use. High molecular weight components which usually increase the viscosity of a resin can be processable with this technology. Next to (meth)acrylate based resins, hot lithography allows the use of alternative chemistry like epoxy based resins [15]. It was also observed that printing at elevated temperatures can reduce the curing time and can positively influence the mechanical properties compared to samples printed at room temperature [16].

To successfully print high performance parts using stereolithography one has to control a number of parameters carefully. Curing time and light intensity have major influence on the

mechanical properties and on the spatial resolution. The temperature at curing has influence on the curing behavior. Furthermore, all the parameters are depending on the resin itself which can contain numerous different components. These components can be mixed in different compositions which makes general assumptions difficult to make. The resin-printer system is very complex because none of its components is fully independent from each other. Small changes in one of the parameters can have severe influence on the printing result. To better understand the layer formation in resin-based 3D printers, one has to first understand the fundamental mechanism that leads to the solidification of the resin. The so-called photopolymerization or photoinduced polymerization will be discussed in a later section.

1.1.3   Application in orthodontics

One of the largest field of application of 3D printing to date is orthodontics. It requires patient specific geometries that are hard to manufacture with conventional manufacturing methods economically. Specifically, so called "aligners" are of major interest to the industry. These are digitally shaped transparent appliances with the purpose of moving a patient's teeth to the desired location. An aligner treatment consists of multiple such individual parts, each of which for the purpose of applying an incremental shift to a set of teeth. Today, aligners are manufactured primarily by 3D printing or milling of molds and subsequent thermoforming of a thermoplastic material [17]. Direct printing of transparent aligners would give an obvious advantage over the established manufacturing method. While the precision that is needed for this application can be achieved easily by stereolithography, the required material properties for a reliable aligner treatment are challenging. Brittle materials cannot be used as fracture in a patient's mouth must not happen. Furthermore, a defined stiffness must be guaranteed for a controlled application of force to the teeth and the force has to be kept above a certain threshold over the lifetime of the aligner. Another challenge is the moist oral environment in which the material must function.

These requirements for a 3D printing material were considered in the planning of the experiments in this work and the presented methods are evaluated with these requirements in mind.

1.2 Photoinduced polymerization

Photoinduced polymerization is a process where, induced by light, reactive molecules are polymerized [18]. These molecules can be monomers with one or more reactive groups, or oligomers which already consist of several repeat units. They can also be equipped with one or more reactive groups. Usually, oligomers for photoinduced polymerization in 3D printing have one reactive group at each end of the molecule [19].

Photoinduced polymerization can be used to solidify a liquid resin and is therefore applicable in a variety of industries [20]. For the polymerization reaction, ionic as well as free radical curing is possible [18]. Due to the usually faster reaction, free radical polymerization of acrylate based resins is preferable in a range of applications including additive manufacturing [21]. In the present work only meth-/acrylate systems have been investigated. Hence, the focus in this section is on radical polymerization.

For starting the reaction, a polymerization initiating species must be present. It is generated by the so called photoinitiator. These are special molecules that form the reactive species when absorbing a photon with a certain energy. Multiple specialized photoinitiators are commercially available for a range of different absorption spectra [22]. After initiation, reactive monomers or oligomers are sequentially added to form a polymer chain until the reaction is terminated. Termination can happen by a termination reaction or if all reactive groups in the material are consumed or 'frozen'. During the polymerization, the molecular weight is increasing which leads to increasingly limited mobility of the unpolymerized molecules. If the mobility is restrained to a point where the reaction partners can't come close to each other no further polymerization reaction can take place.

1.2.1 Radical photopolymerization

This section closely follows [23].

Radical polymerization is a form of chain-growth polymerization in which the reactive center is a radical. The overall polymerization consists of a sequence of reactions.

The first step is the creation of an initiating radical R• by the initiator I. In the case of homolytic dissociation one initiator molecule is cleaved into two radicals. Each of which can

start a polymerization reaction. In the case of photoinitiation, this process is initiated by an energy quantum in the form of a photon $h\nu$. The radical is then adding to a monomer[1] M forming the chain starting radical $M_1\bullet$.

Initiation
$$I + h\nu \longrightarrow 2\,R^\bullet$$
$$R^\bullet + M \longrightarrow M_1{}^\bullet$$
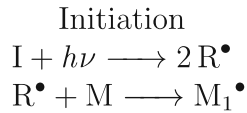
The monomer that bears the radical character then adds another monomer as the chain propagates. The radical character is passed onto the latest added molecule as the chain is growing.

Propagation
$$M_1{}^\bullet + M \longrightarrow M_2{}^\bullet$$
$$M_2{}^\bullet + M \longrightarrow M_3{}^\bullet$$
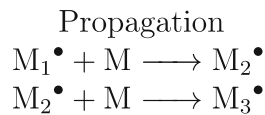
The chain propagation continues as long as monomer species is available in the vicinity of the active chain end, or a termination reaction occurs.

Termination can happen by a combination reaction. In this case two radical polymer chain ends combine to form a chain with the length of the sum of the two chains involved. Or disproportionation where two radical chains react to form two chains. Both chains keep their initial degree of polymerization.

Termination
$$M_n{}^\bullet + M_m{}^\bullet \longrightarrow M_{n+m}$$
$$M_n{}^\bullet + M_m{}^\bullet \longrightarrow M_n + M_m$$
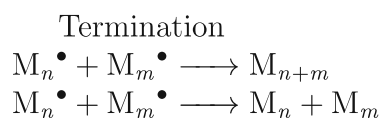
A different type of termination reaction can happen with substances present in the material either deliberately or unintentionally. Some substances are known to be capable of inhibiting

---

[1] A monomer in this context is any reactive group attached to a molecule. Every reactive group of a molecule can be seen as a monomer. Since a molecule can bear multiple reactive groups, it can engage in multiple polymerization reactions.

the polymerization reaction. They can be used to increase the shelf life of reactive resins and are therefore widely used to avoid premature polymerization. Unwanted polymerization inhibition often comes from oxygen as it is a particularly efficient inhibitor and commonly present. It reacts with chain radicals and forms unreactive peroxy radicals.

Oxygen inhibition

$$M_n{}^\bullet + O_2 \longrightarrow M_n{-}OO^\bullet$$
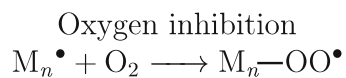
In the case of oxygen inhibition, the polymerization cannot be restarted as the peroxy radicals form dead ends to the chain. Another effect of oxygen worth considering is the quenching of the excited initiator state. This means that the energy coming from the absorbed photon is not dissipated by forming radicals but by energy transfer. Quenching blocks the initiator from forming the initiating species. In this case the initiator remains intact which means that the reaction can be started at a later time during exposure. The effect is a reduced initiation rate. Both oxygen inhibition and oxygen quenching can be avoided if oxygen is excluded from the reaction.

Compared to step growth polymerization, chain growth polymerization leads to a rapid increase in molecular weight starting from the beginning of the polymerization. Large initiation rates lead to high polymerization rates. Therefore, very fast curing can be achieved. But with an increasing number of radicals the chance for termination reactions is also increasing. This has influence on the length of the individual polymer chains and potentially alters the final material properties. The kinetic chain length v, which is the average number of monomer units consumed per initiating radical, is inversely proportional to the initiation rate.

$$v = \frac{R_p}{R_i} \tag{1}$$

Where R_p is the propagation rate, R_i is the initiation rate. A high number of monomer units per polymer chain is therefore in competition with a high initiation rate. [23]

1.2.2 Photoinduced generation of radicals

This section closely follows [23].

In the case of photoinitiation the initiation rate can be expressed as

$$R_i = 2f\phi' I_a \tag{2}$$

Where I_a is the absorbed volumetric light intensity or absorbed volumetric photon density and ϕ' is the quantum yield which is the number of photolysis events per absorbed photon. f represents the efficiency of the initiator radical starting a chain polymerization. The factor of 2 comes from the fact that two radicals are formed from one initiator molecule. The expression $2f\phi'$ then stands for the number of initiated chains per absorbed photon and represent the efficiency of an initiator in a given environment. The absorbed light intensity per unit area I_a' follows from the Beer-Lambert law:

$$I_a' = I_0 - I_0 e^{-\alpha[A]D} \tag{3}$$

Where α is the absorption coefficient, $[A]$ is the concentration of the absorber, I_0 is the incident intensity and D is the depth.

From this consideration one can see that the polymerization rate depends on the distance the light must travel through the absorbing medium. This dependency becomes small if $\alpha[A]D$ becomes small. In this case the exponential expression gets close to one and the dependency on the depth becomes negligible. That is the case when the curing layer is thin, and the initiator concentration is low. Photobleaching of the absorbing substances can also reduce the depth dependency as the absorption coefficient decreases over time. [23]

1.2.3 Network formation

Reactive molecules can have one or more reactive groups. The number of reactive groups is essential for the constitution of the resulting polymer material. First, let's consider the case of monofunctional monomers. Figure 2 shows ten methyl methacrylate molecules in a ball-stick

configuration[2]. A radical provided by the photoinitiator can attack the C=C double bond in one of the monomers and start the chain reaction. Sequentially, monomers are added to the chain, provided that no termination reaction takes place. The result of this process is a linear chain of the monomers (see Figure 3). A material that is polymerized purely from monofunctional monomers consists of chains with statistically distributed length that interact only by physical bonds. The absence of chemical bonds between the polymer chains makes it in principle possible to separate them by dissolution in appropriate solvents. The presence of molecules of higher functionality in the resin changes this behavior fundamentally.

If a polymer chain incorporates a molecule with more than one functional group, the remaining functional group(s) can still engage in a polymerization reaction. In that way the multifunctional molecule can act as a crosslinker between polymer chains, establishing chemical bonding between them (see Figure 4). This has influence on the properties of the resulting material but also on the polymerization process itself. While in the case of monofunctional molecules the molecular weight of the polymer chain is increased by the weight of only one monomer at a time, when a crosslink is established, the resulting molecular weight is the sum of the crosslinked polymer chains. This leads to a faster increase in molecular weight, therefore a faster increase in viscosity. This becomes manifest in an early onset of gelation. Gelation is defined as the point when the material transitions from a predominately viscous behavior to a predominantly elastic behavior. The transition point is called gel point. Intuitively, it is obvious that multifunctional monomers reach the gel point earlier after initiation compared to monofunctional monomers because due to crosslinks it takes less polymerization reactions to reach high molecular weights (see Figure 4). The number of crosslinks in a polymer material can be influenced by the ratio between monofunctional and multifunctional components in a resin. Small multifunctional molecules are often referred to as crosslinkers.

In the cured state, crosslinks play a large role also for the mechanical properties. Linear chains can move easily with respect to each other when the material is strained. Chemical bonds between polymer chains restrict that movement to a certain extent. This can have influence on properties like hardness, tensile strength, storage modulus, loss modulus and glass transition temperature [25], [26].

---

[2] The molecules in the figures were equilibrated using the UFF force field as implemented in Avogadro[24]. No external pressure was applied. That means the molecules in a system under atmospheric pressure would be closer together.
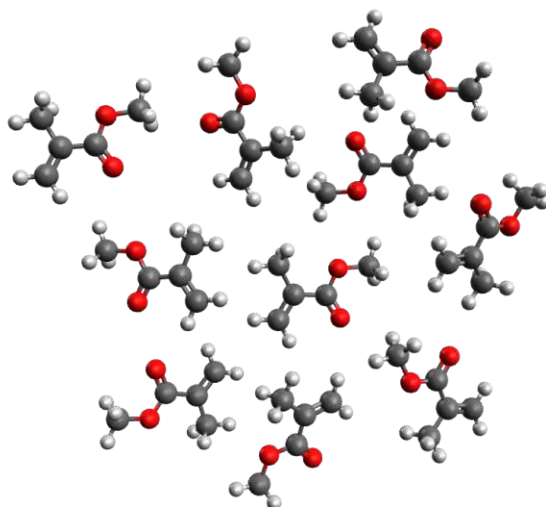
Figure 2: Ten methyl methacrylate molecules. The grey, red and white particles are representing carbon, oxygen and hydrogen atoms respectively. This figure was created using Avogadro [24].
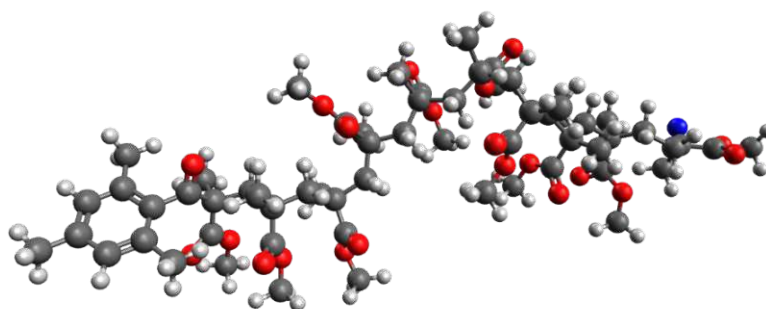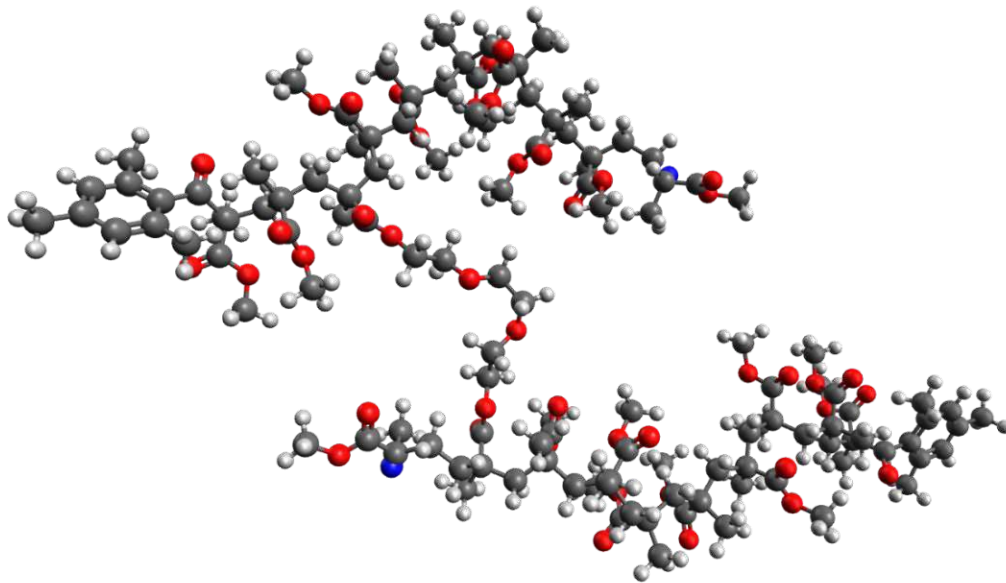

Figure 3: A linear chain of poly-methyl methacrylate. The initiating radical was provided by TPO photoinitiator in the left part of the figure. The radical chain end is represented with a blue marker next to the respective carbon atom. The grey, red and white particles are representing carbon, oxygen and hydrogen atoms respectively. This figure was created using Avogadro [24].

Figure 4: Two poly-methyl methacrylate chains connected by one triethylene glycol methacrylate molecule. This figure was created using Avogadro [24].

1.3   Thermomechanical properties of polymers

Polymers show an incredibly wide range of properties, which qualify them as structural and even functional materials. They can be applied in a variety of highly demanding applications. While it probably makes sense to replace some of the disposable plastics with more sustainable alternatives, others cannot be replaced easily. Some polymer materials are essential for technological applications because of their unique properties. A modern example for the technological relevance is their use as battery materials [27]. Also, the mechanical properties of polymers are vital for a wide range of applications.

The origin for these properties lies in the molecular structure. Polymers consist of chains of monomers which can be arranged in different ways. A number of thermoplastic polymers for example show a semi-crystalline morphology. That means domains of polymer chains with a crystalline arrangement are located within an amorphous matrix. Another type of polymers, ABS for example, shows a matrix-inclusion morphology. The basis for all the different polymer materials are the polymer chains. The length of these chains is arbitrary and there is a variety of monomers available and new ones are constantly being developed. Additionally, the polymer chains can be crosslinked, which obviously influences the properties of the material. There are

also blends of different polymers being used. Copolymers that combine different monomers in one polymer chain are another way to tailor the properties of a polymer material. One can see that the possible combinations are infinite. To understand the origin of the properties and therefore have better guidance for the development of novel materials, researchers have described the fundamental processes happening on a molecular level.

In the high strain realm, the mechanical properties are determined in particular by the ability of the polymer chains to move against each other [28]. One can assume, especially for amorphous polymers, that these movements are thermally assisted relaxation processes happening on the atomistic scale [29]. For these processes to happen, an energy barrier must be overcome which is a statistical process [28]. According to the theory of rate processes [30], the energy barrier for these relaxations to happen is altered by shear stress which makes movements in the direction of the applied shear stress more feasible [31]. A schematic representation of the potential energy is given in Figure 5. An applied stress leads to a lower energy barrier in the direction of the stress. With increasing stress, it becomes increasingly likely that the barrier is overcome. It follows from these considerations that the local height of the energy barrier is connected the local yield stress of a material. It has been shown that polymers show plastic flow at the yield stress, as described by Eyring [32], [33].
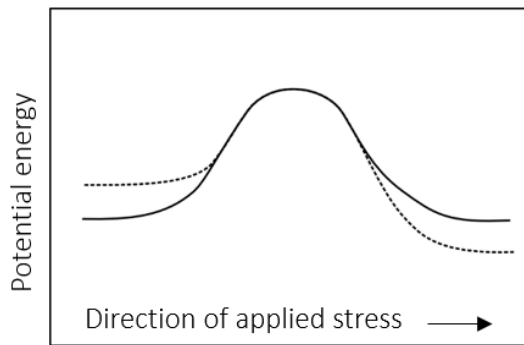

Figure 5: Schematic drawing of the potential energy barrier of a relaxation process without external stress (solid line), and with external stress (dashed line). Representation based on [28].

According to [28], following the Eyring equation [34] the frequency ν of events to cross an energy barrier of the height ΔH is

$$\nu = \nu_0 e^{-\frac{\Delta H}{k_B T}} \tag{4}$$

22

where k_B is the Boltzmann constant, T is the temperature, and ν_0 is a constant. Equation (4) represents the zero stress states. In the presence of stresses Equation (4) becomes

$$\nu = \nu_0 e^{-\frac{\Delta H - V\sigma}{k_B T}} \tag{5}$$

where σ is the applied stress and V is the so-called activation volume. The yield stress can then be expressed as

$$\sigma_Y = \frac{k_B T}{V} ln\left(\frac{2\dot{\varepsilon}}{\dot{\varepsilon}_0} e^{\frac{\Delta H}{k_B T}}\right) \tag{6}$$

[28].

The initial height, however, is influenced by several factors. Considering the amorphous structure of a polymer glass it can be expected that the (local) energy barrier varies throughout a polymer.[3] Obvious factors that influence the energy barrier are the intermolecular interactions and the flexibility of the backbone of the polymer chains. Molecules that interact strongly with each other cannot move as freely as molecules that don't interact much. It is also easier to tear apart flexible chains compared to rigid chains. Hence, different chemical building blocks can be used to influence a polymer's properties. It was observed that whether or not a polymer chain is 'bulky' has influence on the strength values of brittle polymers [35], [36]. Crosslinks between polymer chains are also influencing the molecular configuration and hinder molecular movement. Molecular weight of the polymer chains becomes increasingly important at high strains when the chains start to align [29] and short chains can easily loose grip. The elongation at break tends to increase with increasing molecular weight [37].

---

[3] For reasons discussed in section 1.2, especially photopolymers can show significant spatially differing curing conditions which influence the network topology, and therefore the local potential energy landscape.

1.3.1   Stress strain behavior

Although the large chemical diversity leads to a large variety of mechanical properties among polymer materials, most technologically relevant polymers show analogical response when subject to a constant strain rate. The most prominent analysis method to probe this response is the tensile test. The resulting stress-strain curves can, in most cases, be divided into three sections in which different mechanisms are dominating the material response. These sections are elastic response, plastic response, and fracture. It should be noted that these sections are often not clearly separated and can happen at strains that are orders of magnitude apart. Rubbers for example show elastic behavior at strains that are unreachable for other polymers.

Figure 6 shows typical responses of three different polymer classes. Thermoset materials that show high modulus tend to break at low strains without significant plastic deformation (curve I). Curve II in Figure 6 shows a behavior which is often seen in thermoplastic materials. The stress increases linearly with increasing strain until the material starts to yield. At the end of the curve strain hardening occurs before the material eventually breaks. Rubber networks have small elastic moduli and typically high elongation at break (curve III) compared to thermoset and thermoplastic polymer materials.
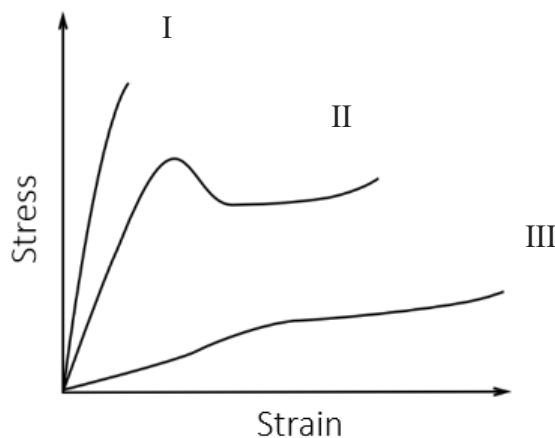

Figure 6: Typical stress-strain response of different polymer materials. After [38].

In general, in the low strain realm, the stress-strain response can be seen as linear elastic. The tensile stress grows linearly with the applied strain and the deformation is recoverable. In

this low strain limit Hooke's law applies. An applied stress leads to an increase of free energy. For materials below their glass transition temperature, this energy is stored as internal energy, and above the glass transition temperature it will be stored by lowering the entropy [39]. This second phenomenon is known as rubber elasticity or entropy elasticity [39], [40]. It is responsible for the unique properties of rubbers. It can be explained phenomenologically by the uncoiling of initially coiled polymer chains upon straining [40], [41]. Releasing the stress leads to re-coiling into a state of higher entropy. For full recovery of strains in rubbers, a network of crosslinked chains is essential [40].

When the stress exceeds the elastic limit of a material, plasticity starts to play an increasingly important role in the stress-strain response. At the yield stress, the stress response curve starts to flatten and some materials show a peak in the stress-strain curve. Plastic strains are by definition not recoverable. After unloading a plastically deformed material, only the elastic deformation is recoverable.

The plastic behavior of polymers involves thermally activated relaxation processes that accumulate with increasing stress [29]. After a significant amount of plastic flow polymer chains start to align and lower the entropy of the material. It can be easily recognized that the resistance to deformation of a material with aligned polymer chains is higher compared to a material in with coiled chains (see Figure 7). This phenomenon is known as strain hardening. This effect is important for toughening polymer materials. Strain hardening has the consequence that a larger volume is engaged in energy dissipation than in non-strain hardening materials [42], [43], [44].
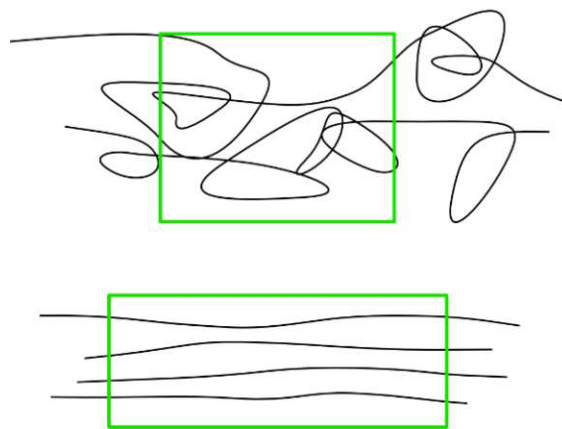

Figure 7: Schematic visualization of strain hardening in a representative volume element. Top: Polymer chains are in a curled-up high entropy state. Bottom: Polymer chains are aligned.

The last section of the stress strain response includes the fracture of the material. During the deformation stresses accumulate locally leading to stress concentrations. From the standpoint of engineering, stress concentrations often happen due the shape and load case of a structural part. Failure is expected to happen in such highly stressed regions. On the material level, stress concentrations occur at imperfections in the bulk of the material or at surface flaws. During plastic flow high stresses can be compensated by local strain concentrations. Fracture occurs when stress concentrations can no longer be compensated and unstable cracks are forming. With this in mind, the strain at break of different types of polymers can be explained on a phenomenological basis. Rubbers can be strained until the polymer chains are fully uncoiled. At this point the crosslinks restrict further chain movements and the increasing stress leads to brittle failure. Tightly crosslinked polymers, such as thermosets, reach that point at much lower strains because the chain length between crosslinks is comparatively short. That is the reason for the high stiffness and low elongation at break of such materials. Certain thermoplastics are known for high elongation at break. This can be explained by long polymer chains that exhibit enough mobility to detangle when strained. Therefore, limiting the buildup of stress concentrations and avoiding premature fracture. These considerations explain why the mechanical properties of polymers are so strongly linked to the architecture of the polymer network.

Besides plastic yielding, polymers show also other mechanisms that dissipate deformation energy, and which are relevant for the tough behavior of some polymer materials. One important phenomenon is crazing. Crazes are micro voids where the faces of the voids are bridged by elongated polymer fibrils [45], [46]. Figure 8 schematically shows the formation of a craze zone followed by a crack. The difference between the crack zone and the craze zone is the bridging of the faces by fibrils in the craze zone. Crazing is a mechanism often occurring pre-fracture if the crazes are not properly stabilized [45]. In Figure 9, a transmission electron microscopy image of a stable craze is shown. One can clearly see the fibrular structure of the craze zone. At the bottom of the void fibrils already started to break down indicating imminent fracture [47].

Crazing and plastic yielding are important energy dissipating mechanisms. They are essential for avoiding stress intensities, therefore, key for tough material behavior. Which mechanism predominately is present, is highly material dependent. The mechanism of plastic deformation is changing significantly with changing chain architecture [47].
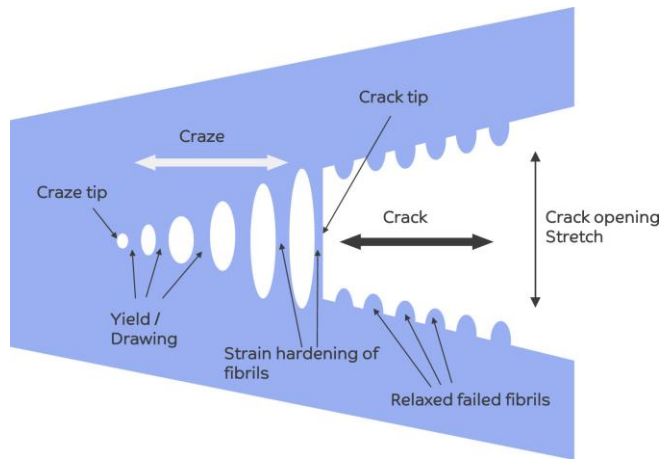
Figure 8: Crack opening with accompanied craze formation. Taken with permission from [48]. Copyright © 2019, Elsevier Ltd.
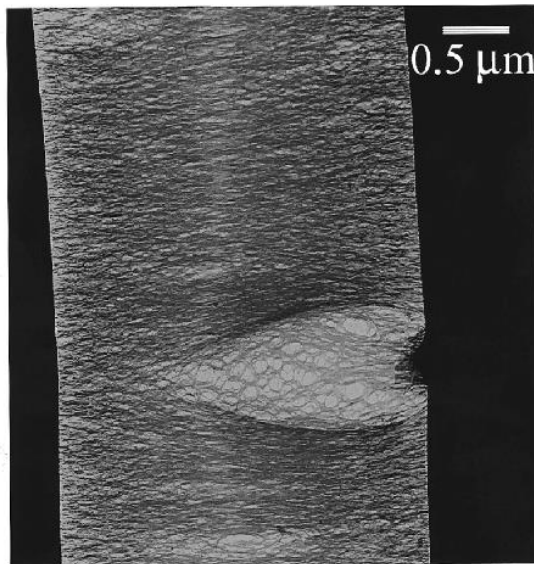

Figure 9: TEM image of a strained poly vinyl cyclohexane thin film. Taken with permission from [47]. Copyright © 2002, American Chemical Society.

1.3.2 Viscoelasticity

When comparing the response of polymers with the response of other solid materials the elastic-plastic nature of polymers stands out. Polymers show viscous response already at low strains. This can be attributed to the relatively high share of free volume in amorphous polymer material that leads to liquid like behavior [49]. The solid like domains will predominantly

respond elastically while the liquid like domains will show viscous behavior. The response of a polymer can therefore be seen a superposition of solid-like and liquid-like behavior [49]. To probe this behavior, the response of a material to either constant external stresses or constant strains can be measured. Also, dynamic probing of the viscoelastic nature of polymers can be used.

1.3.2.1 Creep

The term "creep" relates to the behavior of a material under constant load. The result of a creep experiment is the strain over time. A creep measurement consists of instantaneous loading and maintaining the load for a certain period of time. In Figure 10 a typical strain response to a constant stress is shown. When the load is applied the idealized material reacts with an instantaneous strain increase. The strain is then monotonically increasing and asymptotically approaching a certain strain value.
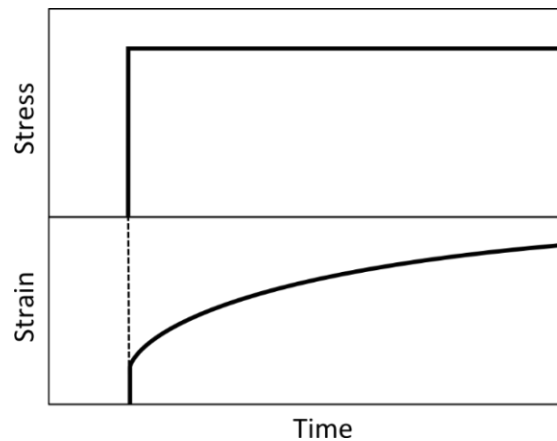
Figure 10: Viscoelastic creep response.

1.3.2.2 Stress relaxation

Stress relaxation is the response of a material to constant strain. Upon stepwise straining the idealized material responds with a step stress. The viscous component is then responsible for the decay of stress. The result of a stress relaxation experiment is the curve of the stress over time (see Figure 11).
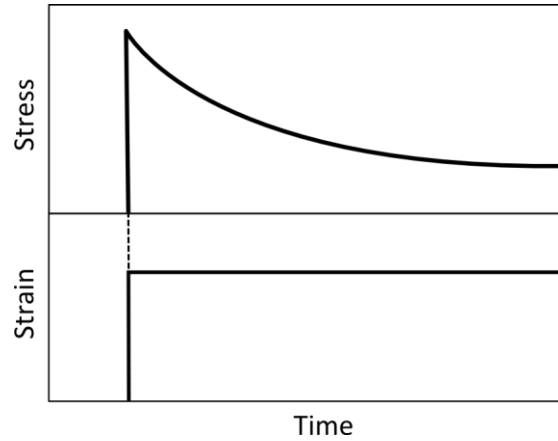
28

Figure 11: Stress relaxation response.

1.3.2.3 Dynamic mechanical analysis

To probe the viscoelasticity of a material a dynamic approach can be used. For this measurement, a sinusoidal strain is applied to the material.

$$\varepsilon = \varepsilon_0 \sin(\omega t) \qquad (7)$$

The measured response is therefore also sinusoidal, as long as the material remains in the linear viscoelastic realm. For that reason, dynamic mechanical measurements are usually conducted using small strains. The phase shift between external load and response can then be taken as a measure for the viscous behavior of a material.

$$\sigma = \sigma_0 \sin(\omega t + \delta) \qquad (8)$$

A perfectly linear elastic material would react instantaneously, and no phase shift is present in the response. A perfectly viscous material reacts with a phase shift of exactly 90 deg.

The response function can be expressed as a linear combination of sine and cosine as

$$\sigma = \varepsilon_0 \, G_1 \sin(\omega t) + \varepsilon_0 \, G_2 \cos(\omega t) \qquad (9)$$

where G_1, the expansion coefficient for the in-phase contribution, is known as the storage modulus, as it describes the energy that is stored as elastic energy, and G_2 describing the energy dissipated by viscous flow [50].

29

Figure 12 shows a typical result of a dynamic mechanical measurement that was done over a temperature range. Ramping up the temperature allows to study relaxation processes in a material which are, as mentioned above, thermally assisted. That means, as the temperature is going up more and more relaxation processes are energetically possible, and less energy is stored as elastic strain energy. The result is a decreasing storage modulus. Most polymers show, next to continuously distributed relaxation processes, characteristic secondary relaxations at distinct temperatures [49]. The primary relaxation is happening at the so-called glass transition temperature. At this temperature region a major drop in storage modulus can be observed as the polymer transitions from a glassy state into a rubbery state [49]. In the case of thermoplasts, the storage modulus will continue to decrease with increasing temperature as the material is approaching its melting region. For crosslinked polymers this is not the case. Crosslinked polymers establish a rubbery plateau at temperatures beyond the glass transition that can be attributed to the crosslinked network structure [51].

Note that different definitions for the glass transition temperature exist. One of the most widely used is defined as the temperature at the peak in the loss factor, or tangent delta. Where tangent delta calculates as

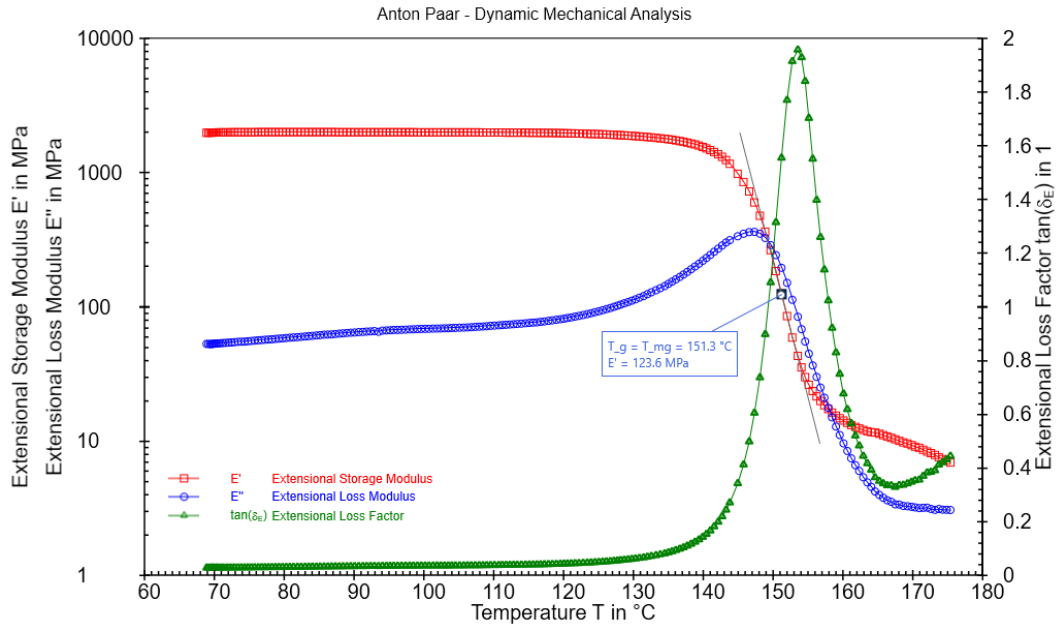$$\tan(\delta) = \frac{G_2}{G_1} \tag{10}$$

[50].

Figure 12: Dynamic mechanical analysis measurement of an amorphous thermoplastic material. Taken from [52].

1.4 Toughening of polymers

The material property of fracture toughness is linked to the ability of a material to resist stress intensities without fracture [53]. Fracture occurs when a stress intensity results in a super-critical crack.

In the framework of linear elastic fracture mechanics, the crack criticality can be assessed using the Griffith criterion [54]. For the simplest case of an infinitely large plane and homogenous stress field it has the form

$$\sigma_f = \frac{K_{IC}}{\sqrt{\pi c}} \tag{11}$$

which says that a crack or flaw propagates if the stress exceeds σ_f. K_{IC} is the critical stress intensity factor for mode 1 crack loading and is a material parameter. The higher this value, the higher is the fracture toughness of a material. c is the size of the crack. It follows that the stress required for fracture is high when the flaw size is low or the value of K_{IC} is high.

31

The stress intensity factor has the following relation with the remote stress

$$K_I = \sigma_\infty \sqrt{\pi c} \qquad (12)$$

According to theory, a sample fractures when K_I becomes super-critical.
With K_I the normal stress along the x axis of the crack can be described as

$$\sigma_{yy} = \frac{K_I}{\sqrt{2\pi x}}, \qquad x > 0 \qquad (13)$$

with x being the Cartesian coordinate along the horizontal crack [54], [55], [56].

The stress at the crack tip is much larger than the far field stress. In the theoretical case of a perfectly sharp crack tip the stress even goes to infinity, following from equation (13) [55]. This, of course, is not true for actual cracks in a real material, as high stresses lead to significant deformation and yielding, the crack tip is blunted and stress is relieved [57]. A material which dissipates strain energy therefore shows less brittle behavior because deformations in areas of high stresses keep the stress intensity sub-critical.

Considering a real material, in the majority of the cases there is not one single dominant flaw. There are multiple flaws statistically distributed in size and number. Fracture of a part can be avoided only if the stress at every single stress intensity is kept sub critical. In materials that are very easily deformed this happens without any modification and large strains can be reached without fracture. For other materials that show brittle behavior, local stress intensities stay localized, and fracture occurs before large volumes of the material start to significantly deform. High deformation volumes are found in materials with pronounced strain hardening. It can lead to higher fracture toughness because strains are more evenly distributed in such materials [42], [43], [44].

Phenomenologically, macroscopic toughness is the result of the sum of microscopic energy dissipating events. This includes mechanisms like shear band yielding and crazing that can happen in polymer materials and dissipate energy by plastic deformation [29]. Ideally, during deformation the stress values in every volume element increases above the yield stress in order to get the maximum deformation while staying below the fracture limit.

Over time, different mechanisms to toughen materials were identified. They can be categorized into mechanisms that act in front of the crack tip, and mechanisms that act behind the crack tip. They are called intrinsic or extrinsic respectively [58]. Extrinsic toughening mechanisms aim at avoiding the crack opening displacement. It is widely used in polymers and known, for example, as fiber reinforcement [59], [60]. Fibers inside a material bridge two areas that are separated by a crack and take load off the crack tip. For practical reasons, adding fibers to a resin is not always possible. Especially in the field of 3D printing, manufacturing of fiber reinforced polymers is challenging. However, there exist methods to 3D print fiber polymer composites [61], [62]. Furthermore, intrinsic mechanisms fail in most brittle materials because they lack the potential for stress relaxing strains. Tightly crosslinked polymers for example will not relax stresses because molecular movements are restricted by covalent bonds. Hence, they are not toughenable by plastic deformation [63], [64].

Intrinsic toughening mechanisms make use of the intrinsic ability of the material to deform under stress [58]. However, materials that are very tough by nature cannot be modified to increase the intrinsic toughness. Naturally tough materials already make use of stress relieving mechanisms and every attempt to add some sort of toughening filler will most likely result in lower toughness, because the filler particles act as flaws inside the material.

A filler material that is frequently used for toughening are elastomer particles or compliant particles in general. They are known to work in a number of different polymer materials and different mechanisms are being discussed in literature. The most accepted mechanism however involves shear deformation of the matrix [64]. Others are cavitation and debonding of particles [65] or increased crazing of the polymer matrix [66]. All these mechanisms require some critical stress to be exceeded in order to happen. The stress field around a rubber particle can provide such stress intensities at which relaxations take place and the material is toughened [67], [68]. However, significant toughening can only happen if these deliberately added stress intensities are homogenously distributed throughout the material. Otherwise, the strains in the vicinity of the particles stay localized, and the particles act as flaws. To induce stable toughening mechanisms, the stress fields induced by the particles have to be just right for a specific material. This of course is depending on the material properties itself, which are generally unknown when dealing with a new material. That means predicting the amount of toughenability is difficult. It depends on the micromechanical behavior of the dissipation mechanisms of the material in question.

Considering the infinitely large number of possible material combinations, a one-for-all formula or simulation that predicts toughening does not seem possible. Numerical computations offer a possibility to improve phenomenological insights. But, the complexity of the response of polymer materials, when it comes to visco-elasto-plastic behavior or different damage mechanisms, makes that a difficult task [69].

The quickest way to assess a material for toughenability is still the experimental route. In the case of photopolymers, it can be done by simply adding so called core shell rubber particles to the resin and deagglomerate them well. Core shell rubber particles are commercially available in large quantities. They consist of an elastic core and a rigid shell and are synthesized by seed emulsion polymerization for the purpose of toughening resins [70]. Figure 13 shows electron microscopy images of core shell rubber particles. The seed emulsion polymerization leads to well-shaped spherical particles with a narrow size distribution [70]. Depending on the polymerization parameters the diameter can be adjusted and particle diameters starting from 125 nm were reported [70].
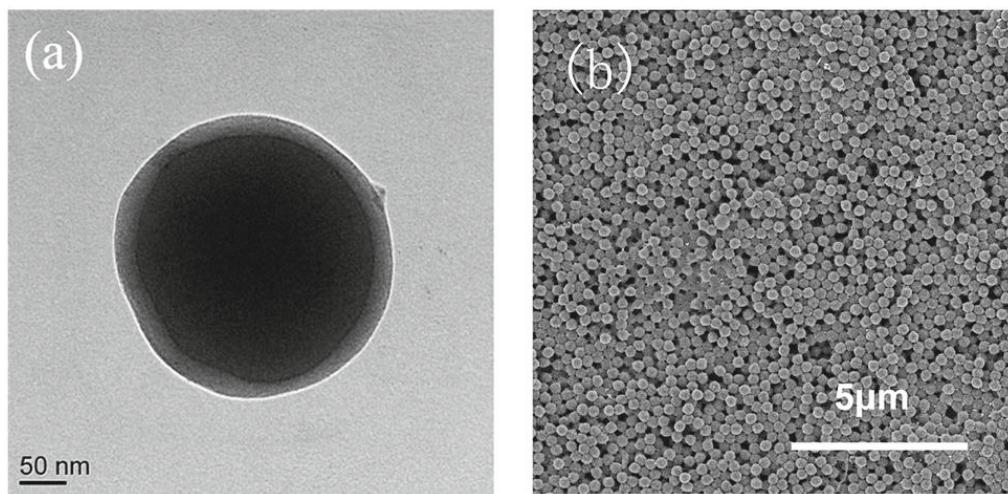
Figure 13: (a) TEM image of a single core shell rubber particle; (b) SEM image of core shell rubber particles. Taken from [70].

1.5 Modeling of photopolymer resins

The formation of a polymer by means of photochemical initiation is a complex process. Different physical and chemical phenomena happen at the same time and the individual processed cannot always be treated as independent from each other. Usually, the suitability of a photopolymer formulation for a given application is determined experimentally and often subsequent iterations in order to receive an optimal resin are required. Development of experimental resins and introducing novel components with unknown properties takes a lot of time and material quantities. It is therefore of interest to find a method that provides relevant information in an early stage of the development process to avoid using lab-resources unnecessarily. Useful information includes information on the reactivity of a given resin formulation and prediction of mechanical properties.

An efficient, universal modeling pipeline would take only the molecular structure of the ingredients and the composition of the resin of interest as input parameters. From that, one could then automatize the screening of several resin formulation and make informed decisions for subsequent experimental studies.

For a successful modeling approach two steps are crucial. First, the modeling on a molecular level must be reasonable. This is controlled by using a force field that can accurately describe the interactions on an atomistic level and model the properties of interest. The second important step is to model the polymer network itself. It was mentioned earlier that the properties are strongly depending on the constitution and especially the crosslink density of a polymer network. Therefore, it is important to get a realistic network structure for further modeling steps.

Molecular modeling has long been used in polymer physics. Molecular modeling has provided insight into the energy barriers present in polymer materials [49], [71].

1.5.1 Molecular dynamics

Molecular dynamics is a method to numerically determine the movements of molecules. The molecules are modeled using particles that interact with each other in a way that is defined by the so-called force field. The force field defines a potential energy function which takes the relative particle positions as arguments. This allows the calculation of forces on each particle. When all the forces are known, Newtonian mechanics is applied to calculate the trajectories of

all the particles in the simulation system. The numerical integration is usually done using the velocity verlet algorithm [72], [73].

Multiple open-source codes are available that have implemented numerical integration algorithms and take force field parameters as input. Among the most widely used code projects are Lammps [74] and Gromacs [75].

The key for a precise simulation is the force field. Force fields use a certain type of potential function for inter particle interactions. A common choice is the Lennard-Jones potential, also called 12-6 potential:

$$E = 4\varepsilon \left[\left(\frac{\sigma}{r} \right)^{12} - \left(\frac{\sigma}{r} \right)^{6} \right] \quad r < r_c \tag{14}$$

as implemented in Lammps [76]. In the above formula r is the distance between two particles, ε is the energy depth and σ is the distance where the function crosses zero. The shape of this potential energy function is given for different values of ε in Figure 14. Increasing ε leads to stronger pair wise interactions between particles. At low distances, the potential energy increases rapidly and models highly repulsive interactions between particles. At a certain value of r the function has a minimum. This minimum marks the equilibrium distance between particles. At high distances, the function asymptotically approaches zero. The total potential energy is the sum over all interactions in a system. When using periodic boundary conditions this sum has infinitely many terms. One way to circumvent this is to use a cutoff radius. This means that pair-wise interactions are only taken into account for pairs with distances up to the cutoff radius. The larger the cutoff, the more pairwise interactions need to be calculated which has negative influence on the computation time. A low cutoff gives larger errors because long range interactions are neglected. Deciding a cutoff distance is therefore a tradeoff between computational performance and precision.
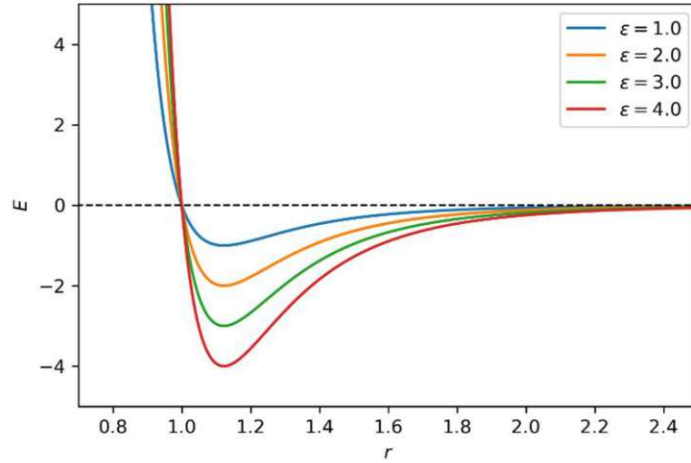
Figure 14: Lennard Jones potential plotted for different values of ε.

Chemical bonds between particles are often modeled using harmonic bonds. The mathematical expression as implemented in Lammps is given in Equation (15) [77].

$$E = K(r - r_0)^2 \qquad (15)$$

The shape of this kind of function for different values of the coefficient K is given in Figure 15. The function is symmetric around r_0 and is rising quadratically in both directions of r.

For modeling molecular systems not only bond lengths are needed, also the shape of molecules is important. The shape can be influenced by three particle and four particle angular potential which often are of harmonic type [78]. With these angular terms, bond angles can be modeled. It is also possible to represent torsion angles called dihedral angles, and improper dihedral angles which are used to control the planarity of molecules (see Figure 16).
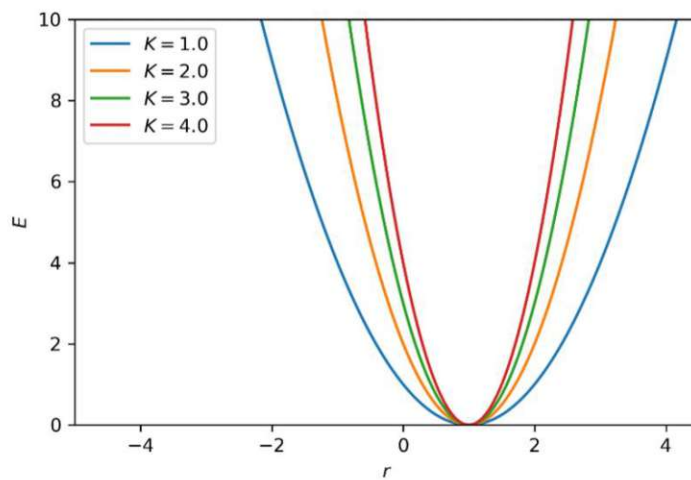
Figure 15: Harmonic potential plotted for different values of K.
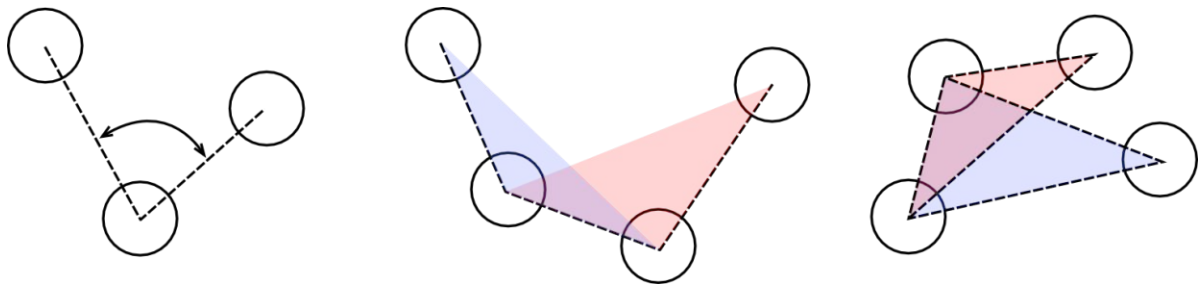
Figure 16: Angle definitions used in molecular dynamics. Left: simple three body angle; Middle: The proper dihedral angle is defined as the angle between the red and blue plane; Right: The improper dihedral angle is defined as the angle between the red and blue plane.

There are two major approaches to modeling molecules. One is to model every single atom that is part of the system of interest. This quickly leads to a high number of particles to consider and many interactions to evaluate. So called coarse grain force fields aim to model systems using fewer individual particles but still achieving reasonable accuracy. This makes the simulation of larger systems computationally feasible, even on machines with limited computational power. The so-called Martini force field aims at providing easy to use coarse grain parameters and guidelines about which chemical groups to model in a single coarse grain bead. It was initially developed to model biomolecular systems, but is also used for polymer simulations [79]–[81].

1.5.2 Simulated polymerization

Modeling a polymer by molecular dynamics can be done by initializing the simulation using pre-defined polymer network structures. This requires to intuitively guess a network topology which gives room for human induced errors. An inaccurately initialized simulation could potentially alter the simulation results and must be avoided. Also, by guessing the network structure it is not possible to gain information on the polymerization process itself, which is quite important for photopolymer materials. These two aspects justify the use of a simulated polymerization approach that allows to automatically prepare polymer network structures and at the same time get information on the reaction kinetics. In the framework of classical molecular dynamics, the bond formation process, which is clearly in the realm of quantum mechanics, cannot be modeled in all its details. But an intuitively reasonable simplification can be made by using a cut off criterion. In molecular dynamics, the positions of all particles are known in principle. It is therefore not difficult to evaluate distances between distinct particles. A reasonable assumption for modeling a polymerization reaction is to allow chemical bonding only if the reaction partners are within a certain distance to each other (see Figure 17).

$$V = 4\varepsilon \left[\left(\frac{\sigma}{r} \right)^{12} - \left(\frac{\sigma}{r} \right)^{6} \right]$$

$$\text{If } r < r_{cutoff}$$

$$V = K(r - r_0)^2$$
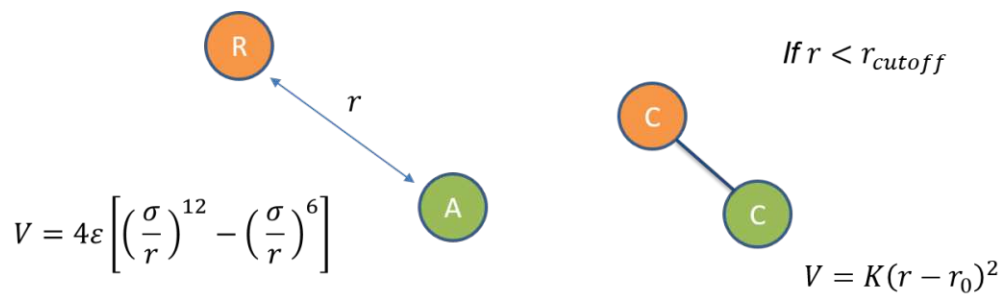
Figure 17: A harmonic bond is established when the distance between particle R and particle A falls below the cutoff distance.

After the formation of a bond all bonded interactions need to be updated, in order to comply to the rules of the chosen force field. This task takes some effort in handling the dynamically changing list of interactions and makes the use of some sort of code necessary. One example of a code that was developed specifically to perform polymerization simulation employing a cutoff criterion is Polymatic [82]. This program is built around Lammps as a simulation engine. Polymatic handles the input files for Lammps that define the bonded interactions and particle types and hands them to Lammps for energy minimization and molecular dynamics runs. The

39

core of the program is a loop that consecutively performs criteria checks, input files updates and starts Lammps for molecular dynamics runs. The loop is kept running until a certain termination criterion is fulfilled. The result is structure file for the polymerized monomers that took only minimal human inputs and still is computationally reasonably. Other information on the polymerization process can be extracted on the way and comes with no extra computational cost.

2 Methods

The following is a list of methods and materials used to obtain the results reported later in this work.

2.1 Computational details

All molecular dynamics simulations were done with Lammps [74]. Reaction simulations were done using Polymatic which basically wraps Lammps as a simulation engine and prepares input files to Lammps accordingly [82].

For initial system preparation the random packing routine *pack.pl*, which is part of the Polymatic package was used. A simulation box large enough to fit all molecules was defined and periodic boundaries were used at all boundaries. The largest molecules were packed first, followed by the remaining molecules in order of descending size. The packed simulation box was then relaxed and equilibrated.

The system for tensile experiment was prepared with 1000 molecules plus 10 molecules set as initiating molecules. The energy of the system was then minimized using *minimize 1.0e-5 1.0e-7 10000 100000* and equilibrated at 300 Kelvin with *fix 1 all npt temp 300 300 100 iso 1 1 1000* for 80000 timesteps with timesteps of 20 fs. Then Polymatic was used for the polymerization of the molecules. The parameters were set to *bonds_cycl = 4* which means a molecular dynamics run of 20000 timesteps with a timestep of 10 fs was started every 4th polymerization step and *md_max* was set to 50. The cutoff setting for bond formation was set to 4.5. For the tensile tests, the structures were taken after polymerization step 600, 700, 800 and 895. All tensile tests were preceded by equilibration at 300 Kelvin for 30000 timesteps with 1 fs. The deformation was done with the deform fix with *erate* set to 1e-7 and the *remap x* keyword was used over 3500000 timesteps. Breaking of the backbone bond was allowed using the *bond/break* fix every 10 timesteps and *Rmax* of 3.6 Angstrom. The pressure at the faces parallel to the deformation direction was kept constant at 1 atmosphere. For plotting the resulting stress in the direction of deformation the average over 1000 timesteps was calculated.

The systems for the kinetic studies were prepared with the same method as the system for the tensile test. System sizes were 1000 molecules in the case of pure methyl methacrylate, 800 molecules in the case of pure TEGDMA, 700 molecules in the case of pure PEGDM700. The mixture consisted of 100 PEGDMA700 molecules, 100 TEGDMA molecules and 1000 methyl methacrylate molecules. The number of initiating molecules was one mol% of reactive groups.

For the simulated DMA experiment the pure TEGDMA system was prepared with 400 TEGDMA molecules and 5 initiating molecules. The mixed system with propyl methacrylate was prepared with 50 mol% of both molecules and 5 initiating molecules. Minimization was done with *minimize 1e-4 1e-6 100 1000* and equilibration at 323 Kelvin for 450000 timesteps with a timestep of 1 fs. A *npt* barostat was active and set to 1 atmosphere and *Pdamp* set to 1000. Polymatic parameters were set as *bonds_cyc = 3* and *md_max = 20*. Molecular dynamics runs were 10000 timesteps long with the same barostat settings as above. Cutoff setting for bond creation was 12.4. A minor change in the file *polym.pl* was necessary to use Polymatic for all-atom radical chain growth polymerization of meth/-acrylates. The code block starting at line 241 must be modified as follows. The specific type numbers must match the definition of the atom types.

```perl
# Update atoms in bonds
    for (my $i=0; $i < scalar(@addBonds); $i++)
    {
        # Atoms in bond
        ($a1, $a2) = @{$addBonds[$i]};
        $sys{'atoms'}{'type'}[$sys{'atoms'}{'bonded'}[$a2][0]] = 12
            if ($sys{'atoms'}{'type'}[$sys{'atoms'}{'bonded'}[$a2][0]]==2);
        $sys{'atoms'}{'type'}[$sys{'atoms'}{'bonded'}[$a2][1]] = 12
            if ($sys{'atoms'}{'type'}[$sys{'atoms'}{'bonded'}[$a2][1]]==2);
        $sys{'atoms'}{'type'}[$sys{'atoms'}{'bonded'}[$a2][2]] = 12
            if ($sys{'atoms'}{'type'}[$sys{'atoms'}{'bonded'}[$a2][2]]==2);
        push(@{$sys{'atoms'}{'bonded'}[$a1]}, $a2);
        push(@{$sys{'atoms'}{'bonded'}[$a2]}, $a1);
    }
```

A single data point for the DMA experiment was created using the following method. First the simulation box was equilibrated at the desired temperature for 25000 fs. Then the box was strained in all three spatial directions with a sinusoidal displacement over 3 periods, each period took 10000 timesteps and the amplitude was 3 percent of the initial box size. The resulting stress was then averaged over 50 timesteps and all three strain directions. A linear combination

of sine and cosine was then fitted to the data points and the coefficients were interpreted as storage modulus and loss modulus respectively as in [83].

2.2 Materials characterization

2.2.1 Tensile test

The tensile tests were conducted either on a Zwick-Roell Z050 or on a Zwick-Roell Z250, at room temperature. The speed of the traverse was set to 5 mm min^{-1}. The tests were run until fracture occurred. The elongation was measured as the distance of travel of the traverse. For each series either five, six or seven specimens were tested. For the analysis of the results only four specimens with the highest elongation at break were taken into account. The results of the other specimens were discarded. The plots in the results section only show the result of the specimen with the highest elongation at break of each series. The mean value of the elongation at break is indicated by a cross on top of the plotted line. The specimen geometry was according to type 5B, ISO 527-2. The specimens were produced by either casting in a silicone mold, 3D printing and subsequent die-cutting, or direct 3D printing (see section 2.4).

2.2.2 Dynamic mechanical analysis

To probe the dynamic mechanical response a DMA 2980 from TA Instruments was used. A forced oscillation of 1 Hz at an amplitude of 10 μm was applied to the specimen in three point bending arrangement. The distance between the supports was 20 mm and the cross section was of rectangular shape. The width of the samples was 5 mm, and the height was 1 mm. The test procedure started with thermal equilibration at -50 °C for 5 min. Then the temperature was ramped up with a speed of 3° min^{-1}.

2.2.3 Stress relaxation

For stress relaxation measurements an RSA-G2 from TA instruments was used in three point bending mode. The sample geometry was of rectangular cross section with a height of 1 mm and a width of 5 mm. The distance between the bearings was 15 mm. The applied strain was kept constant at 2 % during the measurement. Samples were equilibrated at 37 °C for half an hour prior to the measurements. Temperature was maintained constant while the strain was applied. If the measurement was done in wet condition the sample was fully emersed in distilled water during equilibration and measurement.

2.3 Materials

All materials used in the experimental section of this thesis are listed below. They are grouped by their respective main purpose, like increasing the glass transition temperature (Tg modifier), increasing the fracture toughness (toughness modifier) or lowering the viscosity (reactive diluent). One type of photoinitiator was used. One type of core-shell rubber was used in combination with the resins. For the inkjet approaches, two different inks were used together with the inkjet system described in section 2.4.3.

2.3.1 Tg modifiers

The term Tg modifier (TGM) in this work refers to oligomers whose main purpose is to raise the glass transition temperature. As identified in previous works, efficient Tg modifiers are difunctional molecules with a relatively rigid backbone [84], [85]. Tg modifiers can also be referred to as crosslinkers as they are usually rather short comparted to toughness modifiers. In the following, the Tg modifiers used in this work are listed for reference.

Bomar XR-741MS

This is a commercially available urethane based difunctional methacrylate obtained from Dymax Oligomers & Coatings. Find TDS in [86].

LPU624

This compound was synthesized by Miwon Austria F&E, based on TGM1 as developed in [85]. It contains 15 wt% TEGDMA as a reactive diluent.

2.3.2 Toughness modifiers

In order to enhance the toughness of photopolymer networks through optimizing the molecular structure, so-called toughness modifiers (TNM) were developed previously. The molecular weight of these substances is considerably higher than the molecular weight of Tg modifiers. Hence, although difunctional, toughness modifiers are not contributing much to the crosslink density. They rather have the purpose of loosen the polymer network and allow for increased molecular mobility.

TNM2

The underlying oligomer was the second of four oligomers synthesized for the purpose of producing tough photopolymer networks in [85]. For the batch used in this work, TEGDMA was added at a content of 30 wt%. The material was provided by Align Technology.

LPU706NT

LPU706NT is a variation of TNM2, also with TEGDMA as a reactive diluent. The material was produced by Miwon Austria F&E.

2.3.3 Reactive diluents

Diluents modify the viscosity of resins that would otherwise be too viscous to be used for a certain application like additive manufacturing. To avoid leaching and degradation of the mechanical properties, reactive diluents are used as they are incorporated into the polymer network and become an integral part of the material. In the following the reactive diluents used in the experimental part of this work are listed.

HSMA

This monofunctional reactive diluent was developed in [13] for high-temperature application. It was supplied by Align Technology.
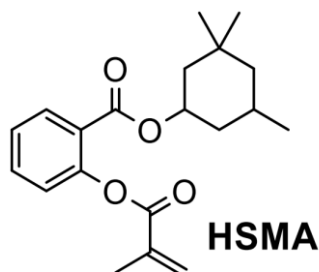
Figure 18: Chemical structure of HSMA. Taken from [13].

MSMA

Another monofunctional reactive diluent similar to HSMA developed in [13]. The material was produced by Evonik.
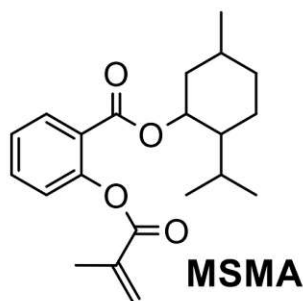
Figure 19: Chemical structure of MSMA. Taken from [13].

TEGDMA

This molecule is a difunctional methacrylate widely used in dental composites as a reactive diluent [87], [88]. It was purchased from Sigma-Aldrich.
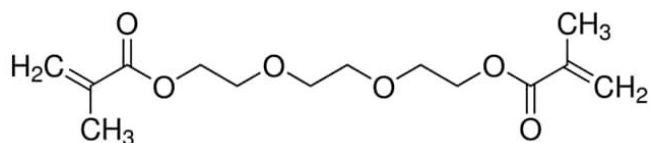
Figure 20: Chemical structure of TEGDMA. Taken from [89].

2.3.4   Photoinitiator

As Photoinitiator, SpeedCure TPO was used. It is a Norrish Type I photoinitiator and was purchased from Lambson. Find TDS at [90]. The purpose of this substance is to provide the initiating species in the resin upon exposure to light.

2.3.5   Core-Shell Particles

Core-shell particles were obtained from Evonik. The specific product used was Albidur EP XP Powder.

2.3.6   Inkjet inks

Two different inkjet inks were used in this work. They are listed below.

TangoPlus

This is a commercially available inkjet ink obtained from Stratasys. It is a ready-to-use inkjet ink and forms a rubber-like material. A small amount of fluorescent dye was added for subsequent analysis with laser scanning microscopy.

Cyanoethyl acrylate

This substance was mixed with a photoinitiator and a small amount of fluorescent dye and used as inkjet ink. The photoinitiator was chosen to allow for separate curing of ink and matrix material. Which means that curing of the ink is possible without curing the base material. This ink was supplied by Bettina Koch. It also forms a rubber-like polymer.

2.4   Sample preparation

Sample preparation included resin preparation which was done as described below for all samples. Shaping was done in one of three ways: either casting, additive manufacturing or additive manufacturing with subsequent die cutting. All preparation methods are described in detail below.

2.4.1   Resin preparation

For preparing the resin, all the ingredients were put into a cup. It was then mixed in a Hauschild Speedmixer until all the solid components were dissolved. In the case of a core-shell particles filled resin, the resin was mixed until no agglomeration was visible. In the case of high viscosity ingredients, the cup was heated in an oven at 90 °C until all components were within a reasonable viscosity range. Prior to use, the resin was degassed, either in a vacuum chamber or with the vacuum function of the Hauschild Speedmixer.

2.4.2   Casting

For preparing the specimens, a silicone mold was used. The liquid resin was poured into the mold and degassed in a vacuum chamber until no air bubbles were visible. If the resin viscosity was too high for degassing the filled mold was put into an oven at 90 °C to lower the viscosity. The filled mold was then put into an oven at the respective temperature for thermal equilibration. After equilibration, the mold was put into an Uvitron Intelliray 400 curing chamber for 300 seconds at full power. The specimens were then extracted from the mold and put in the curing chamber upside down for another 300 seconds at full power. After the curing process, the samples were ground using wet sandpaper. In order to obtain parallel surfaces at the desired height, a stainless-steel sample holder was used for grinding.

2.4.3 Additive manufacturing

For all experiments where 3D printing was required, a hybrid process developed in [91] was used. It was designed to combine DLP 3D printing (Figure 21) with direct inkjet printing. A representation of the process is shown in Figure 22 and Figure 23. The light engine used in this work was a Visitech Luxbeam 4600. This light source projects pixels with a size of 50 µm through a transparent material vat onto the photoreactive resin at a wavelength of 375 nm. The material vat was heated to a temperature of 70 °C. The inkjet printheads used were a Xaar 1003 GS40U, and a Xaar 1003 GS6U. These are printheads for industrial applications, capable of handling a variety of different inks. The ink was supplied via a circulating ink delivery system. To adjust the inkjet settings for good droplet quality a drop watcher, set up together with the inkjet system in [91], was used. A drop watcher is a special optical device for imaging inkjet droplets in-flight. It is based on synchronizing droplet ejection with camera exposure to get the impression of a still-standing drop. For the purpose of this work, however, the drop watcher was only used for initial setup of new inks. It turned out to be practical to validate the droplet quality by simply jetting onto a substrate and observe the droplets via microscope. In this way, also faulty droplet placements could be detected. Furthermore, in some cases, satellite drops were observed on the substrate that could not be visualized using the drop watcher. Cyanoethyl acrylate-based ink was jetted at room temperature. TangoPlus ink was jetted at 40 °C printhead temperature.

For curing the ink, after the jetting process a separate LED array was used. This secondary light source has its peak of the emitted intensity at 455 nm. By using light sources that emit at different wavelengths it is possible to cure the ink without initiating the polymerization of the resin material. For successfully curing the inks used in this work it was necessary to expose in a low oxygen environment. For convenient handling of the LED array a handheld exposure device was crafted from a plastic box which was equipped with a nitrogen inlet to ensure a steady flow of nitrogen during exposure (see Figure 24). All additively manufactured samples were post cured in an Uvitron Intelliray 400 curing chamber for 300 seconds at full power. The samples were then turned upside down and exposed for another 300 seconds.

(a)

1 Light Source (LED 465nm)
2 DMD Chip (dynamic mask)
3 Optics
4 Coating system
5 Tiltable vat
6 Building platform
7 Load cell
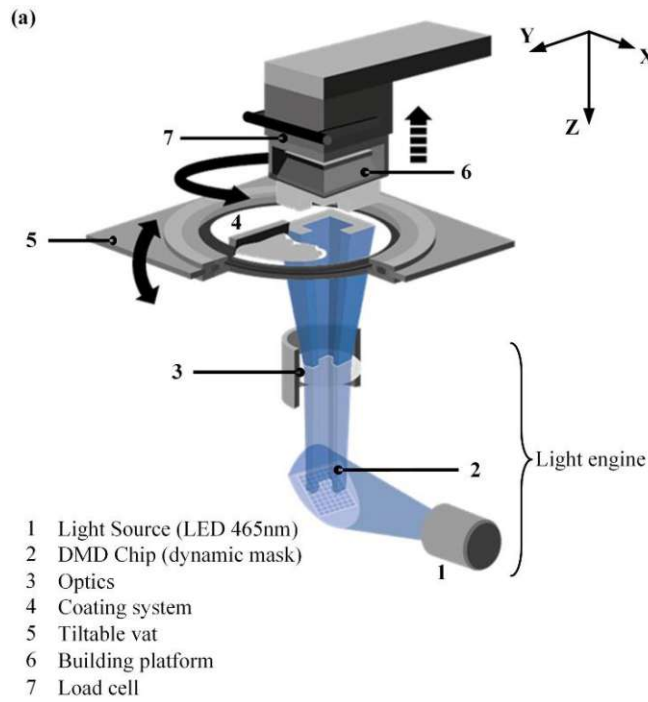
Figure 21: Schematic representation of the 3D printing process. Taken with permission from [92]. Copyright © 2020 Elsevier B.V.

60 °C

40 °C
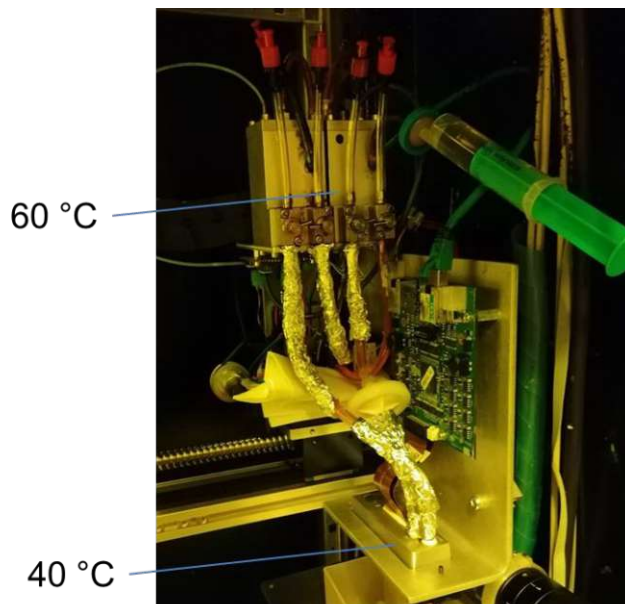
Figure 22: Image of the fluid delivery system. In the top is the ink inlet and outlet tank. In the bottom part is the inkjet printhead. The tubing was insulated with aluminum foil. Tank temperature was set to 60 °C. Temperature measured at the printhead was 40 °C.
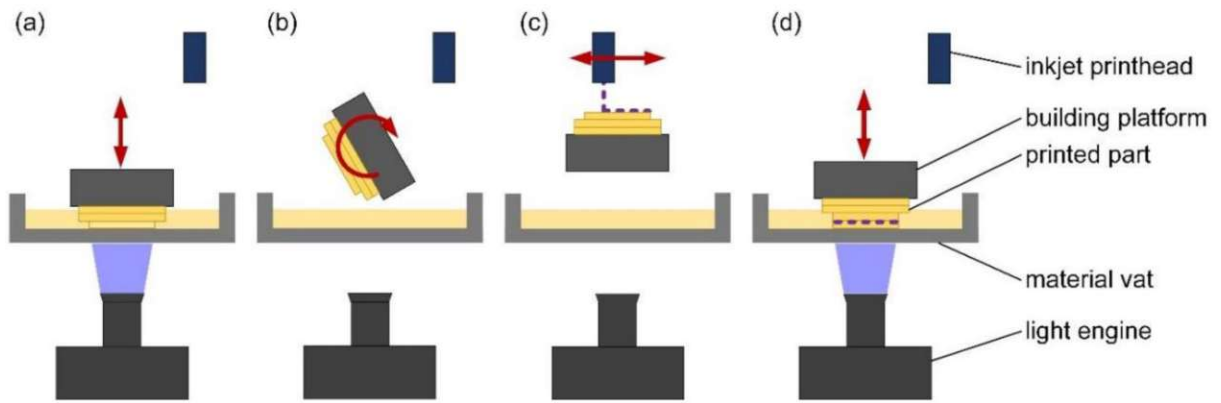
Figure 23: Schematic representation of the hybrid printing process. (a) DLP layer is cured. (b) Building platform is rotated. (c) The DLP-layer functions as substrate for inkjet printing. (d) After rotating the building platform back in its initial position, the next DLP-layer is cured. Taken from [93].
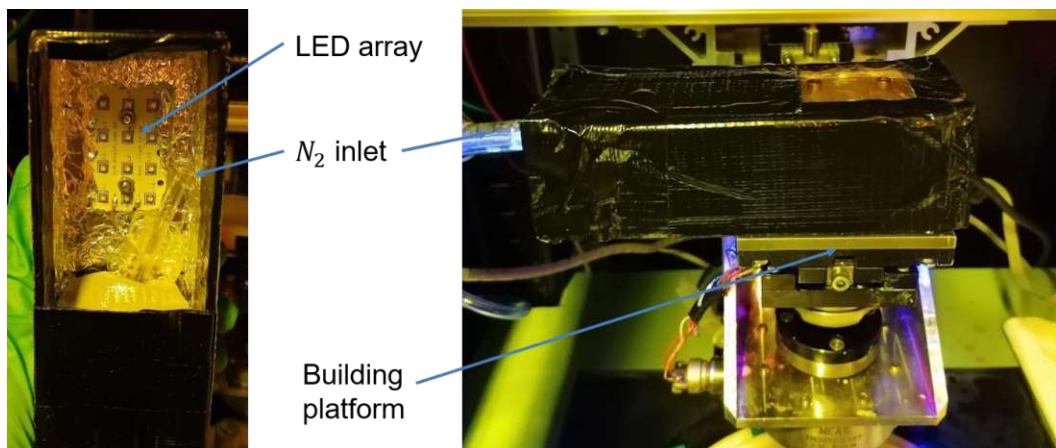
Figure 24: The handheld exposure device used to cure the ink after jetting onto the substrate.

2.4.4 Die cutting

Some samples were printed in a rectangular shape to avoid edge defects arising from inkjet alignment inaccuracy. To obtain tensile specimens a die cutter was used. The cutting edge and the rectangular samples were heated prior to the cutting process to obtain better sample quality. A heating plate at 200 °C was used as a heat source. To apply the force that is required to punch the samples a Zwick Z250 was used in compression mode. For some samples, the cut faces were finished using sandpaper to obtain a smoother surface. Die cut samples are presented in

Figure 25. The method used for each of the samples is stated together with the plot where the respective results are presented.
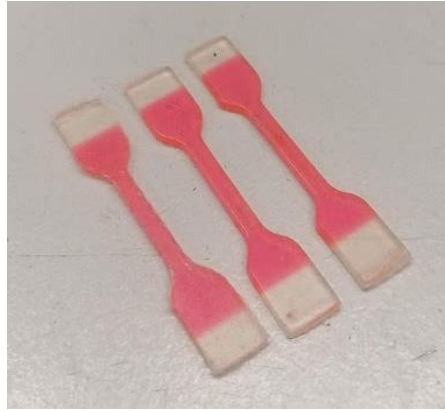
Figure 25: Samples after die cutting.

Note that cut samples are not as smooth as molded samples. Therefore, toughness is decreased for cut samples. Comparing samples prepared with different methods is avoided and is mentioned in the text when necessary.

3 Toughening approaches

3.1 Resin composition

One way of producing a tough polymer is by adjusting the ratios of the constituents. Usually, small multifunctional molecules form brittle networks [21], while molecules with a high molecular weight tend to form polymers with low modulus and high elongation at break. By simply mixing the two substances it is often possible to get an acceptable trade-off. Challenging in this respect can be that by changing from a highly crosslinked network to a coarser network, strength is decreasing. For delicate structural applications, this can be a problem. Therefore, it is of interest to try to understand what influences the material behavior to get the best polymer possible from a given set of constituents.

In the following chapters, a series of measurements are presented to show different materials properties that can be achieved by changing the composition of the resin. As for oligomers, TGM1 and TNM2 (see section 2.3), were used. As reactive diluents, the molecules were chosen to be either monofunctional or difunctional, according to what was to investigate.
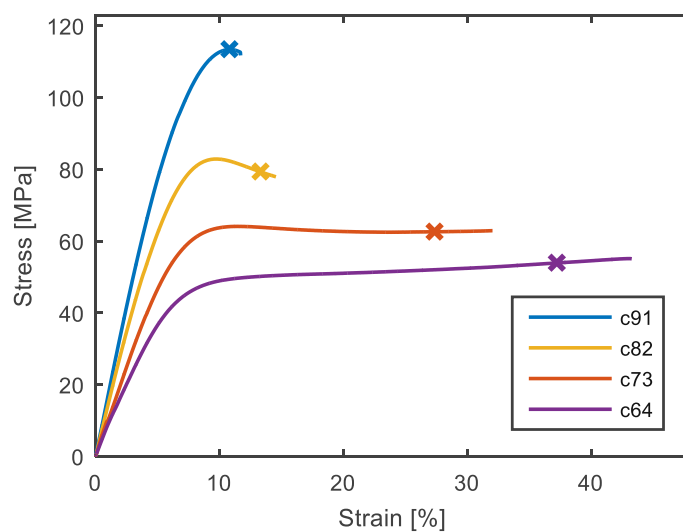
Figure 26: Tensile test of different ratios of TGM1 and TNM2. All samples contain 10 phr MSMA.

Table 2: Resin composition for Figure 26. TPO and MSMA in wt%, resin components in PHR.

	LPU624	TNM2	MSMA	TPO
c91	90	10	10	1
c82	80	20	10	1
c73	70	30	10	1
c64	60	40	10	1

Figure 26 shows the results of the tensile test of materials with different ratios of TGM1 and TNM2. Sample c91 with the highest share of TGM1 has the highest strength and the lowest elongation at break. Whereas sample c64 has the lowest strength and the highest elongation at break. This comes from the lower crosslink density while simultaneously increasing the share of high molecular weight components. Less crosslinks lead to a reduced yield stress in this case and the molecular chains can move relatively easy with respect to each other, therefore reducing the risk of premature fracture. In the case of the highly crosslinked compound, the crosslinks restrain molecular movement and therefore stress intensities cannot be dissipated. Figure 26 shows that varying the share of the constituents is a proper way to adjust the materials properties.

While the elongation at break was increased by approximately 400 %, the number of multifunctional molecules in these samples is still relatively high. To further reduce the crosslink density, multifunctional components can be substituted with monofunctional molecules. This will be discussed in section 3.1.1.

3.1.1 Reduced crosslink density

To investigate the material properties of photopolymers with low crosslink density, TGM1 and TNM2 were synthesized by Bettina Koch using HSMA as a reactive diluent. With this product it was possible to produce samples containing TGM1 and TNM2 as the only difunctional ingredients. Additionally, a high amount of monofunctional reactive diluent was chosen to decrease the crosslink density further. The results of the tensile tests are presented in Figure 27.
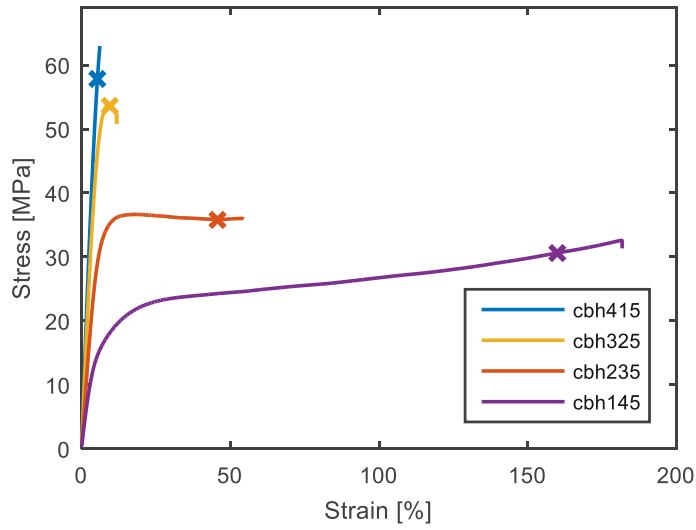
Figure 27: Tensile test of different ratios of TGM1 and TNM2 with a high share of monofunctional reactive diluent.

Table 3: Resin composition for Figure 27. TPO in wt%, resin components in PHR. TGM1B and TNM2B were synthesized in HSMA.

	TGM1B	TNM2B	HSMA	TPO
cbh415	40	10	50	1
cbh325	30	20	50	1
cbh235	20	30	50	1
cbh145	10	40	50	1

It can be seen that the elongation at break varies strongly among the different samples. While for the case with higher crosslink density a factor of four was observed, here a 30-fold increase of elongation at break was measured comparing the samples containing 10 wt% TNM2 and 40 wt% TNM2. It is interesting to note that the elongation at break of cbh415 is lower than for c91 though the ratio of difunctional components is higher in c91. Whereas in the case of 40 wt% TNM2 the elongation at break is higher in the sample with a higher share of monofunctional reactive diluent. This is illustrated in Figure 28.

a)   b)
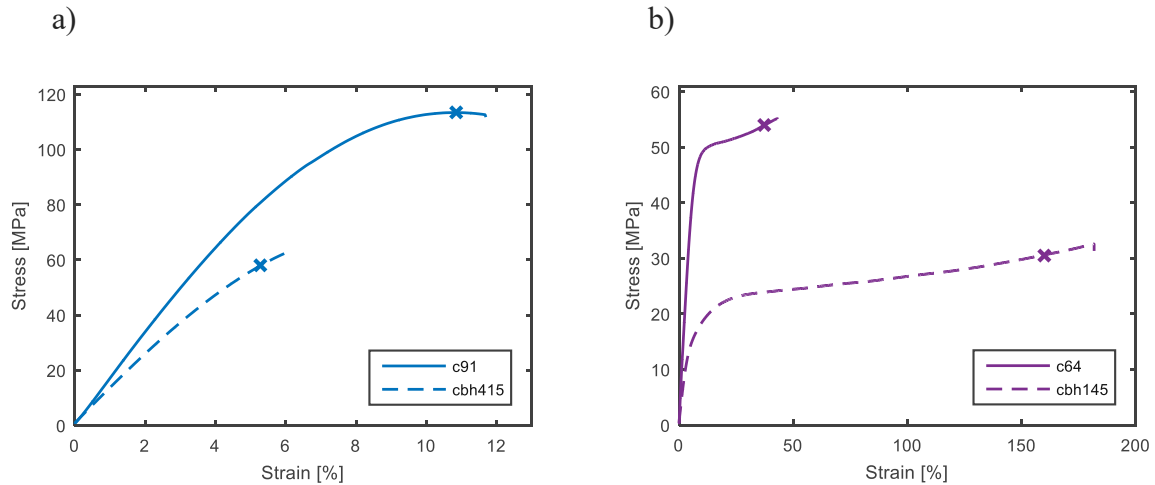
Figure 28: Tensile test results for samples with different crosslinker content.

In the case of few TNM2 the modulus is lower, as expected, for the material with lower crosslink density, but the elongation at break is also lower. That is probably the result of the relatively brittle HSMA[4] (though the crosslink density of poly-HSMA is assumed to be zero) that makes up a large fraction of cbh415. This means that a low crosslink density alone is not the path to a tougher material.

In the case of cbh145, however, the high HSMA content does not seem to harm the toughness of the samples. The HSMA is diluted by large amount of TNM and therefore the brittle nature of HSMA is not present anymore. Another possible explanation for this behavior will be discussed in section 3.2.

3.1.2 Varying crosslinker content

In the section above, it was shown that the material properties are not defined by a single ingredient, they are rather a result of the interplay between all the constituents of a resin. To further investigate the influence of the crosslink density the amount of TEGDMA was varied in different resin formulations.

In Figure 29 the results of the tensile tests for materials with very low crosslink density is presented. In formulation v37 the crosslinks come from the TEGDMA which is present in

---

[4] The haptic perception of photocured poly-HSMA is brittle.

TNM2. For formulation v352 a significant amount of HSMA is substituted by additional TEGDMA which results in a higher number of crosslinks.
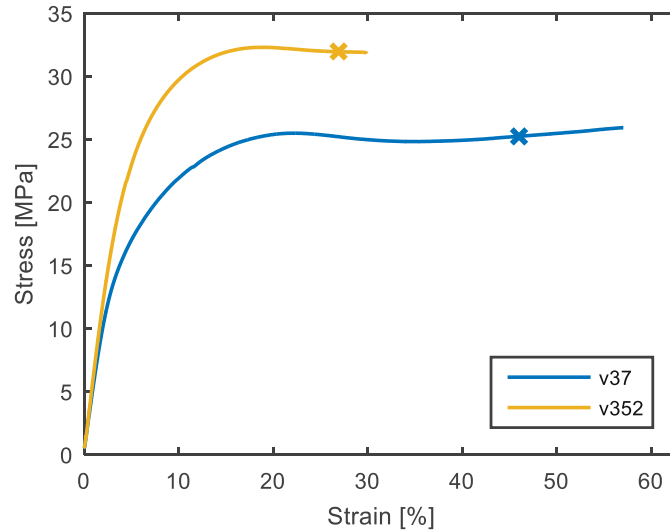
Figure 29:Tensile test results of materials with different amount of crosslinker.

Table 4: Resin composition for Figure 29. TPO in wt%, resin components in PHR.

	TNM2	HSMA	TEGDMA	TPO
v37	30	70		1
v352	30	50	20	1

The effect of the crosslinks is clearly visible in Figure 29. More crosslinks lead to higher strength and lower elongation at break in this case, which is the expected behavior.

Figure 30 shows the results of the tensile tests of different materials where the ratio between LPU and TNM2 was kept constant at 50:50. The material chs20 and the material chs30 contain 20 % HSMA and 30 % HSMA respectively, related to the weight of LPU624 and TNM2. For the samples cteg20 and cteg30 the HSMA was substituted by the difunctional TEGDMA to increase the number of crosslinks.
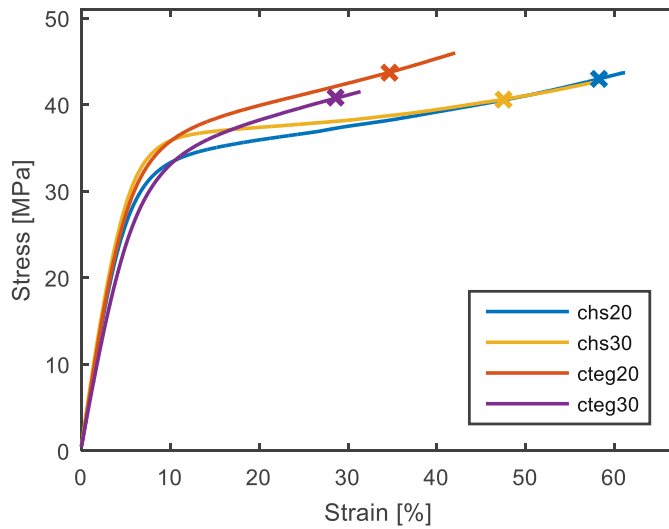
Figure 30:Tensile test results of samples with varying crosslinker content.

Table 5: Resin composition for Figure 30. TPO in wt%, resin components in PHR.

	LPU624	TNM2	HSMA	TEGDMA	TPO
chs20	41.7	41.7	16.6		1
chs30	38.5	38.5	23		1
cteg20	41.7	41.7		16.6	1
cteg30	38.5	38.5		23	1

It can be seen from Figure 30 that the additional crosslinks don't have significant influence on the modulus at low strains. Whereas, the influence is quite pronounced at higher strains, where plasticity is present in the material response. The additional TEGDMA leads to a steeper slope compared to the samples containing HSMA, and the elongation at break is reduced. This behavior is probably a result of reduced mobility within the network when the number of crosslinks is increased. It should be noted that more TEGDMA does not increase the slope further, and more HSMA does not increase the elongation at break.

3.1.3 The role of the toughness modifier

We have seen by now that the tensile properties of a resin system can vary substantially when changing the composition. Highly crosslinked materials show, as expected, low elongation at break, because of the restricted molecular mobility [21]. Low crosslink density materials, however, like HSMA, also tend to show low elongation at break, unless they contain a fair amount of toughness modifier. That means the toughness modifier plays a crucial role in toughening a material. The results presented above have also shown that the effectiveness of the toughness modifier is strongly depending on the distinct material formulation.

The unwanted side effect of the toughness modifier is lower strength, as well as lower modulus. Therefore, it is of interest to use as little TNM as possible, or in other words, maximize the efficacy of the toughness modifier.

To get more information on the toughness modifier, samples were molded using reactive TNM and a non-reactive version of TNM with the same molecular weight[5]. The results of the tensile tests are presented in Figure 31.
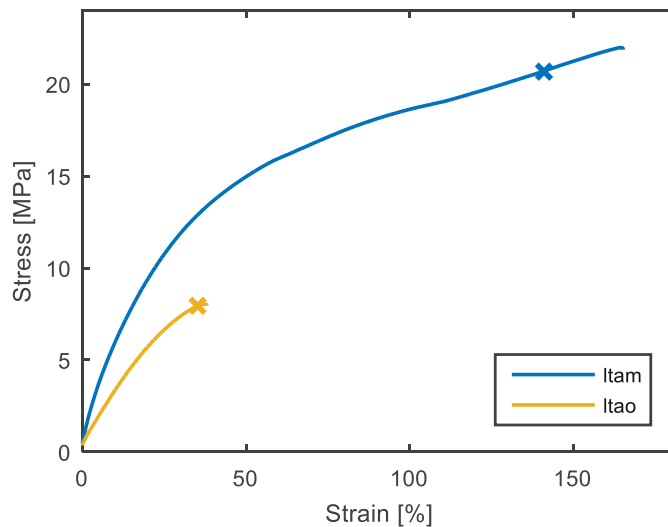
Figure 31: Tensile test results of materials with reactive toughness modifier (ltam) and unreactive toughness modifier (ltao).

---

[5] Both synthesized by Bettina Koch [94].

Table 6: Resin composition for Figure 31. TPO in wt%, resin components in PHR.

	LPU624	TNM	TEGDMA	TPO
ltam	43	40	17	1
ltao	43	40	17	1

The results show that only the TNM-version that reacts with the matrix is effective. Interestingly, the reactive TNM also results in a higher tensile modulus compared to the non-reactive version. It follows that the toughness modifier must be an integral part of the polymer network. It does not simply increase the molecular mobility – like a plasticizer does in a thermoplast – it redistributes, and therefore diminishes, local stress intensities by bridging different domains of a material. It potentially also engages in processes that dissipate energy, like crack bridging and crazing. Crucial for these processes to be significant is the ability of the matrix to allow these kinds of mechanisms. It is clear that if the matrix cracks before yielding, toughening cannot be observed.

It is interesting to note that first, the toughness modifier is efficient when it is well incorporated into the matrix, and second, when the matrix has a certain degree of intrinsic mobility. But point one and two are inversely correlated. As the polymerization proceeds, plasticity is decreased. At the same time, the chances of the toughness modifier to be crosslinked to the polymer network increases with growing degree of polymerization. By considering the fact that molecules with a higher number of functional groups are more likely to be engaged in a polymerization reaction, a possible approach to make the toughness modifier more efficient becomes apparent. That is to increase the functionality of the molecule. This would mean that even if not all of the reactive groups are converted, there is a higher chance that the toughness modifier is anchored in the polymer network, compared to a difunctional toughness modifier.

3.2 Phase separation

It was observed in formulation v37 that the material shows pronounced turbidity after the polymerization process. Therefore, significant light scattering occurs after curing. As source of this scattering, polymerization induced phase separation was identified [95]. Consequently, the produced material consists of separated phases which have differing optical properties and presumably differing mechanical properties. It is known that many structural materials can benefit from a non-homogeneous microstructure. Therefore, it is of interest to study the mechanical properties of phase separated photopolymers.

It is assumed in the following that the material is homogeneous in the resin state. This means that, to form separate phases, a certain degree of diffusion of the constituents is required. Varying the diffusivity by changing the temperature is therefore a way to influence the formation of separated phases. It is demonstrated in Figure 32 that the visible light scattering can be altered by changing the temperature at which the material is cured. The top of Figure 32 shows formulation v37 when cured at an initial temperature of 90 °C. The resin was put into the mold and equilibrated in an oven at 90°C. It was then cured at this elevated temperature. The bottom of Figure 32 shows the same formulation equilibrated at room temperature and cured in the UV chamber.
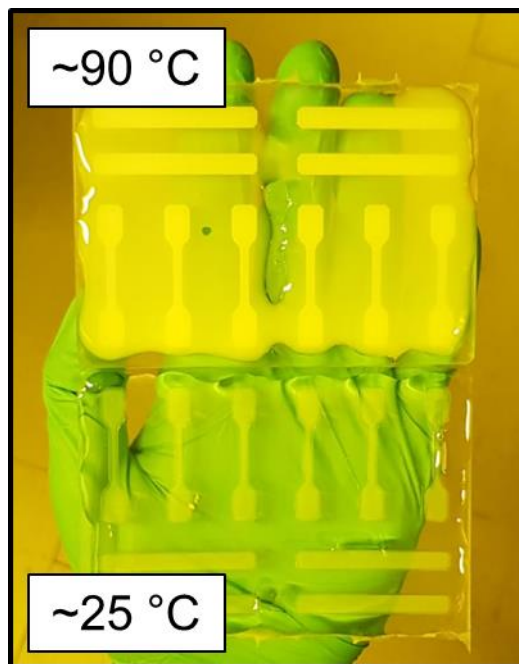
Figure 32: Demonstration of the visible phase separation.

It is clearly visible that the curing temperature plays a major role in the formation of visible phase separation. The material appears white when cured at elevated temperature, which is a sign for diffuse light scattering. In the case of low temperature, the cured material appears to be semi-transparent. The level of visible light scattering is reduce compared to the material cured at high temperature.

To assess the mechanical properties, tensile tests were performed on samples made from formulation v37 cured at different temperatures. The results are plotted in Figure 33.
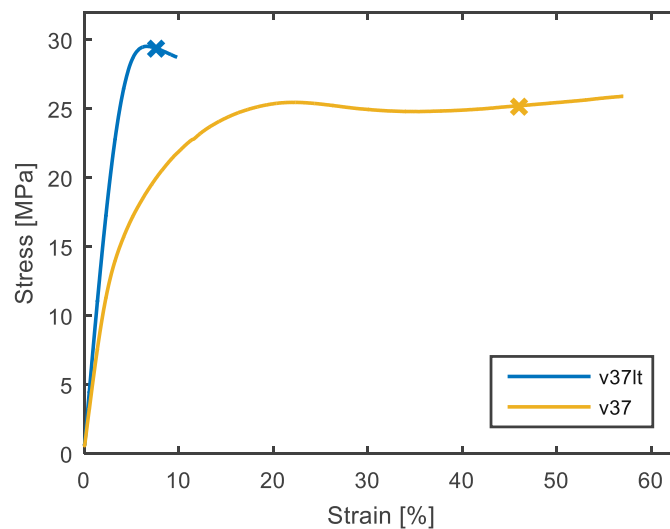
Figure 33: Tensile test results for samples cured at low temperature (v37lt) compared to samples cured at elevated temperatures (v37)

For sample v37lt a special curing method was chosen. After filling the mold, it was put inside a fridge to cool the material in order to suppress phase separation. To reduce the influence of the reaction enthalpy, the material was not cured under continuous radiation, but a UV flash source was used. The resin was exposed to 10 flashes and then put back into the fridge for one minute. This was repeated 10 times. After this the material was put into the continuous UV chamber for the same post processing procedure as sample v37. This was done to ensure similar initiator conversion in both samples.

It can be seen in Figure 33 that the tensile properties differ drastically. The samples cured from a precooled resin show less elongation at break but have higher tensile modulus. Under the assumption of higher double bond conversion of the material cured at higher temperature, the higher elongation at break can be explained by a better incorporation of the toughness

modifier (see Section 3.1.3). We have also seen in Section 3.1.3 that well reacted toughness modifier increases the strength of a material which is in apparent contradiction to what is shown in Figure 33. An explanation to resolve this contradiction is given below where the morphology of the phase separation is discussed.

For a clearer view on the influence of the curing temperature, more samples were produced at different temperatures. The sample curing procedure for samples v37t25, v37t43, v37t65 was as follows. The resin was put into the mold at 90 °C. It was the then degassed to avoid air bubbles. Then the mold was cooled at room temperature while the surface temperature was monitored with an infrared thermometer. It was then put inside the UV chamber at 25 °C, 43°C and 65 °C respectively. The results of the tensile tests are shown in Figure 34 together with the results from Figure 33.
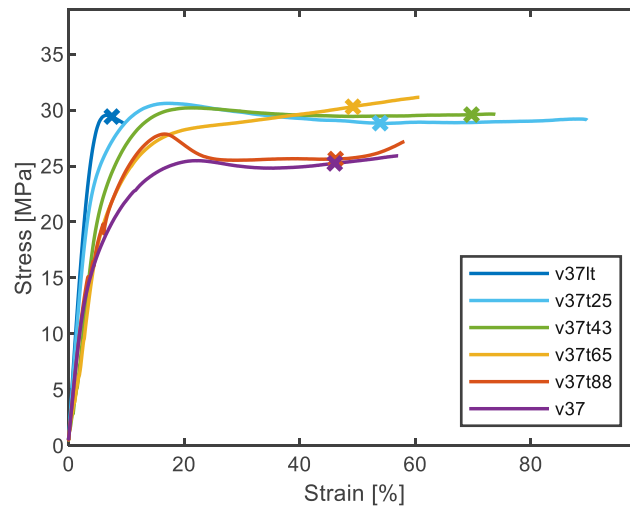
Figure 34: Tensile test results of samples cured at different temperatures.

It can be seen in Figure 34, when comparing the precooled sample v37lt with the sample v37t25, an increase in elongation at break is observed. When the temperature is increased further, the elongation at break is not increased further, but the slope of the curve is changed. In the plastic domain the curve of v37t65 is steeper compared to v37t25 and v37t43. A possible explanation can be found when comparing these results to what was discussed in section 3.1.2, where increasing crosslink density was identified to be responsible for a steeper slope in the plastic domain. It can be concluded that the increased temperature leads to an increase in reactivity. Consequently, the crosslink density is increased.

Sample v37t88 is again flatter. There is also a pronounced yield point visible. This can be attributed to phase separation being the dominant factor for the tensile properties.

To verify the change in modulus, DMA measurements were performed on these materials. The DMA values represent the same trend as the tensile tests indicated, as can be seen in Figure 35.
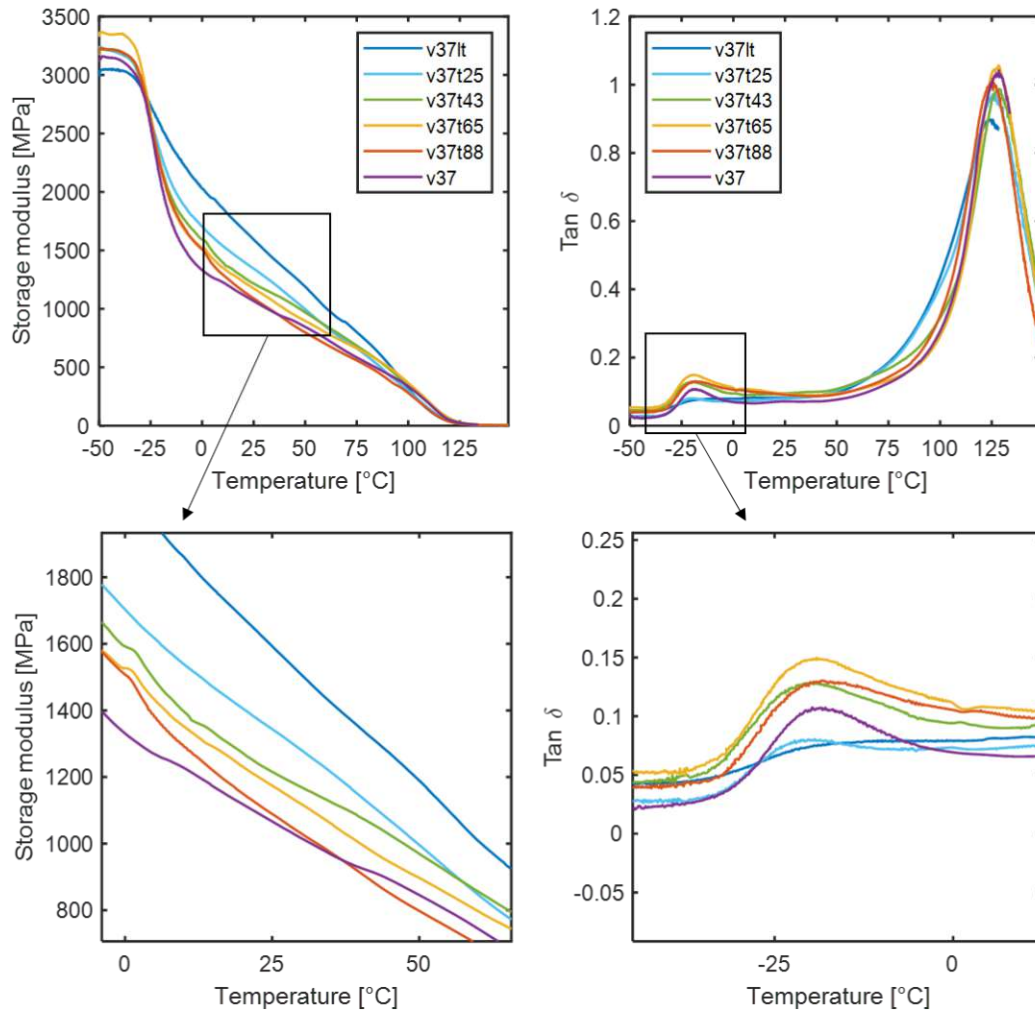
Figure 35: DMA results for samples cured at different temperatures.

The DMA curves also reveal a secondary tangent delta peak at around -20 °C. This peak is more pronounced in the samples that were cured at higher temperatures where phase separation is expected to be more pronounced. A link between secondary tangent delta peak formation and phase separation was reported previously [96], [95].

Another interesting finding, highlighting the importance of the morphology of the microstructure, was revealed by stress relaxation measurements (see Figure 36). The initial

64

stress values again confirm the modulus dependence on the curing temperature. However, evaluating the remaining stress normalized by the initial stress, a sweet spot seems to be at a curing temperature of around 65 °C (see Figure 37).
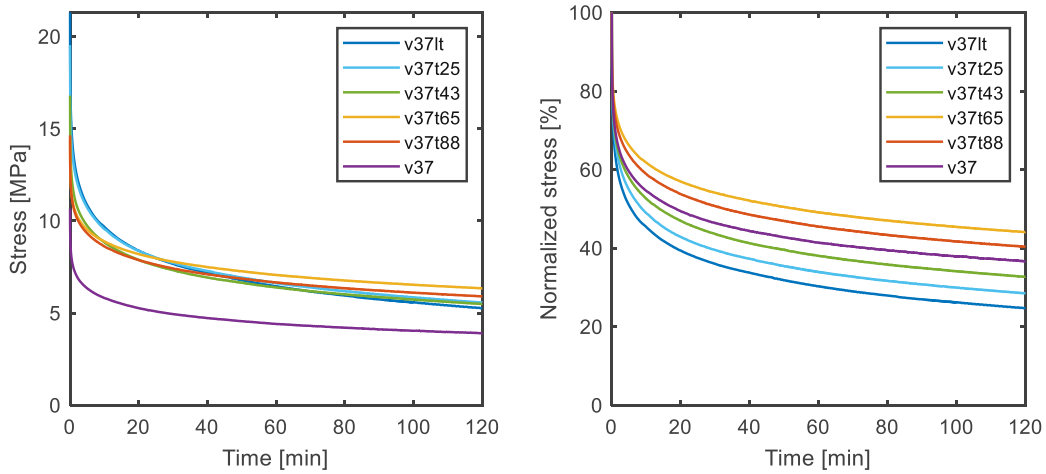
Figure 36: Left: absolute stress relaxation results; right: stress relaxation results relative to their respective maximum stress value.
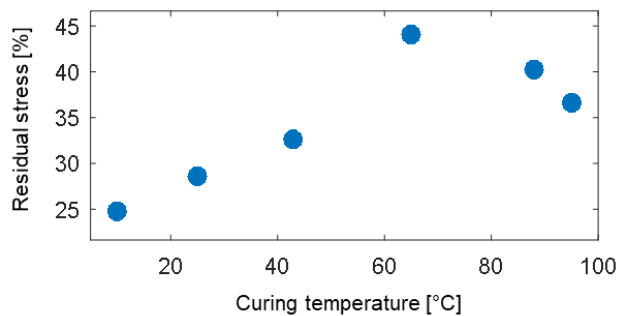
Figure 37: Residual stress values after 2 h stress relaxation for samples cured at different temperatures.

To explain the results presented above, a phenomenological discussion of the constitution of the microstructure is given below.

In the resin state, we assume a homogenous mixture of a high molecular weight component (TNM) and a low molecular weight component (HSMA). This composition is then exposed to a light source and the initiator is starting the polymerization. Due to significant polymerization shrinkage [97], [98], local pressure minima form where the reaction rates are high. This will lead to diffusion of molecules with high mobility in the direction of high reaction rates. It follows from the Rouse model, that the diffusion coefficient is inversely proportional to the polymer length [99], [100]. This means, the diffusivity of the high molecular weight component

can be neglected if $Mw_{high} >> Mw_{low.}$ In the specific case of HSMA mixed with TNM2 we can make this assumption. The low molecular weight component HSMA flows in the direction of high activity, promoting local homo polymerization of this compound. The consequence is static TNM2 molecules forming a matrix in which HSMA rich domains emerge. The higher the temperature, the more complete the phase separation will be. In the extreme case of full phase separation, inclusions of pure poly-HSMA are formed in a Matrix of pure poly-TNM2. With this in mind, the modulus dependence on the curing temperature can be explained. Low curing temperature leads to little phase separation of the initially homogeneous resin. The result is copolymerization of TNM2 and HSMA which gives a relatively stiff material. High temperature curing, in contrast, leads to pronounced phase separation and stiff HSMA rich inclusions within a TNM2 rich matrix. It was shown before, that TNM2 rich materials are less stiff. The stiff HSMA inclusions cannot contribute much to the overall stiffness of the material because they are not interconnected. The result is a material which consists of a soft matrix and inclusions, with relatively low overall stiffness.

3.3 Core-shell-rubber toughening

A convenient way of toughening is to put particles into the resin. These particles act as inclusions that can help toughen a resin. Core-shell particles are widely available. They consist of a soft rubber core and a rigid shell. The following section presents the results from mechanical testing of resin systems already introduced above, mixed with core shell particles.

a)   b)
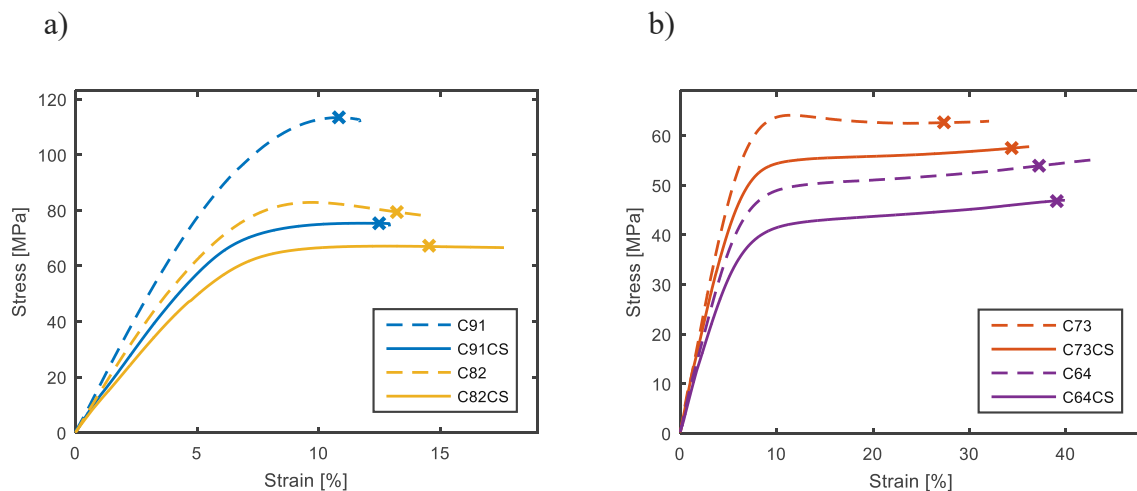
Figure 38: Tensile test results for core-shell toughened materials.

Figure 38a shows the results of the tensile tests for two resin compositions with relatively low amount of toughness modifier. Therefore, the modulus is high and the elongation at break is low. The tensile modulus of the samples with core-shell particles is reduced compared to the reference samples without core-shell particles. This is the expected behavior, because the particles are assumed to have significantly lower modulus than the matrix material. A positive effect on the elongation at break can be seen in both cases but the gains are small. Similar results were obtained with formulations with higher amount of toughness modifier. The results are plotted in Figure 38b. The expected drop in tensile modulus can be seen. For sample C73 there is also a small positive effect on the elongation at break. For material C64 there was only one specimen exceeding the elongation at break of the best specimen of the core shell composite. This cannot be considered as effective toughening. The drop in strength is larger in compositions with higher initial strength. This is due to mixing two materials (core-shell rubber and matrix) that have presumably very different mechanical properties.

a)   b)
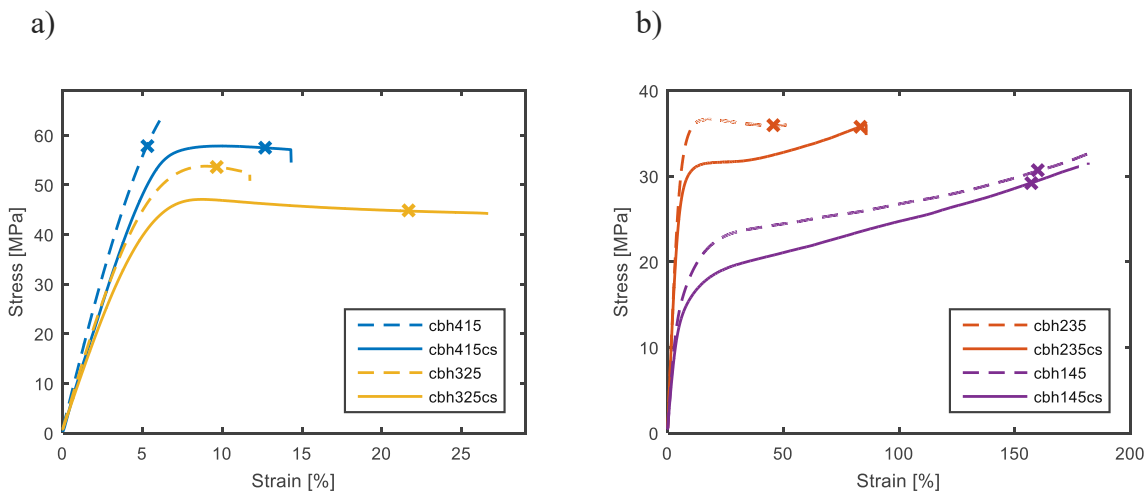
Figure 39: Tensile test results for core-shell toughened material with reduces crosslink density.

Figure 39 shows the results of the tensile tests for matrix compositions that contain no difunctional reactive diluents. Therefore, the crosslink density is lower than in the materials in Figure 38. A more loosely crosslinked network leads to higher molecular mobility and high toughenability is expected. Indeed, the results show very effective toughening with core-shell particles. In the case of cbh415 and cbh325 an increase of strain at break of well above 100% was observed. Only sample cbh145, the material with the highest amount of TNM, did not show any increase in elongation at break. In fact, this matrix material is already very tough which

means the resistance to crack growth is high. Consequently, core-shell particles cannot contribute to the toughness further, and no increase in elongation at break can be observed.
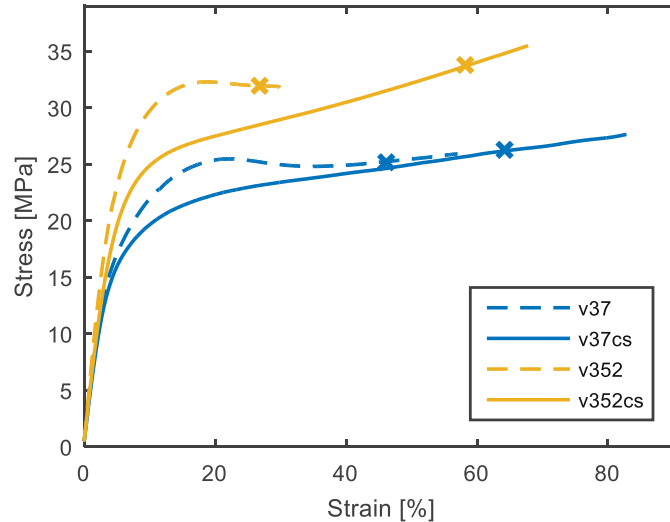
Figure 40: Tensile test results for core-shell toughened materials with different crosslink density.

A direct comparison between two similar materials where the crosslink density is the main difference is shown in Figure 40. It can be seen that the pure matrix with more difunctional reactive diluent breaks at lower strains compared to the material with less crosslinks. When comparing the stress-strain curves of the materials with core-shell particles one can see that the elongation at break do not differ much. The absolute value is indeed higher for the material with lower crosslink density, but the relative increase is higher for the high crosslink version. A possible explanation can be found when looking at the post yielding behavior of both curves. It can be seen that there is more strain hardening in the material with more crosslinks. Strain can therefore be distributed over a large volume more evenly [42], [43], [44].

As shown above, phase separation can have significant influence on the mechanical properties. To investigate the influence of phase separation on the toughening effect of core-shell particles, composites where prepared using a resin which tends to form separated phases. Low temperature curing, as explained above, was used to suppress phase separation to see the toughening in the homogenous matrix. To measure the toughening of the phase separated matrix the same composition was cured at 90 °C, the standard temperature for this work.
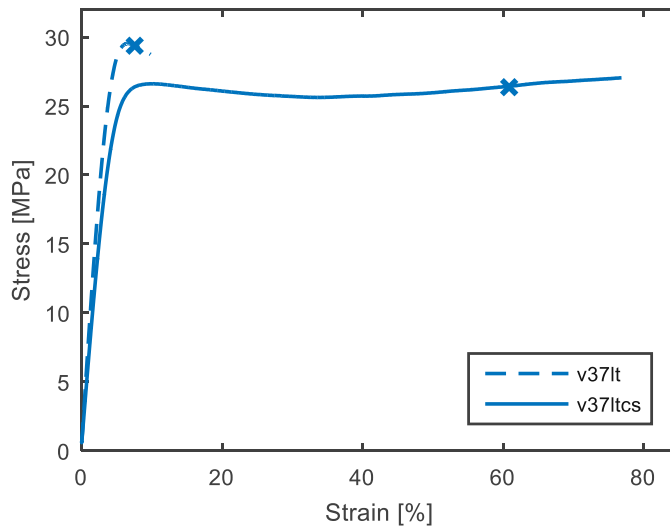
Figure 41: Tensile test results for material v37 cured at low temperature with core-shell particles.

For the material that was cured at low temperature, very effective toughening was observed as shown in Figure 41. Material v37lt shows a relatively low yield stress and is rather brittle. It also contains high molecular weight TNM and due to the reduced temperature at curing, the overall double bond conversion can be assumed to be lower compared to the high temperature cured materials. All these factors probably increase the toughenability of this material.

a)

b)
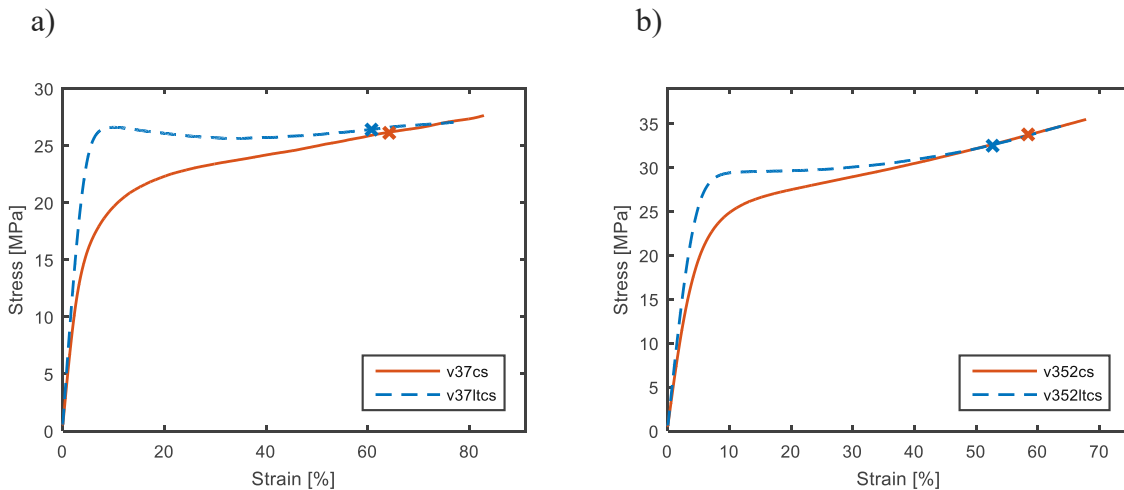
Figure 42: Tensile test results for core shell modified materials cured at high temperature compared to low temperature.

In the high temperature cured version of this material, these factors are not in favor of the toughenability. The toughness is already increased by phase separation leaving less room for potential toughening mechanisms. Figure 42 shows the direct comparison of high temperature

cured materials and low temperature cured materials, both mixed with 10 wt% core-shell particles. That means the difference between the red curve and the blue curve is only the curing temperature. Interestingly, the elongation at break is almost equivalent. This holds for v37 (Figure 42a), and v352 (Figure 42b) where significantly more difunctional reactive diluent was added.

3.4 Inkjet toughening

In all of the previously presented strategies, toughening is applied to the entire volume of a manufactured part. As toughening often comes with unwanted effects, such as reduced tensile modulus, it is of interest to limit the modification to only the volume where it is necessary. These volumes can be domains where the topology, together with a given load case, leads to stress intensities. By selectively toughen only the critical domains it is possible to produce more fail-safe parts while keeping the global properties close to the level of the pristine material. To realize this, a hybrid additive manufacturing process, developed at TU Wien, has been used [91]. With that process it is possible to combine lithography-based 3D printing with inkjet printing. The main advantage of this combination is the possibility to selectively modify materials which can be processed by additive manufacturing. The inkjet system allows to produce high precision material combinations. The ink itself can serve different purposes in an inkjet modified material, [91], [93], [101]. They are discussed separately in the following sections.

3.4.1 Ink as modifier

The inkjet system can be used to apply various different inks to layers produce by the 3D printing process. If the ink has a tendency to diffuse into the substrate, the resulting material is a hybrid of a pre-cured base material modified by the ink that diffuses into the layer. The ink is incorporated into the base material, either by swelling, or by copolymerization with the not yet fully cured material. An ink that meets all the criteria to be used as a modifier is cyanoethyl acrylate. Mixed with a small amount of crosslinker the polymer of this substance gives a highly elastic, low modulus material. In the printed hybrid material, the ink is expected to be present in three different states. These are the pure ink, ink diffused into the base material, and

copolymerization with the uncured base material. To get an estimation of the tensile material properties of the different ink compositions, tensile samples where printed and post processed differently.
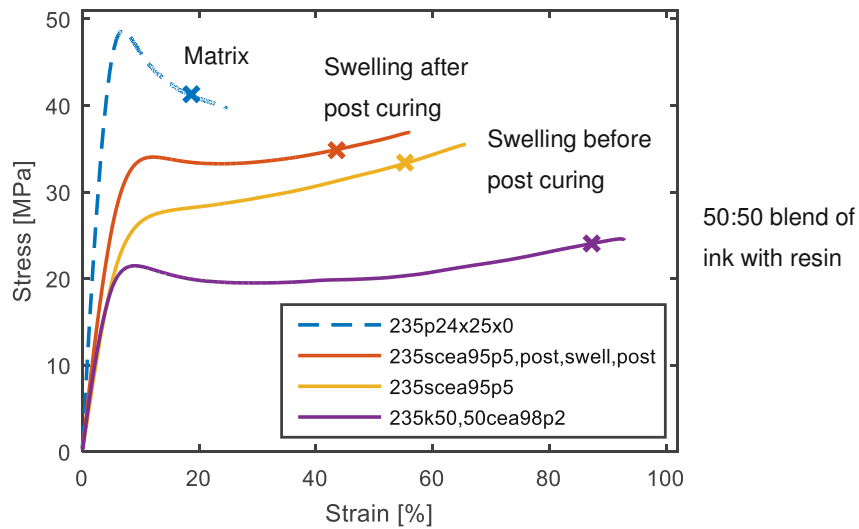
Figure 43: Tensile test results of matrix-ink compositions as they are expected to occur in the final printed part. The matrix material was printed in all three cases. The samples of the purple line were molded.

Table 7: Resin composition for Figure 43 and following. TPO in wt%, resin components in PHR.

	LPU624	TNM2	HSMA	TPO
235	20	30	50	1
334	30	30	40	1
325	30	20	50	1

In Figure 43 the results of the tensile tests of the different ink states are plotted. The probably most common material in a sample printed with the hybrid process is matrix infused with ink before post curing. It can be seen in Figure 43 that the matrix swollen with ink before post curing leads to a significant increase in elongation at break. Also, the matrix soaked after post curing shows high elongation at break. This indicates that there is significant toughening more or less regardless of the curing state of the matrix. The blend of the ink with the matrix was pre cured with the handheld ink exposure device to simulate printing conditions. The elongation at break of this material is very high compared to the other materials. Note that for the blend, ink

with slightly less crosslinker was used. The results indicate that cyanoethyl acrylate is a good choice for selectively toughen urethane-based photopolymer materials.

To proof the concept, a series of samples were printed using the hybrid printing process described above. To make sure no excess uncured resin was present on the substrate, each layer was cleaned prior to jetting. The first cleaning step was mechanically removing the resin with a piece of fabric. The second step was removing the remains with a small amount of acetone on a cloth.
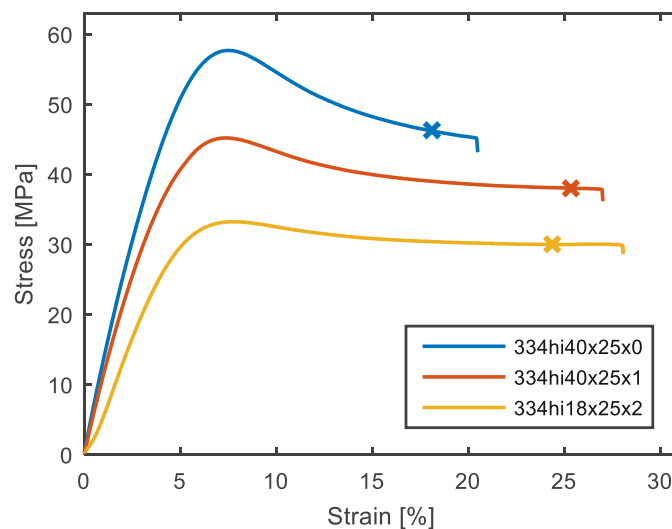
Figure 44: Tensile test results of samples printed with the hybrid printing process.

Figure 44 shows the results of the tensile tests of material 334, manufactured layer by layer with the hybrid 3D printing process. Each layer of base material served as substrate for the subsequent jetting of the ink. The target layer thickness was 25 μm. The specimens represented by the red line were jetted upon once each layer. For the specimens represented by the yellow line, two inkjet cycles were applied to each layer. One can clearly see that with increasing amount of ink the modulus is decreasing. The elongation at break of the material modified with one inkjet cycle each layer profits from the modification. For the material with two inkjet cycles each layer, no further increase in elongation at break could be observed. Figure 44 shows that it is possible to increase the elongation at break by using the hybrid additive manufacturing process. But it is clearly a tradeoff between tensile modulus and elongation at break.

72

While the base material in the preceding case was already relatively tough, Figure 45 shows the effect of the modification on a relatively brittle base material. Material 325 is characterized by a similar tensile modulus as 334, but failure happens well before the yield point.
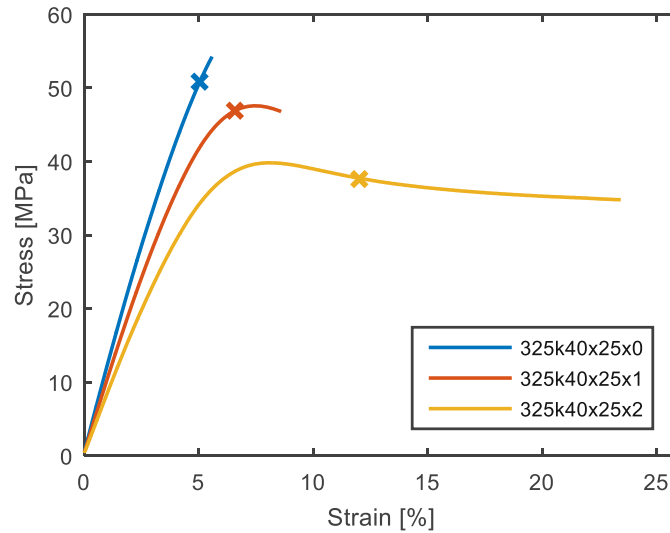
Figure 45: Tensile test results for samples produced with the hybrid printing process. As a matrix a relatively brittle material was chosen.

The red line in Figure 45 represents the material with one ink cycle each layer. This modified material shows higher elongation at break than the unmodified material. The yellow line represents the material with two inkjet cycles each layer. That means double the ink compared to one inkjet cycle. This leads to a doubling of the mean value of the elongation at break. One sample outperformed by more than 100 %, showing the potential of this approach. Modifying a brittle material obviously gives larger relative increase in elongation at break. This comes from the larger difference in mechanical properties of the unmodified base material and the modified material.

To get information on the distribution of the ink inside the additively manufactured parts, laser scanning microscopy (LSM) images were taken from the fracture surface of the specimens, see Figure 46.

a)   b)
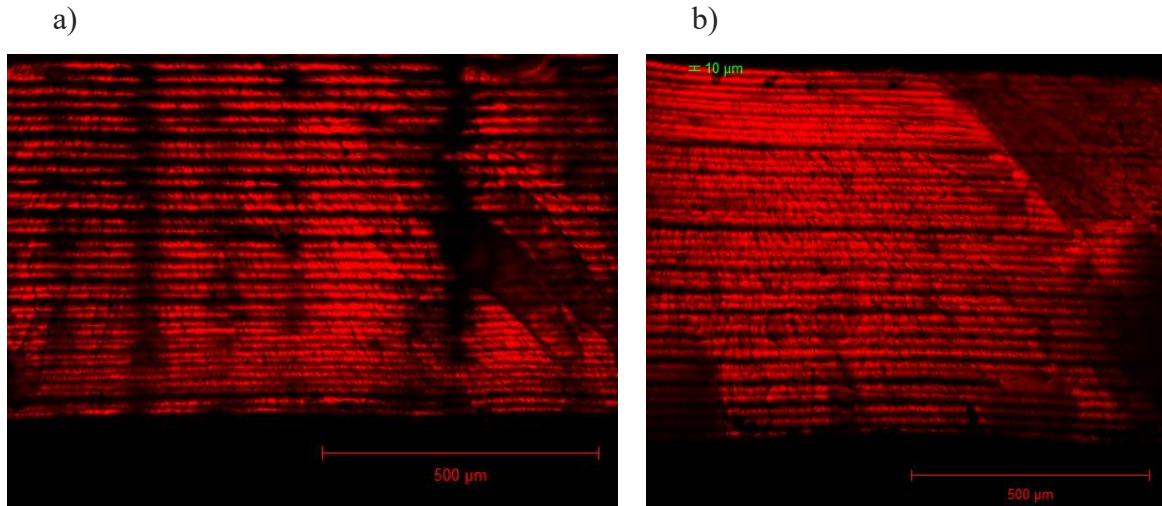
Figure 46: LSM images of the cross sections of samples manufactured with the hybrid printing process. a) one inkjet cycle each matrix layer; b) two inkjet cycles each matrix layer.

The images show that the ink is not diffusing through the whole layers. A periodic change in material properties can be expected. The properties can range from the properties of the pure base material to the pure ink. The gradient must be dependent on the diffusion profile of the ink into the matrix. Figure 46a shows a sample with one inkjet cycle each layer, Figure 46b shows a sample with two inkjet cycles each layer. Subjectively perceived, Figure 46b shows more areas with high concentration of fluorescent dye that was added to the ink. Therefore, it can be assumed that a higher share of base material is modified, which leads to higher elongation at break of the modified material 325.

A variation of the ink-as-modifier approach is presented below. The preceding data was measured from specimens where the ink was applied to flat layers of the cured base material. This led to a top-down diffusion that could not infuse the whole layer. For the following approach, called the fiber approach here, the curing pattern was changed such that individual parallel strands of cured material were obtained. For the exposure pattern, the maximum resolution was used. That means the strands are one pixel wide with one pixel gap between the strands. To achieve such a high resolution, special attention has to be given to the alignment of the focal plane of the DLP projector with the material vat. To demonstrate the integrity of the cured fibers, a couple of strands were pulled from a half-finished sample using a pair of tweezers (see Figure 47).
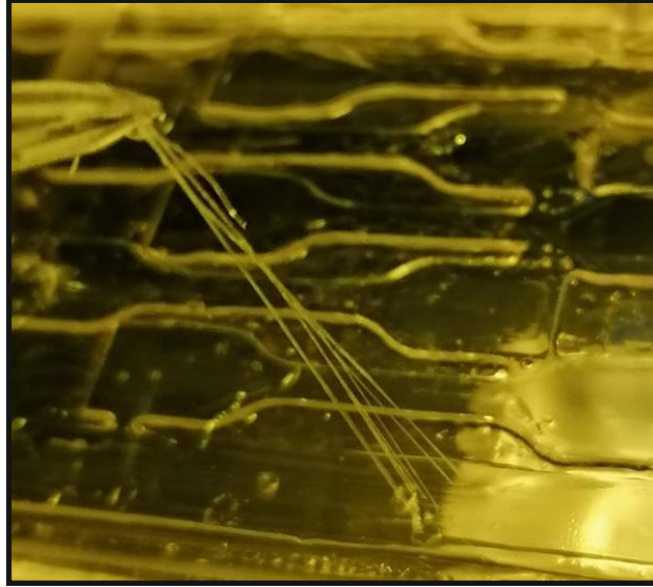
Figure 47: Demonstration of the integrity of the fibers manufactured via DLP exposure.

On this non-continuous substrate, one inkjet cycle and two inkjet cycles were applied. The results of the tensile test are presented in Figure 48. It can be seen that the trend is similar to the results presented in Figure 45. The ink leads to lower modulus, lower yield point and higher elongation at break with a four-fold increase of the elongation at break of the sample with two inkjet cycles, compared to the material with no ink. Also, the elongation at break of the individual specimens within a measurement series appear to be more consistent. The fibers-approach seems to be more effective compared to the continuous layer method.
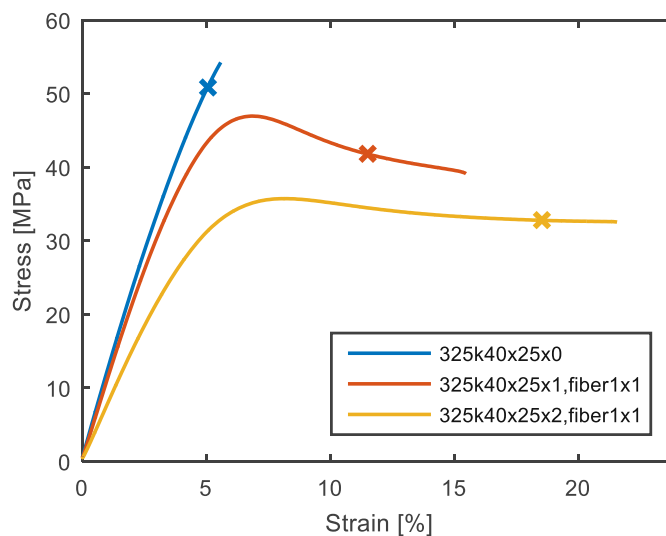
Figure 48: Tensile test results of the samples produced with the fiber approach.

Figure 49 show LSM images of the fracture surfaces of the fiber approach. One can clearly see the pattern that was pre-defined by the DLP exposure. The dark spots represent areas with little ink concentration, whereas the red spots indicate areas with high ink concentration. The width of the dark spots is approximately 50 µm which is the nominal size of a pixel. The images show that the diffusion of the ink was successfully guided to areas where the material was not exposed prior to jetting. This resulted in a thoroughly modified material which led to good toughening results in the tensile test.

a)   b)
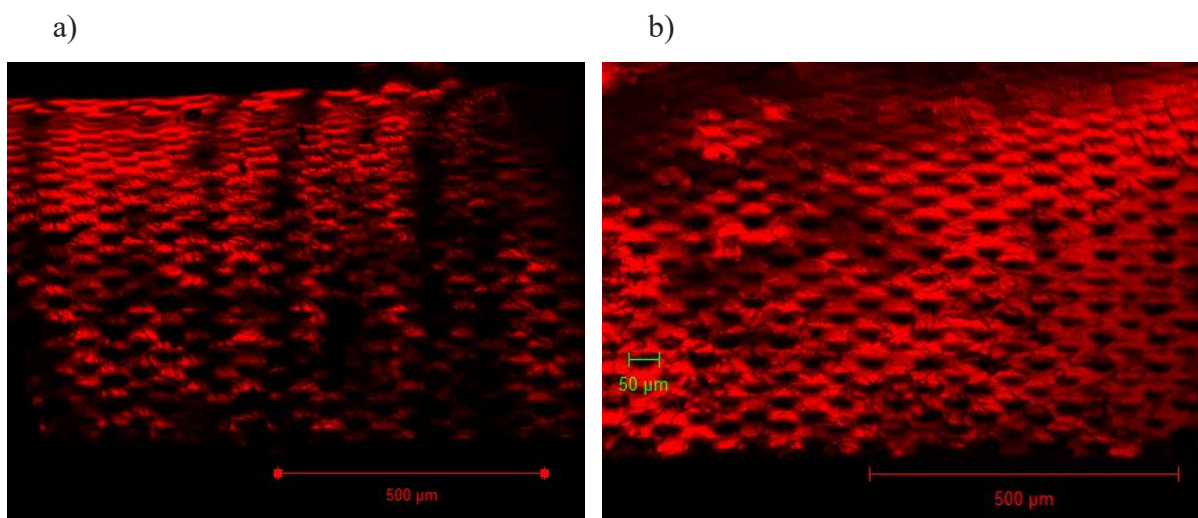
Figure 49: LSM images of the cross section of samples produced with the fiber approach. a) one inkjet cycle each DLP layer; b) two inkjet cycles each DLP layer.

3.4.2   Ink as separating layer

To get separated layers of pure base material it is important that the ink has limited ability to diffuse into the base material. The goal is that the properties of the base materials are unaltered. High stiffness should be retained. This can be achieved by using ink-matrix combinations with low tendency for interdiffusion. One was found to be a commercially available ink called 'TangoPlus' which is a low modulus, rubber-like ink, developed for inkjet 3D printing. The potential toughening with this approach comes from stress decoupling of individual layers, only connected by a low modulus material [102]. The obvious drawback of this approach is the loss of isotropy. Also, the bending modulus is expected to suffer severely.

76

Figure 50 shows the results of the tensile test of a layered material separated by the soft ink and the respective reference matrix material. One can see that the bulk material is relatively brittle and also the layered material does not benefit a lot from stress decoupling. This material has a relatively high crosslink density. Therefore, the potential for plastic strain energy dissipation is assumed to be low. That also means the potential for toughening is low. More toughening effect is expected with materials with higher potential for plastic deformation.
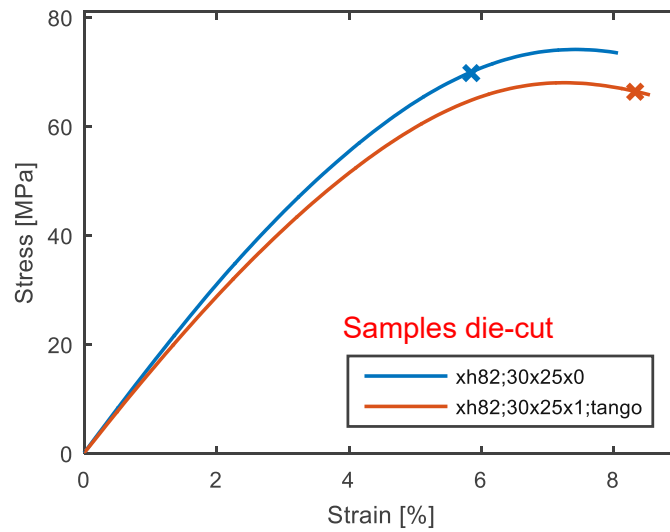
Figure 50: Tensile test results for a laminated material with relatively brittle behavior.

Table 8: Resin composition for Figure 50. TPO in wt%, resin components in PHR.

	XR741MS	HSMA	TPO
xh82	80	20	0.5

In Figure 51 the results for material 64 are plotted. One can see from the blue line that the average elongation at break of this material is larger than the yield strain. That means plastic deformation happens even in the unmodified bulk material. The red, yellow and purple lines represent layered materials with one inkjet cycle, two inkjet cycles and three inkjet cycles respectively. As expected, the tensile modulus is decreasing with higher amount of ink. The elongation at break appears to peak at two inkjet cycles and is then lower with three inkjet cycles, while the expected behavior would be an elongation at break plateau. A possible explanation for this behavior can be found when acknowledging the following. Increasing the

number of inkjet cycles increases the thickness of the ink layer. This thicker interlayer leaves less space for the base-material layer in the DLP step of the additive manufacturing process which bears the major part of the load. At three inkjet cycles the interlayer thickness reaches a point where there is not enough space left to form continuously flawless layers in the DLP step. Flawed layers are expected to have lower elongation at break.
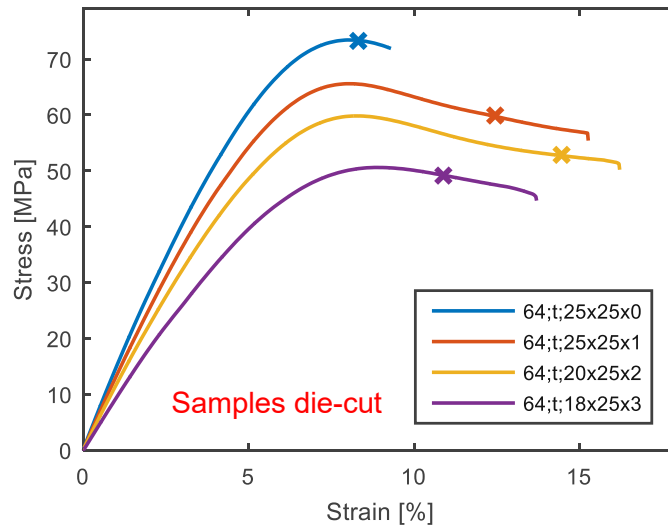
Figure 51: Tensile test results for a laminated material with relatively tough behavior.

Table 9: Resin composition for Figure 51. TPO in wt%, resin components in PHR.

	LPU-624	LPU-706NT	TPO
64	60	40	1

Since material 64 appears to be well toughenable, it was tried to further toughen the material with 10 wt% core shell particles. The results are presented in Figure 52. It can be seen that core shell particles can increase the elongation at break of material 64 (compare Figure 52 blue solid line and blue dashed line). Also, in the case of the layered version, core shell particles give a little extra elongation at break (see Figure 52 red solid line and red dashed line). It must be noted that the effect of the interlayers is much larger than the effect of the core shell particles in this case.

Die approbierte gedruckte Originalversion dieser Dissertation ist an der TU Wien Bibliothek verfügbar.
The approved original version of this doctoral thesis is available in print at TU Wien Bibliothek.
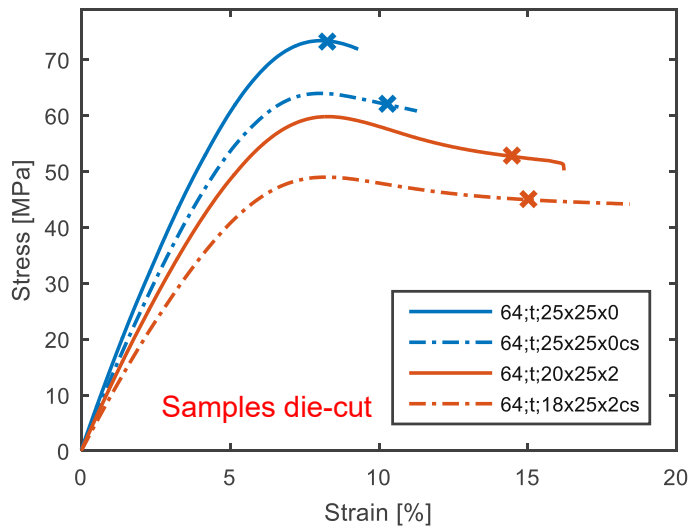
Figure 52: Tensile test results for samples toughened with core shell particles and layers approach.

Fracture surfaces of these samples are interesting because, though the values for elongation at break of the layered samples and the layered samples plus core shell particles are similar, the fracture surfaces look quite different in the SEM images (see Figure 53). One can clearly see the layered structure in both images, but the roughness is much higher at the sample modified with core shell particles. Apparently, the toughness induced by the core shell particles is limited to the fracture zone, otherwise a larger increase in elongation at break would be expected. A reason for the restriction could be the surface roughness of the specimens as a result of die-cutting. Flaws stemming from die-cutting probably lead to severe stress intensities and the plastic strain dissipation cannot percolate through a macroscopic volume.

a)   b)
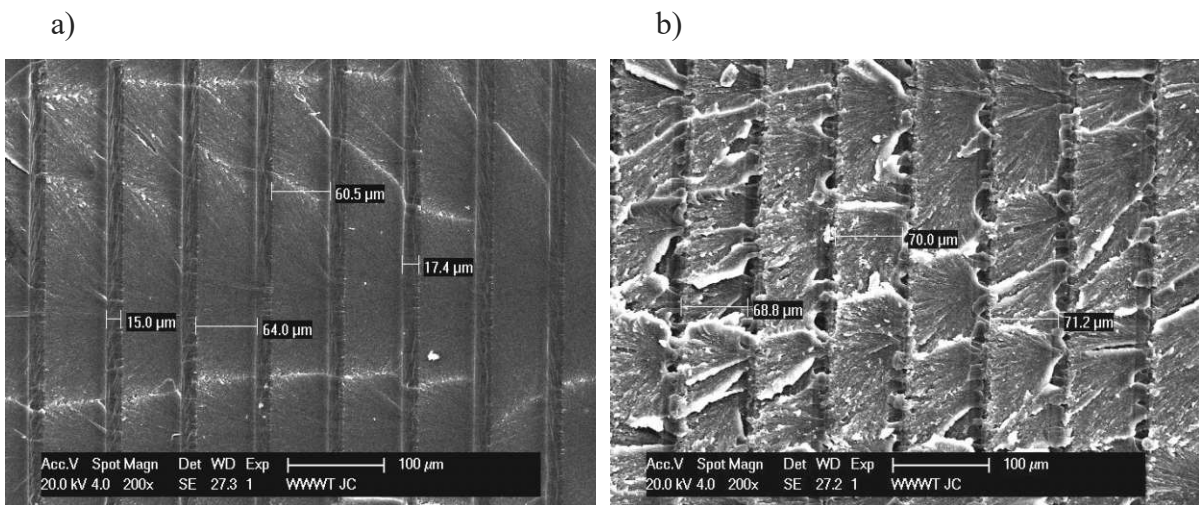
Figure 53: Scanning electron microscopy images of the fracture surfaces of laminates. a) no core shell particles; b) with core shell particles.

3.4.3 Ink as particles

The above presented inkjet approaches have drawbacks regarding loss of stiffness, strength, and breaking of the isotropy of the material. To circumvent these, one can introduce the ink into the base material not in a continuous fashion, but as discrete droplets. Similar to the core shell approach, but on a different length scale. Another difference is that with the inkjet system, the positioning of the inclusions can be set with the precision of the print head, compared to a random arrangement from mixing core shell particles into a resin. For this approach special attention has to be given to droplet quality. To check the quality of the drops, the integrated drop watcher was used. The jetting parameters were adjusted in order to get only main drops without satellite drops. An image of the drops is presented in Figure 54 a.

a) b)
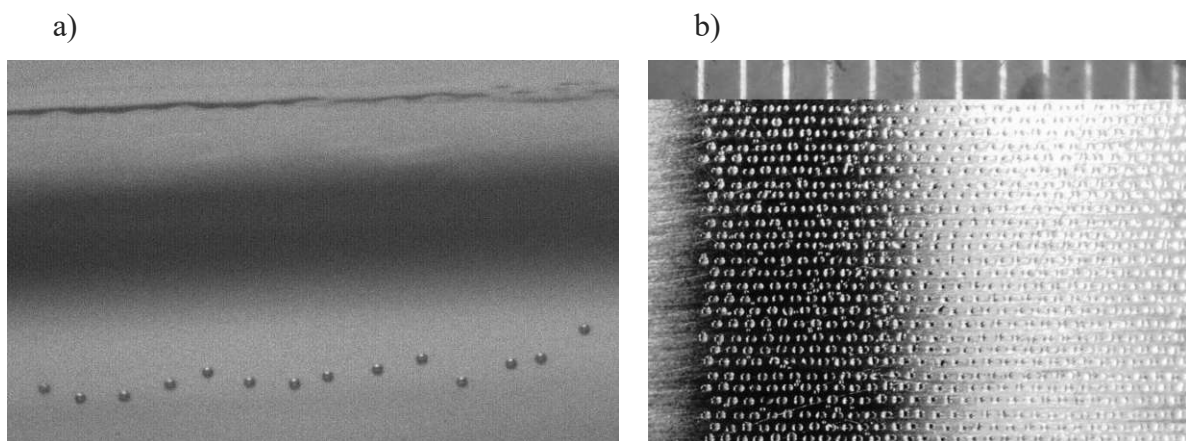
Figure 54: Droplet quality. a) droplets as observed by the drop watcher; b) droplets on the building platform.

Jetting experiments on substrate showed that even when no satellite drops are visible in the drop watcher, they can be present on the substrate. Figure 54 b shows the arrangement of the droplets jetted on the building platform with the optimized parameters. It can be seen that the main drops are arranged in a regular way with occasionally occurring satellite drops in between them. For the results presented below samples were produced with these settings.
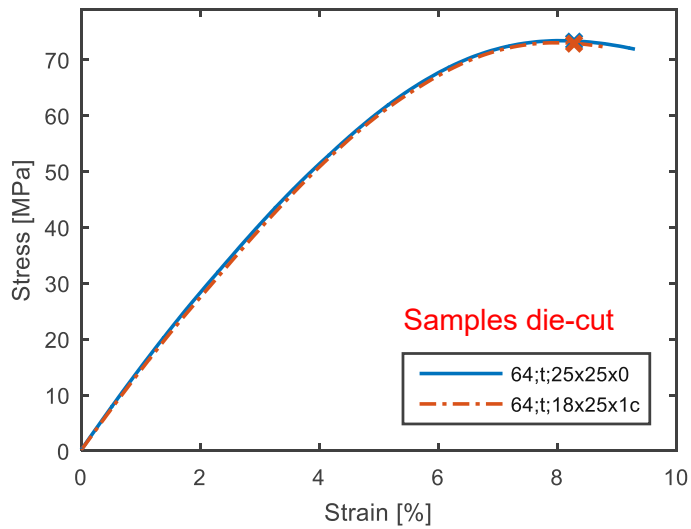
Figure 55: Tensile test results of samples produces with the ink inclusions approach.

Figure 55 shows the results of the tensile test of two different materials. One material was modified using an arrangement of droplets on each layer, the other was not modified. One can see that the results are virtually identical. To see an effect of the modification more ink had to be applied. Because the densest possible arrangement of droplets was already in use, the only way to get more ink inside the material was to stack the drops. To achieve this the inkjet process has to be well reproducible. In order to proof the reproducibility, a stack of three droplets was produced and a top view image was taken using the LSM (see Figure 56).
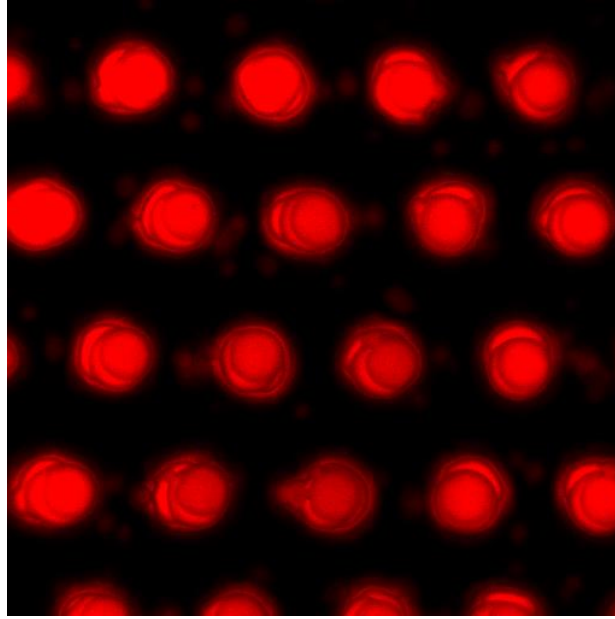
Figure 56: LSM image of stacks of 3 inkjet droplets in top view

It can be seen in Figure 56 that stacking was achieved. The individual droplets are clearly visible. Satellite drops are also visible as faint small drops irregularly placed between the larger main drops. With this approach, samples were manufactured using the hybrid printing process.
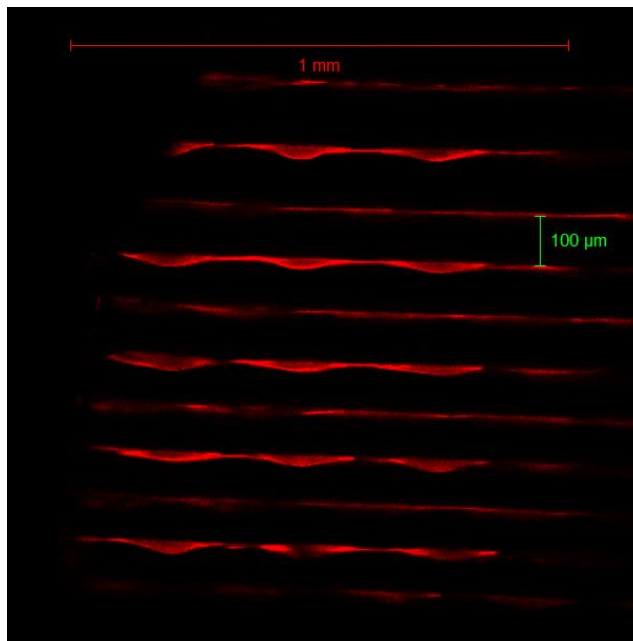
Figure 57: LSM image of the fracture surface of a specimen modified with stacks of 8 drops.

Figure 57 shows that although the stack resembles a snowman-like arrangement in the top view, the drops appear to take less volume than expected in the side view. Also, the layer thickness appears to be much higher than the target of 25 µm. This is probably because of the multiple ink curing steps per matrix layer. In the case of the sample depicted in Figure 57 the material was exposed eight times 5 seconds. Although the main absorbance peaks of the photoinitiators used are far apart, some resin reacted unintendedly during the ink exposure. The result was that some cured material accumulated at the edges of the building platform and did not allow it to reach the desired position.

To investigate the effect of these stacks of droplets on the tensile properties, samples were produced with 5, 8, 11 and 14 droplets stacked on top of each other. To minimize the effect of the die-cutting on the surface quality, the respective surfaces were processed with sandpaper prior to testing. The results are presented in Figure 58.
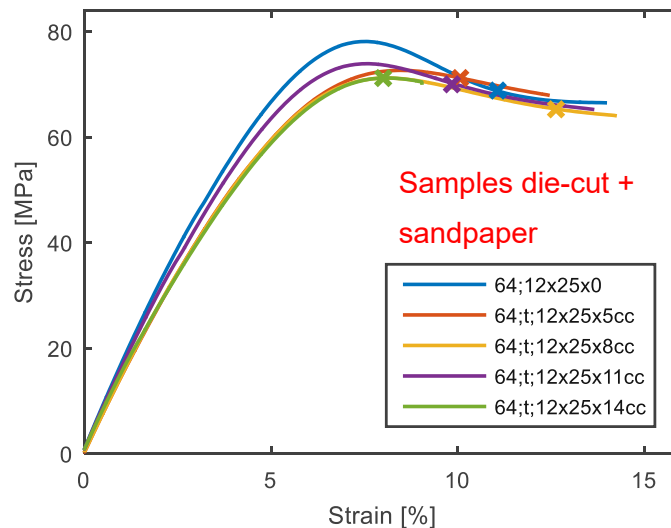
Figure 58: Tensile test results of the ink inclusion approach.

One can see in Figure 58 that the yield stress is decreasing with increasing amount of ink. But the effect on the elongation at break is limited. The reference sample, which is represented by the blue line, is among the best ones in this series of measurements. A little bit of outperformance can be seen in the material with eight-stack, represented by the yellow line in Figure 58. However, the tendency goes to lower elongation at break in the modified samples, with the worst performance of the material with the most ink.

A possible way to increase the influence of the inclusions is to increase the droplet density. As the droplet density was already at the maximum, it was necessary to change the inkjet printhead to a model with smaller droplet volume. For the following results, the printhead with 6 pl nominal droplet volume was used. This allowed for a denser packing of the droplets on the substrate without the droplets being in contact with each other.
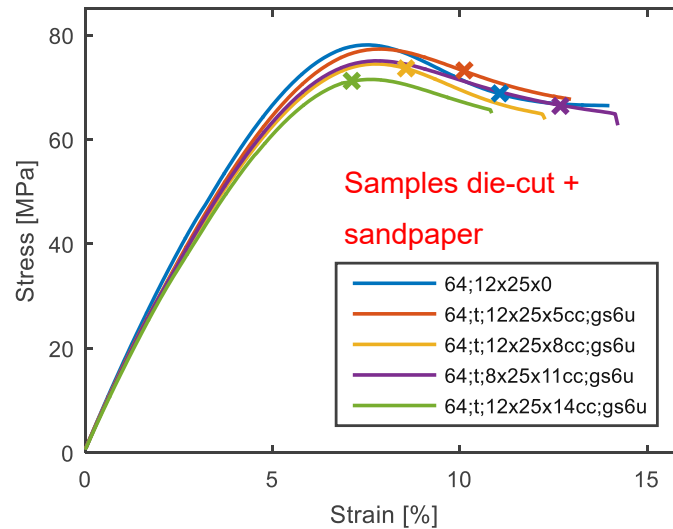
Figure 59: Tensile test results of the ink inclusion approach with smaller droplet size.

In Figure 59, the results of the tensile tests of the samples produced with smaller droplet volume are plotted. Compared to the results with larger droplets the curves are very similar. The reference samples are again among the best ones. Outperformance this time comes from the 11-stack sample compared to the 8-stack sample in Figure 58. The material with most ink has again the lowest elongation at break.

In both cases, the results indicate that the inclusions do not contribute to the toughness, as they have little to no positive effect on the elongation at break. They rather act as flaws inside the matrix. A reason for this could be the shape of the inclusions that can be seen in Figure 57. It can be seen that the inclusions are rather flat. This geometry acts as a notch where stress intensities can occur and therefore lead to premature fracture.

3.5 Unwanted side effects

Every modification of the resin or polymer possibly leads to compromising some other aspect of the material unintentionally. This might not be a problem if one is aware of the magnitude of the effect and adaption is possible. The modifications presented above were observed to, on the one hand, alter the processability, and on the other hand, compromise the properties of the final polymer material.

Changing the composition of the resin to favor toughness includes adding high molecular weight components. This inevitably leads to an increase in resin viscosity. As the stereolithography process is rather sensitive to the resin viscosity, processability might be compromised. This has led to the invention of hot lithography [14]. By adding the possibility to heat the resin in the printer, the processing window can be expanded, and more and more high molecular weight components can be added. Exploring the limits of hot lithography is a subject of ongoing developments an of industrial relevance. Only if tough high performing 3D printing materials are available, a wide industrial adoption of the technology seems possible.

Curing kinetics and green part strengths have to be monitored carefully when modifying a resin. Reducing the amount of crosslinkers to increase the molecular mobility will require higher double bond conversion in the green part. This leads to longer processing times.

Adding particles to the resin also increases the viscosity and makes resin handling more of a challenge. Inhomogeneities in general also alter the visual appearance by acting as centers of light scattering. This can influence the curing precision as the scattered light potentially cures areas that are not exposed to the primary light source. Also, curing depth is limited in a scattering resin. If visible light is scattered, the material will be opaque. This can be an issue in some applications where aesthetics plays a role.

Stiffness and strength are of high technological importance. When adding a compliant, low modulus second phase, it is no surprise that the values for stiffness and strength are decreasing. This behavior was observed in all measurements presented above. But this does not always have to be the case. It was observed in [103] that by promoting the interfacial bonding between particles and matrix, the strength can be kept high while still substantially increasing the elongation at break. However, it is assumed that this can only be achieved using a matrix material with specific mechanical properties which are hard to pin down.

Structural parts are often used in applications where they have to bear stresses permanently without losing their geometrical integrity. Therefore, long term stability is a key asset of a high-

performance polymer. To have information on the material behavior at persistent strain, stress relaxation experiments were conducted. Figure 60 shows the result for different resin formulations, containing different amounts of TNM, TGM and reactive diluent components. All tensile test results of the materials presented in the following were already shown above. As a reminder, Table 10 sums up all the different compositions from Figure 60.

The highest initial stresses are reached by the material formulations cd37, cd352 and cd334. What they have in common is that they all contain 20 wt% of the TG modifier LPU-624. As already shown by the tensile tests, LPU-624 helps increasing the stiffness of a formulation. However, in terms of relative stress relaxation, if much monofunctional reactive diluent is added, the remaining stress is lower compared to the other formulations (see cd37, cd352 and cd334 in Figure 60). This indicates a dependence of the drop in relative stress on the crosslink density. This correlation shows also in the right plot in Figure 60. The samples with the highest remaining stress are the ones with extra bifunctional reactive diluent added to the resin. But the formulation might not be exclusively responsible for the stress relaxation properties. Other possible factors are phase separation and water uptake. Phase separation was observed in v37 and v352, where the characteristic secondary tan delta peak was measured by DMA (see Figure 61). These two materials show the lowest bending stiffness in Figure 60 but no significant correlation of the remaining stress could be observed.
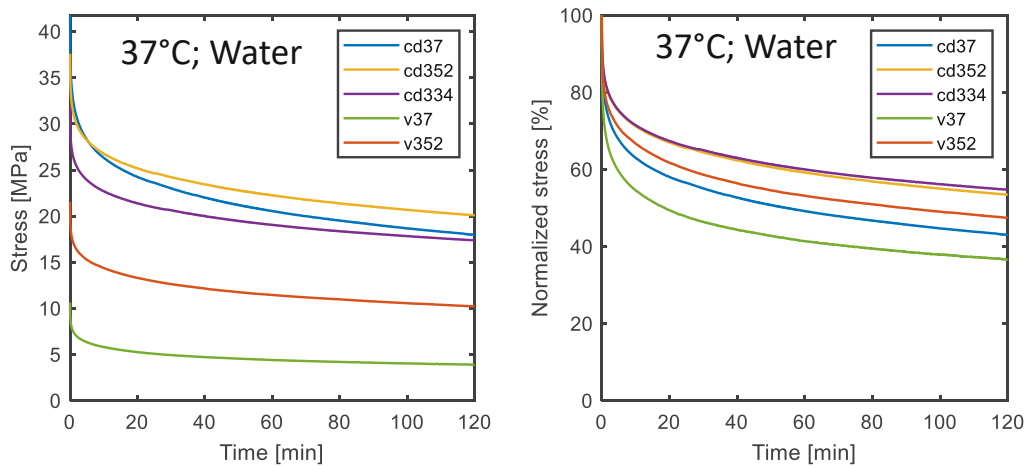
Figure 60: Stress relaxation results for different resin formulations at 37 °C in water. Left: absolute values; right: relative to the respective initial stress.

Table 10: Resin compositions of the materials in Figure 60. Resin components in PHR. With 1 wt% TPO.

	LPU-624	TNM2	HSMA	TEGDMA	D3MA
cd37	20	10	70		
cd352	20	10	50		20
cd334	20	10	30		40
v37		30	70		
v352		30	50	20	
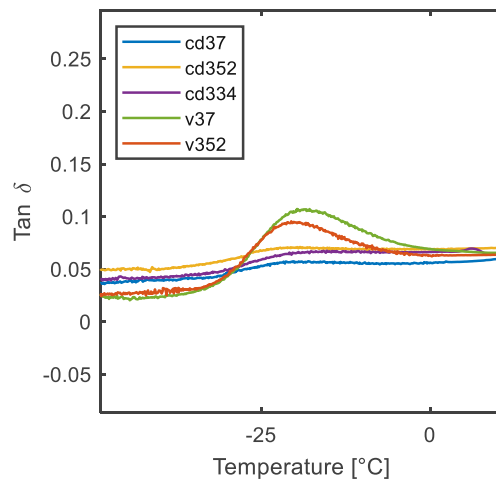
Figure 61: Secondary tan delta peak, indicating phase separation [96], [95].

A direct comparison of samples soaked in water with dry samples suggest that the influence of water uptake is more significant than the influence of phase separation. Materials v37 and v352 were measured both in dry condition and immersed in water (see Figure 62). For material v352 the initial stress values are very similar when comparing wet and dry samples. Over the course of the measurement the drop in stress is larger in the sample measured in wet condition. For material v37 significantly different initial stress values were measured, indicating that a relatively high share of water diffused into the sample already at the start of the measurement. The relative stress relaxation results (Figure 62 right) makes it obvious that for both materials the wet samples showed less remaining stress compared to the dry samples. Comparing the two materials, sample v352 performed significantly better. The higher crosslink density in v352, coming from the additional bifunctional reactive diluent, slows down the water diffusion into the polymer [104]. Consequently, choosing a low crosslink density can compromise the stress relaxation properties in moist condition or wet environments.
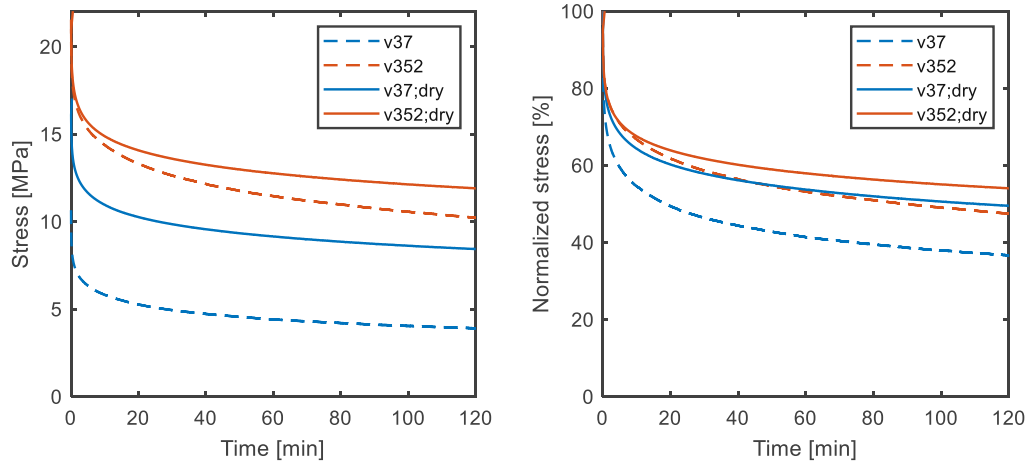
Figure 62: Stress relaxation results of samples measured in dry condition compared to samples measured in wet condition. Left: absolute values; right: relative to the respective initial stress.

For inkjet toughening the expected drop in bending stiffness was also verified in stress relaxation measurements. Jetting a low stiffness material between the DLP manufactured layers lowers the inter-layer stiffness. This lowers the overall stiffness of the part as can be seen in Figure 63. More inkjet layers result in lower bending stiffness, with the lowest stiffness found in the sample manufactured with the fiber approach. More ink also results in less relative remaining stress as shown in Figure 63 right. However, the elongation at break was significantly increased with the soft ink, as can be seen in Figure 64.
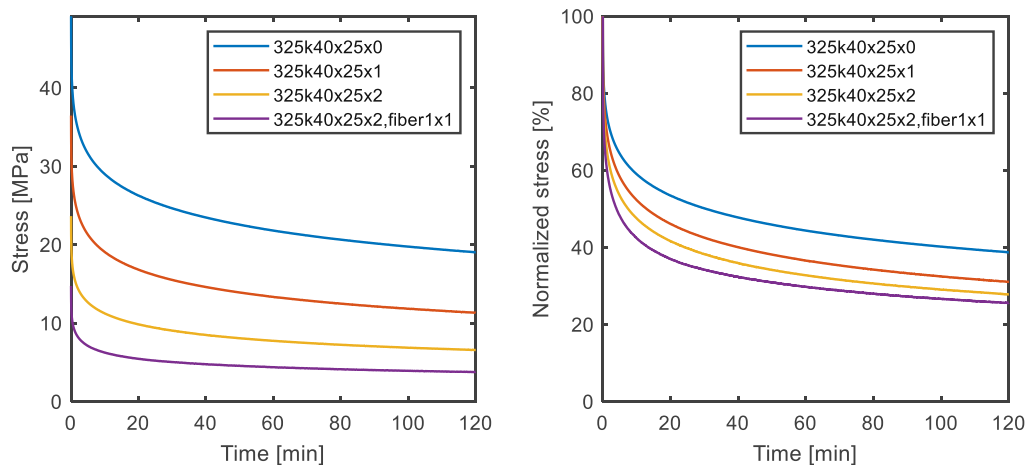
Figure 63: Stress relaxation results for different inkjet toughening approaches.

The stress relaxation measurements revealed a sharp drop in remaining stress after 2 hours when comparing the samples with no ink and with one inkjet cycle. However, doubling the

88

amount of ink only led to a minor decrease of remaining stress compared to the sample with one inkjet cycle per lithography-manufactured layer. The elongation at break was substantially increased. Another increase in elongation at break with only mild reduction of remaining stress was measured with the fiber approach. The amount of ink used for the sample marked with the yellow circle and the purple circle is equivalent. Only the exposure strategy was changed. The elongation at break for this sample almost reached 20 percent while the remaining stress after two hours was comparable to the samples with continuously cured DLP layers.
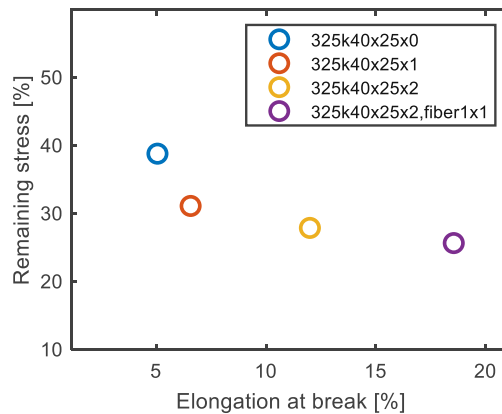
Figure 64: Remaining stress after 2 hours at constant strain over average elongation at break.

Figure 65 shows stress relaxation measurements of samples with reactive toughness modifier compared non-reactive toughness modifier. It can be seen that the initial stress is larger for the sample with reactive toughness modifier, confirming the higher stiffness measured by tensile test. This agreement indicates that the influence of water uptake in this case is likely only a minor effect[6]. However, the magnitude of decrease in remaining relative stress is comparable, so an influence of water uptake cannot be ruled out. It was shown earlier that the use of the reactive toughness modifier leads to higher elongation at break. Consequently, promoting the incorporation of the toughness modifier into the polymer network was the only method found to increase the toughness, and at the same time, leads to higher remaining stress in a stress relaxation experiment.

---

[6] Compare the large effect of the water uptake in sample v37 in Figure 62. The water uptake led to a significant decrease in initial bending stress and also led to lower relative stress.
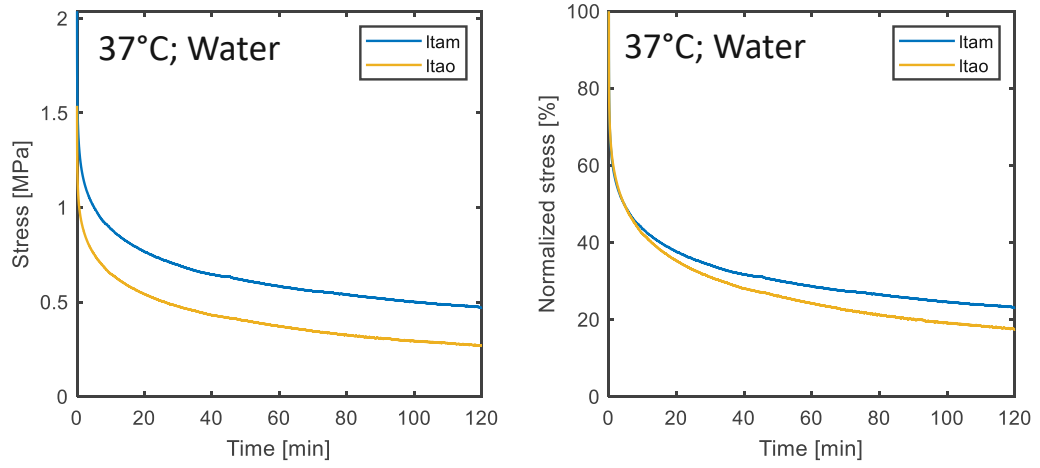
Figure 65: Stress relaxation results for polymers with reactive (ltam) and non-reactive (ltao) toughness modifier.

4 Simulation results

The aim of this chapter is to elaborate on the question if a molecular dynamics simulation approach can give additional information which is valuable in the process of resin development. It was shown in the experimental part of this work, that not only the composition of the resin but also the curing conditions and resulting microstructure are defining the mechanical properties of a photopolymer (see section 3.2). However, these relations are not clear a priori, especially when dealing with novel formulations where no prior knowledge exists. Further, some aspects are not accessible experimentally which limits the possibility to study the mechanisms. Only a proper modeling of the polymer network can give insights on some of the defining relations. Another drawback of the purely experimental route is that it requires synthetization of all constituents of formulations of interest. Only then, after an often lengthy process, the usability can be verified through testing.

A successful simulation route provides information on the target material before the main lab work begins. This information would help decide if certain strategies are feasible and reveals possible strengths and weaknesses of an approach.

The following three subchapters present the results of different studies that were done to evaluate the usability of molecular dynamics simulations for making statements about a certain photopolymer system. Especially interesting in the framework of stereolithography are the reaction kinetics of a resin/initiator system and the mechanical properties of the resulting polymer network. The information on the kinetics was extracted from the simulated polymerization step. The mechanical properties were evaluated using the polymer networks created with said simulated polymerization.

4.1 Reaction kinetics

The information on the reaction kinetics from the Polymatic script comes as the number of created bonds and the number of attempts to establish a bond. The number of established bonds can then be converted into double bond conversion and plotted over the total number of attempts

taken by the algorithm. This gives a visualization of the bond formation over time that the algorithm has performed and the reaction kinetics over a pseudo time. Though the number of attempts correspond to a simulation time, the conversion to a real time is not meaningful. This is because the number of timesteps of a single simulation was chosen arbitrarily. Further, a simple cutoff criterion does not well represent a real bond formation, which would require a thorough quantum mechanical description. The following results therefore only have qualitative meaning.

Figure 66 shows the double bond conversion as calculated from the number of established bonds over the total number of attempts for a simulation of pure methyl methacrylate in a coarse grain representation. The coarse graining was done according to [105]. The plot shows a linear increase of conversion in the beginning. In the early phase of the simulation the mobility of the molecules is high and reaction partners are found whenever the program tries to form a bond. This behavior continues up until approximately 60 % double bond conversion. The curve starts to flatten significantly which means that more and more attempts are necessary to increase the double bond conversion. The reaction is slowing down as a result of decreasing number of reactive species and increasing molecular weight of the polymer chains. The latter reduces the mobility of the system. Hence, it takes longer for the reaction partners to diffuse and satisfy the cutoff criterion. Note that no artificial charge to increase the attraction of active and reactive species was set. The potential reaction partners are approaching by simple diffusion. At approximately 80 % double bond conversion. The simulation was aborted automatically because the termination criterion was fulfilled. At this point no bond was formed within the specified number of attempts, because of restricted diffusion of the remaining monomer units.
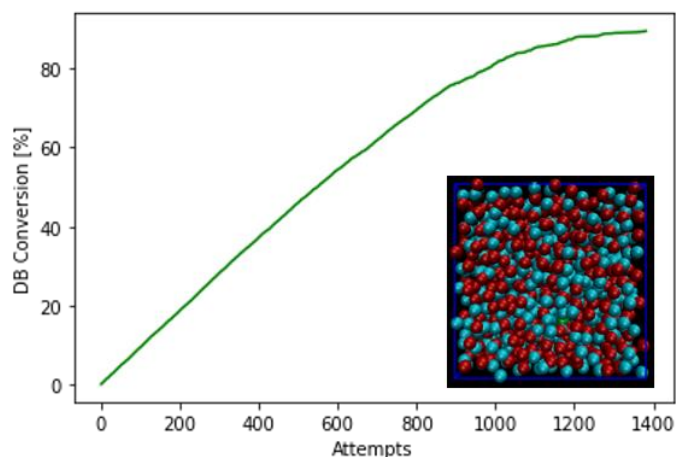
Figure 66: Double bond conversion over the number of bond forming attempts for pure methyl methacrylate.

Frequently, difunctional molecules are used in photopolymer resin. One example is TEGDMA. To model TEGDMA, two methyl methacrylate molecules were linked with two beads representing the ether groups [105]. Figure 67 shows the simulated polymerization of pure TEGDMA. In the early stage of the simulation the increase is again linear over the number of attempts. This is because the mobility is still high and reaction partners can be found easily. The curve starts flattening at approximately 35 % double bond conversion. And not long after the first flattening occurs the simulation stops abruptly. In the case of difunctional molecules a polymer network is formed when the resin is polymerized. That leads to a much faster decrease in mobility compared to a purely monofunctional resin where the molecular weight is only increasing linearly. At a certain point, the molecules are virtually 'frozen'. No more reactions can take place although there are still plenty of reactive groups available.
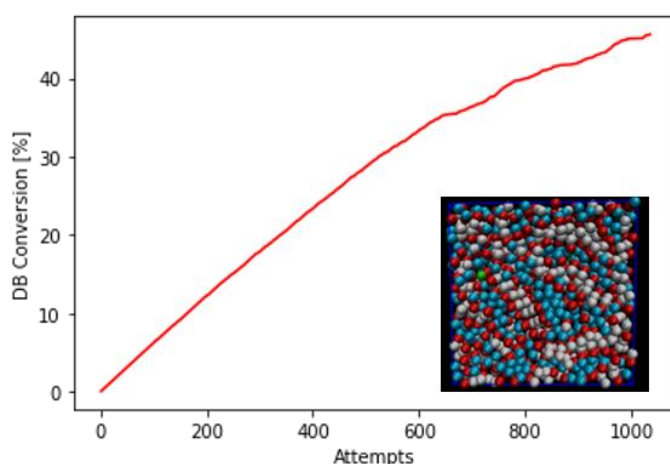
Figure 67: Double bond conversion over the number of bond forming attempts for pure TEGDMA.

Increasing the length of the spacer between two methyl methacrylate molecules gives polyethylene glycol dimethacrylate (PEGDMA). The molecular weight is defined by the length of the spacer. High molecular weight compounds are especially interesting for 3D printing resins, as discussed in the experimental section of this work. They can help increasing the toughness of a material but also reduces the reactivity.

For the following demonstration, a coarse grain representation of PEGDMA with a molecular weight of 700 was used. The orange line in Figure 68 shows the double bond conversion of pure PEGDMA700 over the total number of attempts. In this simulation the linear range is very small. It takes significantly longer to find reaction partners compared to the simulation of smaller molecules. Further, the final number of reacted end groups is well below 10 %. Far lower than in the simulations shown before. The blue line in Figure 68 represents PEGDMA700 together with reactive diluents. As diluents methyl methacrylate and TEGDMA were used. This leads to much higher reactivity of the overall resin. The linear range is comparable with the pure reactive diluents shown above. The shape of the blue curve resembles the curve of pure TEGDMA, but higher double bond conversion was reached. The low molecular weight components exhibit enough mobility to establish a polymer network including PEGDMA with high double bond conversion. The low mobility of PEGDMA is overcome and high reactivity can be achieved. Figure 69 shows the respective simulation boxes. The left frame shows the simulation box filled with PEGDMA700. Reactive beads are colored blue. To form bonds, the blue beads need to come close to each other. In the case of high molecular weight compounds, the distance to cover is relatively large. The right image in Figure 69 shows the diluted case for comparison. The blue beads are much closer to each other. Also, the small molecules provide a mobile species and keep the reaction alive. The polymerization can proceed longer. The diluted system reacts faster and reaches higher double bond conversion compared to the pure system.
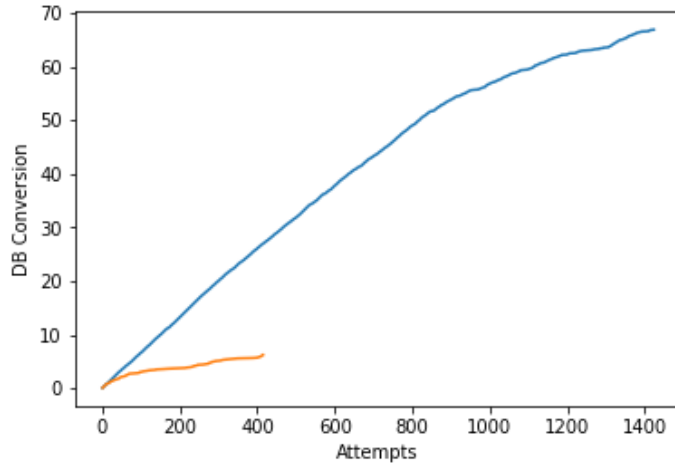
Figure 68: Double bond conversion over the number of bond forming attempts for pure polyethylene glycol dimethacrylate (orange line) and diluted polyethylene glycol dimethacrylate (blue line). 100 PEGDMA; 100 TEGDMA; 1000 MMA.
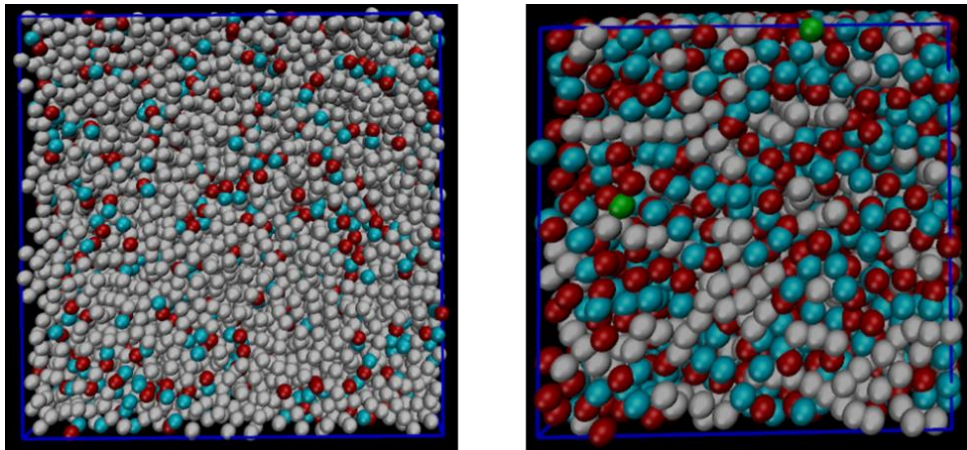
Figure 69: Initial structure of pure polyethylene glycol dimethacrylate (left) and diluted (right).

4.2   Simulated dynamic mechanical response

In this chapter the results of the small strain dynamically deformed simulations are presented. The simulations were set up to resemble a DMA experiment. This means, a periodic strain was applied to a simulation box. As the output the normal stress values were evaluated. If the material responds linearly, which was assumed in all cases, the response function is of harmonic shape which means a function of type $A * \sin w + B * \cos w$ can be fitted to the data

points. From the factor A the storage modulus can be calculated and from factor B the loss modulus can be calculated [83]. Figure 70 shows an example of what the results of the simulation look like. The green dashed line corresponds to the deformation of the simulation box. The blue dots are the normal stress data points. The harmonic response is clearly visible, though the variance of the points is still high. At high temperatures, as the thermal fluctuations become increasingly pronounced, the variance of the data points is increasing. The fitting function, which is the orange line in Figure 70, still seems to be reasonable.
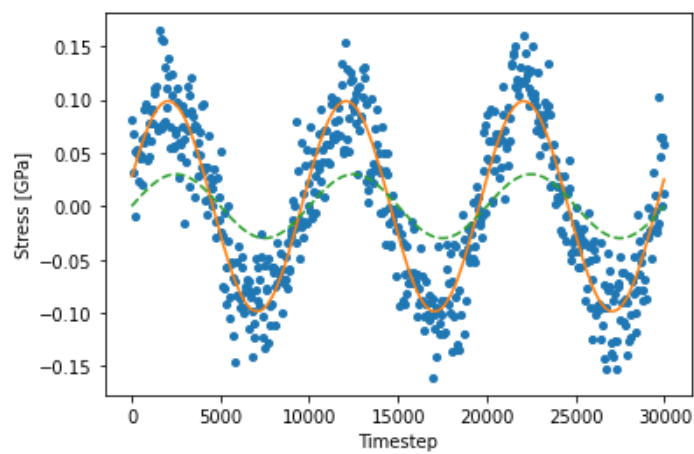
Figure 70: Result of a simulated dynamic mechanical analysis measurement.

To get to a single data point in Figure 71 the simulation was repeated in all three spatial directions and averaged. This was done at various temperatures to evaluate the dependence of the coefficients on the temperature. Similar as in a physical dynamic mechanical experiment.

Figure 71 shows the results of the simulated dynamic mechanical measurement together with the result of a physical measurement. The horizontal axis shows the temperature at which the measurement or the simulation was conducted, and the vertical axis shows the storage modulus. The different colors correspond to different double bond conversions of the same initial simulation box. The data files were simply extracted at different stages of the simulated polymerization. What can be seen is that with lower double bond conversion the values for the storage modulus are lower, which is the expected behavior. More crosslinks lead to a solidification of the material. Therefore, higher double bond conversion usually results in higher storage modulus. Comparing the simulated values with the values from the experiment, one can see that the simulation with 82 % double bond conversion is in good agreement. Considering

the temperature dependence, it can be seen that the values tend to decrease with increasing temperature. The slope however is steeper in the experimental curve compared to the simulated values.
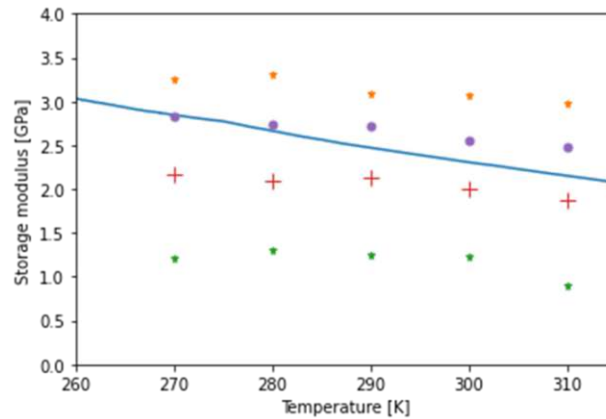
Figure 71: Simulated dynamic mechanical analysis measurement. Solid line: physical measurement; orange: 95 % double bond conversion; purple: 82 % double bond conversion; red: 71 % double bond conversion; green: 48 % double bond conversion.

To study the behavior at higher temperatures the simulation was continued until 680 Kelvin. This was done for TEGDMA with a double bond conversion of 82 %, as this was the material that best agreed with the physical measurement, and TEGDMA diluted with a small monofunctional substance. The monofunctional component significantly lowers the crosslink density, as monofunctional molecules are only capable of forming linear chains. Therefore, a lower storage modulus was expected for the diluted simulation. The results shown in Figure 72 confirm this expectation. The curve of the diluted simulation is well below the pure TEGDMA. The curves appear to be more or less parallel until approximately 600 Kelvin. The simulation containing the monofunctional diluent starts to flatten here. The results shown in Figure 73 also reflects this. In this figure the tangent of the phase shift angle is shown. This value is of special interest because the maximum of this curve is commonly taken as a definition for the glass transition temperature. One can see that in the low temperature realm the values are close together. The curve representing the diluted case shows a steeper increase with temperature. This corresponds to the more liquid like behavior of this material compared to the pure TEGDMA which has more crosslinks. At around 600 Kelvin the curve starts to establish a peak which potentially corresponds to the glass transition of the simulated material. Note however, that the fluctuations are increasing with higher temperatures. The loss modulus is even more

susceptible to fluctuation than the storage modulus. The variance of the loss modulus explains the extreme outlier at 660 Kelvin.

The comparison with the physical measurement at elevated temperatures revels a shortcoming of this specific simulation approach. As visible in Figure 71, the simulation underestimates the temperature dependency. The simulation still shows high storage modulus values at temperatures where the measured values are virtually zero. This behavior is probably inherent to the force field in use here. Bond potentials are modeled with harmonic bonds which are of symmetric shape. This can be a good approximation at a certain temperature, but when the temperature differs significantly from this reference temperature, the error increases. The same is true for non-bonded interactions. The precision is only sufficient at the reference temperature.
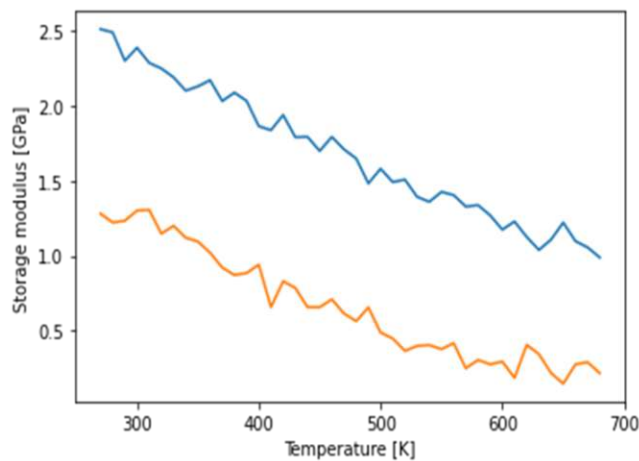
Figure 72: Simulated storage modulus over a large temperature range. Blue: pure TEGDMA; orange: 50 % TEGDMA plus 50 % propyl MA.
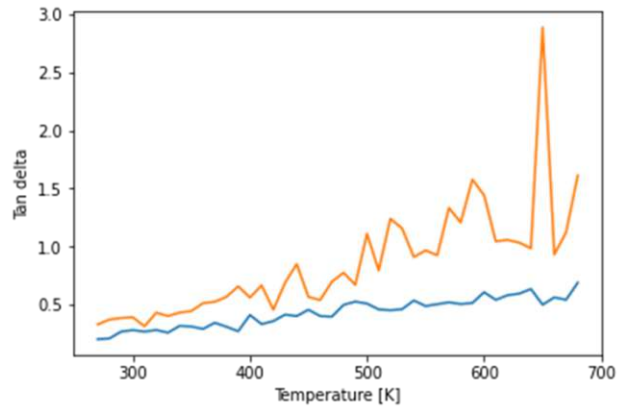
Figure 73: Simulated tan delta over a large temperature range. Blue: pure TEGDMA; orange: 50 % TEGDMA plus 50% propyl MA.

4.3 Simulated tensile response

A highly important test for a structural material is the tensile test, as it reveals the stiffness and strength of a material in a simple load case. The successful simulation of this test would be valuable in a resin development process.

To measure the tensile response, the simulation box was deformed in one spatial direction while a barostat was used to maintain a constant stress at the faces parallel to the direction of deformation. The stress at the face perpendicular to the direction of deformation was interpreted as tensile stress and used as raw data. To obtain reasonably smooth response curves, it is important to average out thermal fluctuations which was done after the simulation by calculating the time average of the tensile stress. To allow for scission of the polymer chains, the bond break fix was used in all tensile simulations.

Figure 74 shows the result of a tensile simulation of poly MMA at a double bond conversion of 90 %, which was the maximum double bond conversion reached in the simulated polymerization. It can be seen that there is a relatively linear increase of stress at low strains, in agreement with expectations. At around 5 % strain the slope of the curve starts to flatten, until the maximum stress is reached at around 10 % strain. Maximum stress exceeding 80 MPa. Stress values are overlapped by thermal fluctuations making the interpretation of stresses difficult. Another factor that has to be taken into account is that due to the small sample size that was chosen in favor of low computational cost, even minor relaxation processes during the deformation can lead to significant changes in measured stress. Other than in physical

99

experiments, stress peaks are not cancelling out in the large volume under strain. After the maximum stress is reached, a softening region can be observed between 10 % and 15 % strain. Stress is released due to chain scission and subsequent relaxation processes that are a direct consequence. At strains above 25 % the material starts to harden again. This is indicated by a larger slope in the high strain realm. At 35 % strain the simulation was stopped. No fracture occurred during the simulated tensile test.

For comparison, Figure 75 shows physical tensile tests of poly MMA at different ambient temperatures from [106]. It can be seen that strength is decreasing with elevated temperatures. Also, the elongation at break is higher with higher temperatures.
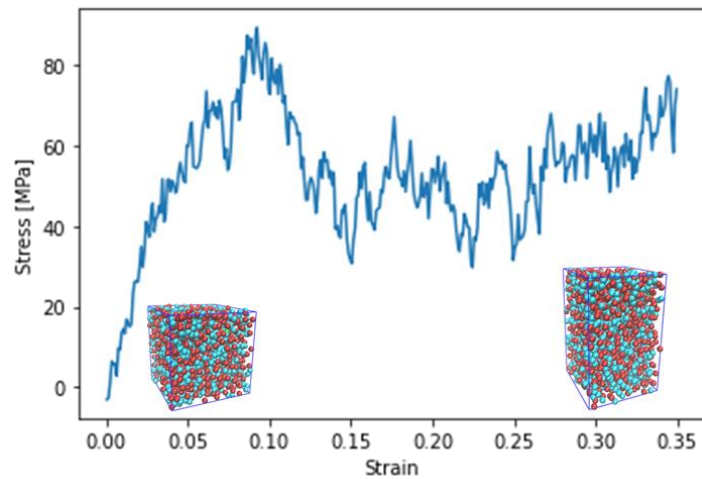
Figure 74: Simulated tensile test of poly MMA.
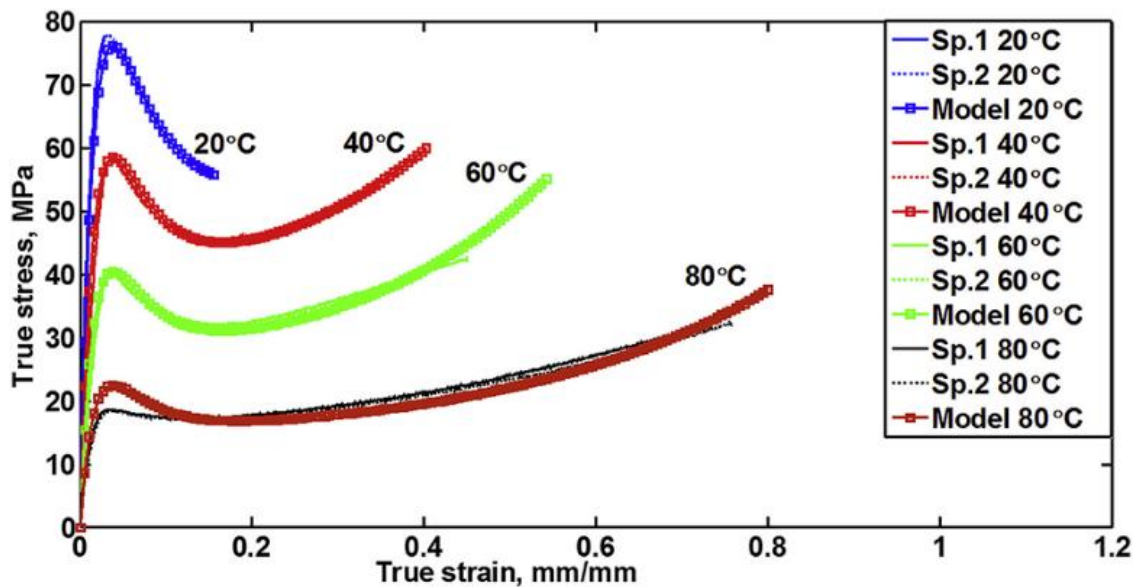
Figure 75: Experimental and modeling data of poly MMA obtained in [106]. Figure taken with permission from [106]. Copyright © 2016, Elsevier Ltd.

Figure 76 shows the simulated tensile tests for different double bond conversions of poly MMA. The blue line again is the poly MMA version with the highest double bond conversion reached in the simulation. The orange line represents 80 % double bond conversion. Compared to the blue line, the yield stress is significantly lower at 60 MPa. After a clear maximum in the stress-strain response, a similar curve was observed, including pronounced softening followed by strain hardening. The location of the yield point of this simulation agrees very well with the measurement at 40 °C from [106] (compare Figure 75). Going even lower with the double bond conversion, the tensile response becomes very flat. At 60 % double bond conversion no yield point can be observed. The lower the double bond conversion, the more the material response is dominated by a liquid-like behavior.
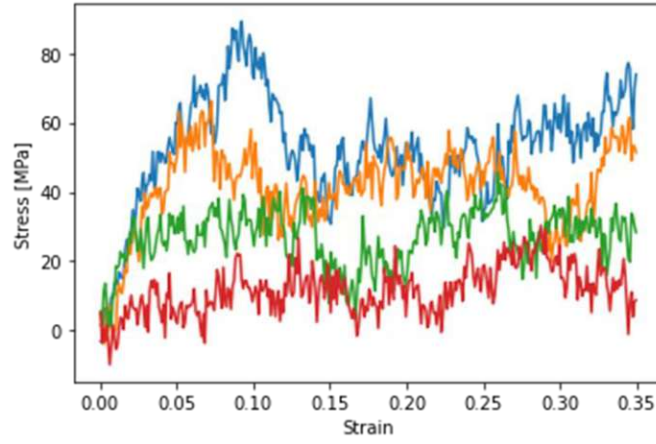
Figure 76: Simulated tensile test of poly MMA. Blue: 90 % double bond conversion; orange: 80 % double bond conversion; green: 70 % double bond conversion; red: 60 % double bond conversion.

5 Summary

Additive manufacturing is a promising technology because it offers several benefits compared to traditional manufacturing methods. However, for a wide adoption in industry, a number of challenging aspects need to be resolved. A major knock-out criterion are insufficient material properties. Only if the material properties of additively manufactured parts are competitive compared to more established methods, manufacturers will be willing to invest time and money in this emerging technology.

Additive manufacturing based on vat polymerization offers high resolution and scalability that makes it interesting for industrial applications. However, this method is bound to photopolymers which are often brittle. Most currently available systems rely on strongly crosslinking photoresins. The resulting highly crosslinked polymer will be stiff and strong, but unfortunately will show low fracture toughness, which limits the number of accessible applications.

The goal of this work was to investigate strategies to understand and modify photopolymers in order to increase the fracture toughness of additively manufactured parts. Hence, paving the way for a broader industrial application of additive manufacturing.

In the first part of this work it was investigated how much changing the resin components can influence the material properties. The used oligomers were toughness- and tg- modifiers developed previously. They were designed to yield transparent polymers with balanced material properties [13], [85]. It was found that the intrinsic toughness can be modified substantially and also the toughenability is influenced by the resin composition. Essential for the effectivity of the toughness modifier is a sufficient incorporation of the molecules into the polymer network.

As a first approach to deliberately add a microstructure, core shell rubber particles were used in the resins. For materials with high initial elongation at break no significant toughening with 10 wt% core shell particles was found. Also, it was observed that no toughening effect occurred in highly crosslinked materials. A high crosslink density restricts dissipative mechanisms which are necessary for a toughening effect [64]. However, for materials with low initial toughness and relatively low crosslink density the elongation at break could be increased. The best relative increase in elongation at break was from 5 % to over 60 % with material v37lt.

For compositions rich in HSMA and TNM2, pronounced phase separation was observed visually. To control the degree of phase separation, the temperature at curing was varied and the influence on the mechanical properties was assessed. It was found that the phase separation changes the mechanical properties drastically. The tensile modulus was found to decrease with elevated curing temperature. This is in contrast to what was expected intuitively. Typically, higher curing temperature leads to higher conversions and consequently stiffer polymers. It was concluded that the degree of phase separation, and not the change in crosslink density, predominantly is responsible for the change in mechanical properties. The change in stiffness over the curing temperature can be explained by considering a matrix-inclusion topology, where the matrix consists of a TNM2 rich phase and the inclusions consist of a stiff HSMA rich phase. Therefore, a higher degree of separation of the two components leads to a softer matrix which is responsible for the lower overall stiffness of the composite. The highest elongation at break was found with the material cured at 25 °C.

As a way to add topology in a controlled fashion, a combination of inkjet with vat curing, developed previously in [91], was assessed. This technology offers the possibility to use an inkjet printhead to apply a secondary material to a layer manufactured by a stereolithography process. Three different strategies to use inkjet as toughening method were characterized. Ink can be used to modify the base polymer by diffusion and incorporation, it can be used to separate individual layers to avoid crack propagation, and to introduce particles that serve the same purpose as core shell particles. For the modification of the base polymer, cyanoethyl acrylate was used as ink, which was found to diffuse into the base polymer well and forms a relatively tough material after a secondary curing step. With this method an approximately five-fold increase in elongation at break could be measured with only mildly decreasing strength. The elongation at break was increase from 5 % to 25 % while the strength decreased from 50 MPa to 40 MPa. Given the highly effective toughening and the great positional accuracy of the inkjet technology, this combination offers high potential for selective toughening in 3D printing. The advantage of selective toughening over global toughening is that the compromise between toughness and strength must be made only in areas of a part where it is required by the application. The other domains of a part remain unaltered and keep initial mechanical properties. This makes it interesting for additive manufacturing of high-performance polymer parts.

Chapter 4 is focused on molecular dynamics simulations to model the properties of photopolymers and the formation thereof. This section was motivated by the complexity of the

polymerization reaction and the vast space of different possible compositions and properties. It was seen in the earlier chapters that the origin of the mechanical properties is not always clear and is hard to pin down with experimental methods. Modeling of the polymer network can give additional information on the topology of the polymer and can help to learn about the structure-property relations in photopolymer materials. With continuously increasing availability of computational resources, simulation methods will play an increasing role for the material sciences in the future.

To create a polymer network using molecular dynamics, a reactive polymerization simulation was applied. For this purpose, Polymatic [82] was used to crosslink reactive groups during molecular dynamics simulations. With this method it was possible to extract information about the double bond conversion rates during the polymerization of different compositions. It was found that the reaction of monofunctional molecules phases out slowly at relatively high conversions. In contrast, the simulation of purely difunctional molecules stopped relatively abruptly at lower double bond conversions. Further, the case of high molecular weight molecules in reactive diluent was tested. As expected, the simulation of the pure high molecular weight system was reacting very slowly and stopped early. The low mobility of the few reactive groups is causing a very inactive system. In the case of reactive diluent being present, the reaction proceeded much faster and to higher conversions. The small molecules provide enough mobility to keep the reaction running.

The dynamic mechanical properties were assessed by periodically straining the simulation cell and measure the stress response of the system. The resulting values were time averaged and fitted with the response function. From this fit, the storage modulus and loss modulus could be extracted, and the phase shift could be determined. For pure TEGDMA the storage modulus value was in excellent agreement with experimental data at 270 Kelvin. For higher temperatures, the experimental values decline faster than the simulated values. A possible explanation for this is that the used force field is not applicable at high temperatures.

To get information on the high strain response, simulation cells were strained up to 35% and the stress response was measured. The yield point for poly methyl methacrylate at a double bond conversion of 80 percent was found to be at a stress of approximately 60 MPa and at a strain of approximately 6 percent, which is in good agreement with tensile test results from literature. Also, a post yield strain hardening behavior could be simulated which is a typical behavior of many photopolymers analyzed in this work.

The simulation results show that with relatively easily available methods, photopolymers can be simulated to a reasonable agreement with experimental values. This motivates a continuing integration of simulation methods into the development process of photopolymer materials.

6 Figures

7 References

[1] B. G. Compton and J. A. Lewis, "3D-Printing of Lightweight Cellular Composites," *Adv. Mater.*, vol. 26, no. 34, pp. 5930–5935, 2014, doi: 10.1002/adma.201401804.

[2] C. W. Hull, "Apparatus for production of three-dimensional objects by stereolithography," US4575330A, Mar. 11, 1986 Accessed: Nov. 23, 2021. [Online]. Available: https://patents.google.com/patent/US4575330A/en?q=chuck+hull+stereolithograpy&oq=chuck+hull+stereolithograpy&sort=old

[3] W. E. Frazier, "Metal Additive Manufacturing: A Review," *J. Mater. Eng. Perform.*, vol. 23, no. 6, pp. 1917–1928, Jun. 2014, doi: 10.1007/s11665-014-0958-z.

[4] Y. Lakhdar, C. Tuck, J. Binner, A. Terry, and R. Goodridge, "Additive manufacturing of advanced ceramic materials," *Prog. Mater. Sci.*, vol. 116, p. 100736, Feb. 2021, doi: 10.1016/j.pmatsci.2020.100736.

[5] M. Valente, A. Sibai, and M. Sambucci, "Extrusion-Based Additive Manufacturing of Concrete Products: Revolutionizing and Remodeling the Construction Industry," *J. Compos. Sci.*, vol. 3, no. 3, Art. no. 3, Sep. 2019, doi: 10.3390/jcs3030088.

[6] W. Sun *et al.*, "The bioprinting roadmap," *Biofabrication*, vol. 12, no. 2, p. 022002, Feb. 2020, doi: 10.1088/1758-5090/ab5158.

[7] T. Swetly, J. Stampfl, G. Kempf, and R.-M. Hucke, "Capabilities of additive manufacturing technologies (AMT) in the validation of the automotive cockpit," *RTejournal - Forum Für Rapid Technol.*, vol. 2014, no. 1, Jul. 2014, [Online]. Available: http://www.rtejournal.de/ausgabe11/3957

[8] G. M. Tartaglia *et al.*, "Direct 3D Printing of Clear Orthodontic Aligners: Current State and Future Possibilities," *Materials*, vol. 14, no. 7, Art. no. 7, Jan. 2021, doi: 10.3390/ma14071799.

[9] N. Shahrubudin, T. C. Lee, and R. Ramlan, "An Overview on 3D Printing Technology: Technological, Materials, and Applications," *Procedia Manuf.*, vol. 35, pp. 1286–1296, Jan. 2019, doi: 10.1016/j.promfg.2019.06.089.

[10]   S. D. Nath and S. Nilufar, "An Overview of Additive Manufacturing of Polymers and Associated Composites," *Polymers*, vol. 12, no. 11, Art. no. 11, Nov. 2020, doi: 10.3390/polym12112719.

[11]   C. Hull, "On Stereolithography," *Virtual Phys. Prototyp.*, vol. 7, no. 3, pp. 177–177, Sep. 2012, doi: 10.1080/17452759.2012.723409.

[12]   M. Hailing, "Untersuchung der Auswirkung eines monofunktionellen Reaktivverdünners auf das 3D-Druckverhalten von Photopolymeren," TU Wien, Wien, Bachelor Thesis, Apr. 2020.

[13]   M. Kury, "Tough photopolymers for 3D printing," Doctor's Theses, TU Wien, 2020.

[14]   M. Pfaffinger, "Hot Lithography – New Possibilities in Polymer 3D Printing," *Laser Tech. J.*, vol. 15, no. 4, pp. 45–47, 2018, doi: 10.1002/latj.201800024.

[15]   C. Dall'Argine, A. Hochwallner, N. Klikovits, R. Liska, J. Stampf, and M. Sangermano, "Hot-Lithography SLA-3D Printing of Epoxy Resin," *Macromol. Mater. Eng.*, vol. 305, no. 10, p. 2000325, 2020, doi: https://doi.org/10.1002/mame.202000325.

[16]   B. Steyrer, B. Busetti, G. Harakály, R. Liska, and J. Stampfl, "Hot Lithography vs. room temperature DLP 3D-printing of a dimethacrylate," *Addit. Manuf.*, vol. 21, pp. 209–214, May 2018, doi: 10.1016/j.addma.2018.03.013.

[17]   Y. M. Bichu *et al.*, "Advances in orthodontic clear aligner materials," *Bioact. Mater.*, vol. 22, pp. 384–403, Apr. 2023, doi: 10.1016/j.bioactmat.2022.10.006.

[18]   J. W. Verhoeven, "Glossary of terms used in photochemistry (IUPAC Recommendations 1996)," *Pure Appl. Chem.*, vol. 68, no. 12, pp. 2223–2286, Jan. 1996, doi: 10.1351/pac199668122223.

[19]   J. Aerykssen and J. Piceno, "New Developments in Acrylate Oligomers for 3D Printing," Bomar, White Paper. Accessed: May 07, 2022. [Online]. Available: https://bomar-chem.com/resources/resource-library

[20]   J. V. Crivello and E. Reichmanis, "Photopolymer Materials and Processes for Advanced Technologies," *Chem. Mater.*, vol. 26, no. 1, pp. 533–548, Jan. 2014, doi: 10.1021/cm402262g.

[21]   S. Clark Ligon-Auer, M. Schwentenwein, C. Gorsche, J. Stampfl, and R. Liska, "Toughening of photo-curable polymer networks: a review," *Polym. Chem.*, vol. 7, no. 2, pp. 257–286, 2016, doi: 10.1039/C5PY01631B.

[22]   J. P. Fouassier, X. Allonas, J. Lalevée, and C. Dietlin, "Photoinitiators for Free Radical Polymerization Reactions," in *Photochemistry and Photophysics of Polymer Materials*, John Wiley & Sons, Ltd, 2010, pp. 351–419. doi: 10.1002/9780470594179.ch10.

[23]   G. Odian, "Radical Chain Polymerization," in *Principles of Polymerization*, 4th ed., John Wiley & Sons, Ltd, 2004, pp. 198–349. doi: 10.1002/047147875X.ch3.

[24]   "Avogadro - Free cross-platform molecular editor," *Avogadro*. https://avogadro.cc/ (accessed Jan. 17, 2022).

[25]   C. T. Ratnam, M. Nasir, and A. Baharin, "Irradiation crosslinking of unplasticized polyvinyl chloride in the presence of additives," *Polym. Test.*, vol. 20, no. 5, pp. 485–490, Jan. 2001, doi: 10.1016/S0142-9418(00)00063-5.

[26]   R. Schwalm, "CHAPTER 6 - Structure–Property Relationships," in *UV Coatings*, R. Schwalm, Ed. Amsterdam: Elsevier, 2007, pp. 160–178. doi: 10.1016/B978-044452979-4/50006-8.

[27]   A. Saal, T. Hagemann, and U. S. Schubert, "Polymers for Battery Applications—Active Materials, Membranes, and Binders," *Adv. Energy Mater.*, vol. n/a, no. n/a, p. 2001984, doi: 10.1002/aenm.202001984.

[28]   I. M. Ward and J. Sweeney, "Non-linear Viscoelastic Behaviour," in *Mechanical Properties of Solid Polymers*, 3rd ed., John Wiley & Sons, Ltd, 2012, pp. 285–318. doi: 10.1002/9781119967125.ch11.

[29]   A. S. Argon, Ed., "Plasticity of glassy polymers," in *The Physics of Deformation and Fracture of Polymers*, Cambridge: Cambridge University Press, 2013, pp. 228–272. doi: 10.1017/CBO9781139033046.010.

[30]   S. Glasstone, K. J. Laidler, and H. Eyring, *The theory of rate processes : the kinetics of chemical reactions, viscosity, diffusion and electrochemical phenomena*, 1. ed.. New York, NY [u.a.]: McGraw-Hill, 1941.

[31]   "Mechanics of Materials," in *An Introduction to Materials Engineering and Science*, John Wiley & Sons, Ltd, 2003, pp. 380–536. doi: 10.1002/0471473359.ch5.

[32]   C. Bauwens-Crowet, J. C. Bauwens, and G. Homès, "Tensile yield-stress behavior of glassy polymers," *J. Polym. Sci. Part -2 Polym. Phys.*, vol. 7, no. 4, pp. 735–742, 1969, doi: 10.1002/pol.1969.160070411.

[33]   Y. Liu and R. W. Truss, "A study of tensile yielding of isotactic polypropylene," *J. Polym. Sci. Part B Polym. Phys.*, vol. 32, no. 12, pp. 2037–2047, 1994, doi: 10.1002/polb.1994.090321210.

[34]   G. Halsey, H. J. White, and H. Eyring, "Mechanical Properties of Textiles, I," *Text. Res.*, vol. 15, no. 9, pp. 295–311, Sep. 1945, doi: 10.1177/004051754501500901.

[35]   P. I. Vincent, "The tough-brittle transition in thermoplastics," *Polymer*, vol. 1, pp. 425–444, Jan. 1960, doi: 10.1016/0032-3861(60)90059-8.

[36]   P. I. Vincent, "A correlation between critical tensile strength and polymer cross-sectional area," *Polymer*, vol. 13, no. 12, pp. 558–560, Dezember 1972, doi: 10.1016/0032-3861(72)90116-4.

[37]   R. W. Nunes, J. R. Martin, and J. F. Johnson, "Influence of molecular weight and molecular weight distribution on mechanical properties of polymers," *Polym. Eng. Sci.*, vol. 22, no. 4, pp. 205–228, 1982, doi: 10.1002/pen.760220402.

[38]   W. Grellmann, S. Seidler, and V. Altstädt, *Kunststoffprüfung*, 3., Aktualisierte Aufl. München: Hanser, 2015.

[39]   A. S. Argon, Ed., "Small-strain elastic response," in *The Physics of Deformation and Fracture of Polymers*, Cambridge: Cambridge University Press, 2013, pp. 90–111. doi: 10.1017/CBO9781139033046.006.

[40]   A. S. Argon, Ed., "Rubber elasticity," in *The Physics of Deformation and Fracture of Polymers*, Cambridge: Cambridge University Press, 2013, pp. 148–173. doi: 10.1017/CBO9781139033046.008.

[41]   L. R. G. Treloar, *The Physics of Rubber Elasticity*. OUP Oxford, 1975.

[42]   J. A. W. van Dommelen, W. A. M. Brekelmans, and F. P. T. Baaijens, "Micromechanical modeling of particle-toughening of polymers by locally induced anisotropy," *Mech. Mater.*, vol. 35, no. 9, pp. 845–863, Sep. 2003, doi: 10.1016/S0167-6636(02)00307-1.

[43]   V. Tvergaard and J. W. Hutchinson, "The relation between crack growth resistance and fracture process parameters in elastic-plastic solids," *J. Mech. Phys. Solids*, vol. 40, no. 6, pp. 1377–1397, Aug. 1992, doi: 10.1016/0022-5096(92)90020-3.

[44]   R. J. M. Smit, W. A. M. Brekelmans, and H. E. H. Meijer, "Predictive modelling of the properties and toughness of polymeric materials Part III Simultaneous prediction of micro- and macrostructural deformation of rubber-modified polymers," *J. Mater. Sci.*, vol. 35, no. 11, pp. 2881–2892, Jun. 2000, doi: 10.1023/A:1004715707138.

[45]   A. S. Argon, Ed., "Crazing in glassy homo- and hetero-polymers," in *The Physics of Deformation and Fracture of Polymers*, Cambridge: Cambridge University Press, 2013, pp. 342–390. doi: 10.1017/CBO9781139033046.013.

[46]   A. J. Kinloch and R. J. Young, "Crazing," in *Fracture Behaviour of Polymers*, A. J. Kinloch and R. J. Young, Eds. Dordrecht: Springer Netherlands, 1995, pp. 147–181. doi: 10.1007/978-94-017-1594-2_5.

[47]   C. Y. Ryu, J. Ruokolainen, G. H. Fredrickson, E. J. Kramer, and S. F. Hahn, "Chain Architecture Effects on Deformation and Fracture of Block Copolymers with Unentangled Matrices," *Macromolecules*, vol. 35, no. 6, pp. 2157–2166, Mar. 2002, doi: 10.1021/ma011576r.

[48]   R. Deblieck, B. Gerets, M. Boerakker, H. Caelers, A. Wilbers, and T. Boonen, "Relation between life time, failure stress and craze microstructure in polyethylene as evidenced by fracture surface texture analysis after an accelerated Full-Notch Creep Test," *Polymer*, vol. 176, pp. 264–273, Aug. 2019, doi: 10.1016/j.polymer.2019.04.033.

[49]   A. S. Argon, Ed., "Linear viscoelasticity of polymers," in *The Physics of Deformation and Fracture of Polymers*, Cambridge: Cambridge University Press, 2013, pp. 112–147. doi: 10.1017/CBO9781139033046.007.

[50]   I. M. Ward and J. Sweeney, "Linear Viscoelastic Behaviour," in *Mechanical Properties of Solid Polymers*, Third Edition., John Wiley & Sons, Ltd, 2012, pp. 87–117. doi: 10.1002/9781119967125.ch5.

[51]   J. P. Brutman, D. J. Fortman, G. X. De Hoe, W. R. Dichtel, and M. A. Hillmyer, "Mechanistic Study of Stress Relaxation in Urethane-Containing Polymer Networks," *J. Phys. Chem. B*, vol. 123, no. 6, pp. 1432–1441, Feb. 2019, doi: 10.1021/acs.jpcb.8b11489.

[52]   Atroiss, *Typisches DMA Thermogramm eines amorphen Thermoplasten (Polycarbonat) gemessen im Dual Cantilever Deformationsmodus mit einer Messfrequenz von 1 Hz und einer Heizrate von 2 K/min. Die Glasübergangstemperatur, bestimmt gemäß ISO 6721-11, beträgt 151.3°C.* 2019. Accessed: Feb. 11, 2022. [Online]. Available: https://commons.wikimedia.org/w/index.php?curid=83161241

[53]   J. Stampf and O. Guillaume, "308.106 Biocompatible Materials," Vienna, Austria, Feb. 14, 2022.

[54]   A. A. Griffith and G. I. Taylor, "VI. The phenomena of rupture and flow in solids," *Philos. Trans. R. Soc. Lond. Ser. Contain. Pap. Math. Phys. Character*, vol. 221, no. 582–593, pp. 163–198, Jan. 1921, doi: 10.1098/rsta.1921.0006.

[55]   G. R. Irwin, "Analysis of Stresses and Strains Near the End of a Crack Traversing a Plate," *J. Appl. Mech.*, vol. 24, no. 3, pp. 361–364, Sep. 1957, doi: 10.1115/1.4011547.

[56]   H. Tada, P. C. Paris, and G. R. Irwin, "The Stress Analysis of Cracks Handbook, Third Edition," Jan. 2000, doi: 10.1115/1.801535.

[57]   R. M. McMeeking, "Finite deformation analysis of crack-tip opening in elastic-plastic materials and implications for fracture," *J. Mech. Phys. Solids*, vol. 25, no. 5, pp. 357–381, Oct. 1977, doi: 10.1016/0022-5096(77)90003-5.

[58]   R. O. Ritchie, "The conflicts between strength and toughness," *Nat. Mater.*, vol. 10, no. 11, Art. no. 11, Nov. 2011, doi: 10.1038/nmat3115.

[59]   M. A. Ghalia and A. Abdelrasoul, "7 - Compressive and fracture toughness of natural and synthetic fiber-reinforced polymer," in *Mechanical and Physical Testing of Biocomposites, Fibre-Reinforced Composites and Hybrid Composites*, M. Jawaid, M. Thariq, and N. Saba, Eds. Woodhead Publishing, 2019, pp. 123–140. doi: 10.1016/B978-0-08-102292-4.00007-2.

[60]   D. K. Rajak, D. D. Pagar, P. L. Menezes, and E. Linul, "Fiber-Reinforced Polymer Composites: Manufacturing, Properties, and Applications," *Polymers*, vol. 11, no. 10, Art. no. 10, Oct. 2019, doi: 10.3390/polym11101667.

[61]   S. M. F. Kabir, K. Mathur, and A.-F. M. Seyam, "A critical review on 3D printed continuous fiber-reinforced composites: History, mechanism, materials and properties," *Compos. Struct.*, vol. 232, p. 111476, Jan. 2020, doi: 10.1016/j.compstruct.2019.111476.

[62]   S. H. R. Sanei and D. Popescu, "3D-Printed Carbon Fiber Reinforced Polymer Composites: A Systematic Review," *J. Compos. Sci.*, vol. 4, no. 3, Art. no. 3, Sep. 2020, doi: 10.3390/jcs4030098.

[63]   A. C. Meeks, "Fracture and mechanical properties of epoxy resins and rubber-modified epoxy resins," *Polymer*, vol. 15, no. 10, pp. 675–681, Oct. 1974, doi: 10.1016/0032-3861(74)90060-3.

[64]   R. Bagheri, B. T. Marouf, and R. A. Pearson, "Rubber-Toughened Epoxies: A Critical Review," *Polym. Rev.*, vol. 49, no. 3, pp. 201–225, Aug. 2009, doi: 10.1080/15583720903048227.

[65]   A. S. Argon and R. E. Cohen, "Toughenability of polymers," *Polymer*, vol. 44, no. 19, pp. 6013–6032, Sep. 2003, doi: 10.1016/S0032-3861(03)00546-9.

[66]   S. Wu, "Phase structure and adhesion in polymer blends: A criterion for rubber toughening," *Polymer*, vol. 26, no. 12, pp. 1855–1863, Nov. 1985, doi: 10.1016/0032-3861(85)90015-1.

[67]   Y. Huang and A. J. Kinloch, "Modelling of the toughening mechanisms in rubber-modified epoxy polymers," *J. Mater. Sci.*, vol. 27, no. 10, pp. 2753–2762, May 1992, doi: 10.1007/BF00540702.

[68]   M. Ishikawa and I. Chiba, "Toughening mechanisms of blends of poly(acrylonitrile-butadiene-styrene) copolymer and BPA polycarbonate," *Polymer*, vol. 31, no. 7, pp. 1232–1238, Jul. 1990, doi: 10.1016/0032-3861(90)90213-I.

[69]   R. A. Pearson, "Introduction to the Toughening of Polymers," in *Toughening of Plastics*, vol. 759, 0 vols., American Chemical Society, 2000, pp. 1–12. doi: 10.1021/bk-2000-0759.ch001.

[70]   C. Xu *et al.*, "Enhanced toughness and thermal conductivity for epoxy resin with a core–shell structured polyacrylic modifier and modified boron nitride," *RSC Adv.*, vol. 9, no. 15, pp. 8654–8663, Mar. 2019, doi: 10.1039/C8RA10645B.

[71]   M. Hutnik, A. S. Argon, and U. W. Suter, "Quasi-static modeling of chain dynamics in the amorphous glassy polycarbonate of 4,4'-isopropylidenediphenol," *Macromolecules*, vol. 24, no. 22, pp. 5970–5979, Oct. 1991, doi: 10.1021/ma00022a012.

[72]   L. Verlet, "Computer 'Experiments' on Classical Fluids. I. Thermodynamical Properties of Lennard-Jones Molecules," *Phys. Rev.*, vol. 159, no. 1, pp. 98–103, Jul. 1967, doi: 10.1103/PhysRev.159.98.

[73]   W. C. Swope, H. C. Andersen, P. H. Berens, and K. R. Wilson, "A computer simulation method for the calculation of equilibrium constants for the formation of physical clusters of molecules: Application to small water clusters," *J. Chem. Phys.*, vol. 76, no. 1, pp. 637–649, Jan. 1982, doi: 10.1063/1.442716.

[74]   A. P. Thompson *et al.*, "LAMMPS - a flexible simulation tool for particle-based materials modeling at the atomic, meso, and continuum scales," *Comput. Phys. Commun.*, vol. 271, p. 108171, Feb. 2022, doi: 10.1016/j.cpc.2021.108171.

[75]   M. J. Abraham *et al.*, "GROMACS: High performance molecular simulations through multi-level parallelism from laptops to supercomputers," *SoftwareX*, vol. 1–2, pp. 19–25, Sep. 2015, doi: 10.1016/j.softx.2015.06.001.

[76]   "pair_style   lj/cut   command   —   LAMMPS   documentation." https://docs.lammps.org/pair_lj.html (accessed Feb. 15, 2022).

[77]   "bond_style   harmonic   command   —   LAMMPS   documentation." https://docs.lammps.org/bond_harmonic.html (accessed Feb. 17, 2022).

[78] J. A. Harrison, J. D. Schall, S. Maskey, P. T. Mikulski, M. T. Knippenberg, and B. H. Morrow, "Review of force fields and intermolecular potentials used in atomistic computational materials research," *Appl. Phys. Rev.*, vol. 5, no. 3, p. 031104, Sep. 2018, doi: 10.1063/1.5020808.

[79] S. J. Marrink, H. J. Risselada, S. Yefimov, D. P. Tieleman, and A. H. de Vries, "The MARTINI Force Field: Coarse Grained Model for Biomolecular Simulations," *J. Phys. Chem. B*, vol. 111, no. 27, pp. 7812–7824, Jul. 2007, doi: 10.1021/jp071097f.

[80] S. J. Marrink and D. P. Tieleman, "Perspective on the Martini model," *Chem. Soc. Rev.*, vol. 42, no. 16, pp. 6801–6822, Jul. 2013, doi: 10.1039/C3CS60093A.

[81] T. E. Gartner and A. Jayaraman, "Modeling and Simulations of Polymers: A Roadmap," *Macromolecules*, vol. 52, no. 3, pp. 755–786, Feb. 2019, doi: 10.1021/acs.macromol.8b01836.

[82] L. J. Abbott, K. E. Hart, and C. M. Colina, "Polymatic: a generalized simulated polymerization algorithm for amorphous polymers," *Theor. Chem. Acc.*, vol. 132, no. 3, p. 1334, Jan. 2013, doi: 10.1007/s00214-013-1334-z.

[83] J. Shen *et al.*, "Molecular dynamics simulations of the structural, mechanical and visco-elastic properties of polymer nanocomposites filled with grafted nanoparticles," *Phys. Chem. Chem. Phys.*, vol. 17, no. 11, pp. 7196–7207, 2015, doi: 10.1039/C4CP05520A.

[84] P. Dorfinger, "Toughening of photopolymers for lithography-based 3D-printing," Doctor's Theses, TU Wien, 2016.

[85] G. Harakály, "Tough photopolymers for Hot Lithography application," Doctor's Theses, TU Wien, 2019.

[86] "Bomar® XR-741MS Difunctional Aliphatic Polyester Urethane Methacrylate." https://dymax-oc.com/images/pdf/pds/xr-741ms.pdf (accessed Nov. 17, 2021).

[87] E. Asmussen and A. Peutzfeldt, "Influence of UEDMA BisGMA and TEGDMA on selected mechanical properties of experimental resin composites," *Dent. Mater. Off. Publ. Acad. Dent. Mater.*, vol. 14, no. 1, pp. 51–56, Jan. 1998, doi: 10.1016/s0109-5641(98)00009-8.

[88] J. L. Ferracane, "Resin composite—State of the art," *Dent. Mater.*, vol. 27, no. 1, pp. 29–38, Jan. 2011, doi: 10.1016/j.dental.2010.10.020.

[89] "Tegdma." https://www.sigmaaldrich.com/AT/de/search/tegdma?focus=products&page=1&perpage=30&sort=relevance&term=tegdma&type=product (accessed Nov. 26, 2022).

[90] "SpeedCure TPO an energy curing product from Lambson." https://www.lambson.com/energy-cure/view,speedcure-tpo_157.htm (accessed Nov. 17, 2021).

[91] S. Baumgartner, "Development of a 3D-printing process for colored dental ceramics and selective modification of polymers," Doctor's Theses, TU Wien, Vienna, Austria, 2018.

[92] S. Baumgartner, R. Gmeiner, J. A. Schönherr, and J. Stampfl, "Stereolithography-based additive manufacturing of lithium disilicate glass ceramic for dental applications," *Mater. Sci. Eng. C*, vol. 116, p. 111180, Nov. 2020, doi: 10.1016/j.msec.2020.111180.

[93] J. Stögerer, S. Baumgartner, A. Hochwallner, and J. Stampfl, "Bio-Inspired Toughening of Composites in 3D-Printing," *Materials*, vol. 13, no. 21, Art. no. 21, Jan. 2020, doi: 10.3390/ma13214714.

[94] B. Koch, "Tailored urethane methacrylates for tough, thermoplastic-like photopolymers via hot lithography," Master's Thesis, Technische Universität Wien, Vienna, 2019.

[95] C. R. Szczepanski, C. S. Pfeifer, and J. W. Stansbury, "A new approach to network heterogeneity: Polymerization induced phase separation in photo-initiated, free-radical methacrylic systems," *Polymer*, vol. 53, no. 21, pp. 4694–4701, Sep. 2012, doi: 10.1016/j.polymer.2012.08.010.

[96] J. H. Kim, F. E. Karasz, and M. F. Malone, "Effects of phase separation on the mechanical properties of polystyrene/poly(vinyl methyl ether) blends," *Polym. Eng. Sci.*, vol. 31, no. 13, pp. 981–987, 1991, doi: https://doi.org/10.1002/pen.760311308.

[97] M. P. Patel, M. Braden, and K. W. M. Davy, "Polymerization shrinkage of methacrylate esters," *Biomaterials*, vol. 8, no. 1, pp. 53–56, Jan. 1987, doi: 10.1016/0142-9612(87)90030-5.

[98] M. Dewaele, D. Truffier-Boutry, J. Devaux, and G. Leloup, "Volume contraction in photocured dental resins: The shrinkage-conversion relationship revisited," *Dent. Mater.*, vol. 22, no. 4, pp. 359–365, Apr. 2006, doi: 10.1016/j.dental.2005.03.014.

[99] M. Muthukumar and A. Baumgaertner, "Diffusion of a polymer chain in random media," *Macromolecules*, vol. 22, no. 4, pp. 1941–1946, Apr. 1989, doi: 10.1021/ma00194a071.

[100] M. Muthukumar and A. Baumgaertner, "Effects of entropic barriers on polymer dynamics," *Macromolecules*, vol. 22, no. 4, pp. 1937–1941, Apr. 1989, doi: 10.1021/ma00194a070.

[101] J. Stögerer, "Hybrid material toughening of photopolymers in 3D printing," Thesis, Wien, 2022. Accessed: Nov. 26, 2022. [Online]. Available: https://repositum.tuwien.at/handle/20.500.12708/20298

[102] J. Wiener, H. Kaineder, O. Kolednik, and F. Arbeiter, "Optimization of Mechanical Properties and Damage Tolerance in Polymer-Mineral Multilayer Composites," *Materials*, vol. 14, no. 4, Art. no. 4, Jan. 2021, doi: 10.3390/ma14040725.

[103] J. Cloos, "Toughening of photopolymers used for lithography-based additive manufacturing," Master's Thesis, TU Wien, Vienna, 2021.

[104] Y. Wu, S. Joseph, and N. R. Aluru, "Effect of Cross-Linking on the Diffusion of Water, Ions, and Small Molecules in Hydrogels," *J. Phys. Chem. B*, vol. 113, no. 11, pp. 3512–3520, Mar. 2009, doi: 10.1021/jp808145x.

[105] G. Campos-Villalobos, F. R. Siperstein, and A. Patti, "Transferable coarse-grained MARTINI model for methacrylate-based copolymers," *Mol. Syst. Des. Eng.*, vol. 4, no. 1, pp. 186–198, Feb. 2019, doi: 10.1039/C8ME00064F.

[106] A. A. Abdel-Wahab, S. Ataya, and V. V. Silberschmidt, "Temperature-dependent mechanical behaviour of PMMA: Experimental analysis and modelling," *Polym. Test.*, vol. 58, pp. 86–95, Apr. 2017, doi: 10.1016/j.polymertesting.2016.12.016.

CURRICULUM VITAE

Education

2018 – today	**Doctoral Program in Technical Sciences** Technische Universität Wien Thesis: *Toughening and Modeling of Photopolymers used in 3D Printing* Lecture highlights: Theoretical Molecular Chemistry, Nonlinear Finite Element Methods, VSC-School II: Course in High-Performance Computing
2016 – 2018	**Master of Science – Material Sciences** Technische Universität Wien Thesis: *Influence of Core-Shell Particles on the Properties of Materials for Stereolithography* Lecture highlights: Theoretical Chemistry, Computational Materials Science, High Performance Ceramics, Surface Physics, Organic Chemistry, and Polymer Chemistry
2012 – 2016	**Bachelor of Science – Physics** Technische Universität Wien Thesis: *Investigation of the Thermoelectric Effect in Heusler Compounds* Lecture highlights: Quantum Mechanics, Statistical Mechanics, Mathematical Methods in Physics
2006 – 2011	**Matura – Mechanical Engineering** Höhere Technische Bundeslehranstalt Steyr Automotive engineering

Employment

06/2018 – today	**Technische Universität Wien** Institute of Materials Science and Technology Project Assistant Working together with a team of researchers and an international industry partner on novel 3D printing materials for biomedical application.
2013 – 2016	**LernQuadrat GmbH** Freelance tutor for mathematics and engineering subjects
07/2011 – 03/2012	**Austrian Red Cross** Civilian community service Assistant Paramedic
08/2005	**ZF Steyr Präzisionstechnik GmbH** Internship Quality management

Skills

<u>Molecular modeling</u>: Force field based molecular dynamics simulations (Lammps, Gromacs), Linux based high performance computing
<u>Engineering</u>: Finite element simulations in structural mechanics (Ansys, Abaqus, Comsol), fluid dynamics basics, CATIA, Solidworks
<u>Programming</u>: Python, Matlab; basics in: C, C++
<u>Language</u>: Fluent in English and German

Journal Publications

C. Dall'Argine, **A. Hochwallner**, N. Klikovits, R. Liska, J. Stampf, and M. Sangermano, "Hot-Lithography SLA-3D Printing of Epoxy Resin," *Macromolecular Materials and Engineering*, vol. 305, no. 10, p. 2000325, 2020, doi: https://doi.org/10.1002/mame.202000325.

J. Stögerer, S. Baumgartner, **A. Hochwallner**, and J. Stampfl, "Bio-Inspired Toughening of Composites in 3D-Printing," *Materials*, vol. 13, no. 21, Art. no. 21, Jan. 2020, doi: 10.3390/ma13214714.

A. Hochwallner and J. Stampfl, "A Martini 3 coarse-grain model for the simulation of the photopolymerizable organic phase in dental composites," *RSC Adv.*, vol. 12, no. 19, pp. 12053–12059, 2022, doi: 10.1039/D2RA00732K.

Conference Presentations

A. Hochwallner and J. Stampfl, "Watching Polymer Networks Form: Molecular Dynamics Simulation of the Chain Growth Polymerization of Photopolymers," presented at the EUROMAT 2021 - European Congress and Exhibition on Advanced Materials and Processes, Sep. 17, 2021.

A. Hochwallner and J. Stampfl, "Molecular Dynamics Simulation of the Mechanical Properties of Photopolymers used in 3D-Printing," presented at the ESIAM21 - The second European Conference on the Structural Integrity of Additively Manufactured Materials, Sep. 08, 2021.

A. Berg, B. Koch, **A. Hochwallner**, J. Stampfl, C. Grasl, and F. Moscato, "Magnetic Resonance Microscopy for the non-destructive analysis of polymer micro structures produced using additive manufacturing," presented at the Proc. Joint Meeting of Dreiländertagung & Multinational Congress on Microscopy, Wien, Aug. 22, 2021.

B. Koch, **A. Hochwallner**, R. Liska, and J. Stampfl, "Ink development for the fabrication of digital materials with increased fracture toughness," presented at the ESIAM21 - The second European Conference on the Structural Integrity of Additively Manufactured Materials, Aug. 09, 2021.

M. Ahmadi, **A. Hochwallner**, O. Andriotis, P. Thurner, and J. Stampfl, "Phase separation in (Meth)acrylate-based photopolymers," presented at the ESIAM21 - The second European Conference on the Structural Integrity of Additively Manufactured Materials, Aug. 09, 2021.

A. Hochwallner and J. Stampfl, "Molecular Dynamics Simulation of the Dynamic Mechanical Response of Photopolymerized Methacrylate Networks," presented at the vESPS21 - Virtual European Symposium of Photopolymer Sciences, Jun. 15, 2021.

Conference Posters

M. Ahmadi, **A. Hochwallner**, O. Andriotis, P. Thurner, and J. Stampfl, "Characterization of phase-separated (Meth)acrylate photopolymers," presented at the EUROMAT 2021 - European Congress and Exhibition on Advanced Materials and Processes, Sep. 13, 2021.